CHARACTERIZATION OF PEPTIDE RELEASE FROM NEURONAL CELLS WITH MICROFLUIDICS AND MASS SPECTROMETRY

BY

MING ZHONG

DISSERTATION

Submitted in partial fulfillment of the requirements
for the degree of Doctor of Philosophy in Chemistry
in the Graduate College of the
University of Illinois at Urbana-Champaign, 2012

Urbana, Illinois

Doctoral Committee:

Professor Jonathan V. Sweedler, Chair
Professor Ryan C. Bailey
Professor Martha U. Gillette
Professor Ralph G. Nuzzo

ABSTRACT

The nervous system is a complex network of a large number of neurons, and the neuronal communication between these cells often relies on chemical signals. Deciphering these signaling molecules, including neuropeptides, is an important but challenging task. Microfluidic technology allows the manipulation of mass-limited samples and the control of the extracellular microenvironment, making it well suited for studying neurons. In this work, we developed several microfluidic devices that can be interfaced to matrix-assisted laser desorption/ionization (MALDI) mass spectrometry (MS) for characterization of neuropeptide release in response to chemical stimulation. One of the microdevices contains an inlet reservoir connected to three sampling channels. Neurons are loaded into the inlet, and the surrounding chemical environment is precisely controlled. The analytes are collected onto a derivatized surface as the media in the reservoir flow through the channel. After that, the surface is interrogated with offline MALDI-MS imaging. This device allows the temporal analysis of the stimulation event, by sequentially sampling the media in different channels. In another device, one single neuron is loaded inside the microchannel, and the releasate is collected in the downstream, enabling single cell analysis. Microfluidics even allows subcellular regions of a neuron to be separately manipulated. In the compartmentalized device, three parallel large channels are connected by small interconnects, and under appropriate conditions, the neurites from cells loaded into the main channel can grow through the interconnects and enter into the adjacent channels. The fluidic environment in each channel can be individually controlled.

This dissertation also presents a unique method to quantify peptides based on the adsorption length in a microchannel. The device used here contains a cell chamber and a long serpentine channel. As the ability of a surface to adsorb an analyte is fixed per area, a larger amount of analyte covers a longer section of the channel. Experiments with standards confirmed the expected linear relationship of the sample amount and the adsorption length. By applying this approach to a small number of *Aplysia* bag cell neurons, the determined amounts of peptides released from a single neuron agreed with other methods. Our quantitation method provides a simple, label-free, and robust way for quantitation of mass-limited samples within microfluidic devices.

To my parents and family

ACKNOWLEDGEMENTS

I would like to take the opportunity here to express my deepest gratitude to everyone who has been supporting my Ph.D. studies at the University of Illinois, Urbana-Champaign. First of all, I would thank my supervisor, Prof. Jonathan V. Sweedler, for his always support and guidance during my research. He is very knowledgeable and knows how to encourage students when they encounter difficulties. I appreciate all the insightful suggestions he gave to me to make my dissertation research so smooth. He is a good teacher. I learned a lot from him about how to address research topics in a systematic and scientific way. Moreover, I want to thank him for giving me the flexibility to try different approaches during my Ph.D. research.

I enjoy every moment I have spent at the Sweedler group. The group members here are always willing to offer help when needed. I want to specially thank Dr. Chang Young Lee for his technical assistance to my research projects. He is very intelligent and knows a lot about engineering. I know whenever I need help, I can get it from him. It has been my great pleasure to work with him for the past two years. I am also thankful to Dr. Kyubong 'Q" Jo and Dr. Michael L. Heien, our previous group members, for introducing me into this research subject and training me on how to make microfluidic devices and to use the mass spectrometer when I first started the research. The members of the microfluidics subgroup also include Callie Croushore, Sam-ang Supharoek, and Amy Maduram, who are extremely helpful and willing to share their expertise, during cooperation as well as the monthly subgroup meeting. They are not only my coworkers, but also my personal friends. Besides, I am grateful to Dr. Stanislav S. Rubakhin and Dr.

Elena Romanova for their helpful discussions on cell manipulation, and Stephanie Baker for editing my manuscripts. Of course, I also acknowledge all the Sweedler group members, for their kindness and support throughout my Ph.D. studies.

My research work involved cooperation with the Gillette and Nuzzo groups at UIUC. I want to thank Dr. Larry J. Millet and Anika Jain from the Gillette group for sharing their expertise in PDMS extraction and cell handling, and Dr. Matthew E. Stewart and Audrey Bowen from the Nuzzo group for assistance in device fabrication. I am very thankful to Kathleen Motsegood, who manages the clean room at the Beckman Institute, for all the training and support I received from her.

I would also want to express my appreciation to Prof. Ryan C. Bailey, Prof. Martha U. Gillette, and Prof. Ralph G. Nuzzo for serving on my dissertation committee and for offering insightful and helpful advice on my literature seminar, preliminary exam, and original research proposal.

Last but not the least, I would give my special and sincere gratitude to my parents and my wife. I am the only child of my parents, and I understand they have dedicated all themselves to my personal growth. From them, I have learned how to face challenges, to appreciate the life we have, and to be optimistic about the future. Speaking with them on the phone every Friday night is the happiest time of my life in the US.

TABLE OF CONTENTS

LIST OF TABLES

LIST OF FIGURES

CHAPTER 1

INTRODUCTION AND DISSERTATION OVERVIEW

1.1 Background

In the nervous system, a large number of neurons form a complex highly-branched network. For example, the human brain contains about 10^{12} neurons with the estimated number of 10^{15} connections.[1] Neuronal communication often relies on chemical signals. Knowledge of a complement of these signaling molecules provides novel insights into the key effectors in neuronal repair and restoration of function, and provides clues to the possible treatments of neurodegenerative diseases, which are of rising concern with the aging of our population. In the Sweedler group at the University of Illinois, Urbana-Champaign, we are interested in understanding the detailed chemical information contained in neuron-neuron interactions by using a broad array of analytical techniques and different model organisms.

The specific category of signaling molecules I have been studying is neuropeptides. In a neuronal network, peptides can function as neurotransmitters (act on neurons in the immediate vicinity), neuromodulators (influence the response of a neuron to an input), neurohormone (function at a distance from the sites of release), or trophic factors (stimulate neuronal growth).[2] Investigation of peptide release presents challenges due to their small amounts and structural diversity. The overarching goal of my dissertation research is to develop suitable microanalytical platforms to define and

sample extracellular environments surrounding neurons, down to subcellular regions, for determination of identities, quantities, and dynamics of neuropeptide release. The primary technology utilized in this research is microfluidics, since microfluidic technology is well suited for manipulation of small-volume samples and control of local chemical environment with high spatial resolution. For detection of neuropeptides, mass spectrometry is used due to its rich information content and high sensitivity. We have selected *Aplysia californica* as the model organism to validate our microfluidic systems because of its well-characterized nervous system and biochemical properties. In particular, bag cell neurons from the *Aplysia* abdominal ganglion can be stimulated with an elevated potassium concentration, leading to depolarization of the cell membrane and release of several known neuropeptides.[3, 4]

1.2 Introduction to Microfluidics

Since microfluidics was first introduced[5], it has been used throughout analytical chemistry and biological sciences.[6] Microfluidics, by broad definition, is a technology that utilizes fluids contained in the micron scale. Because of the small sizes, microfluidic technology offers advantages such as control of local microenvironment, manipulation of small-volume samples, minimal reagent consumption, portability, and integration of multiple components in a single device, enabling "lab on a chip".[6, 7] The advantages of microfluidics lies on the distinct fluidic characteristics associated with the small dimension of the microchannel. A good understanding of fundamentals of fluid mechanics in the microfluidic system helps in design of microfluidic chips tailored to specific applications. Here I present some of the most important principles and equations

for microfluidics pertinent to this dissertation. For detailed description of fluid mechanics, please refer to Ref. 8.

The most prominent phenomenon of fluids in the microchannel is the laminar flow. The behavior of mass transfer in a flow is determined by the Reynolds number, which describes the ratio of inertial forces to viscous forces, is defined as[8]:

$$\mathrm{Re} = \frac{dv\rho}{\mu} \tag{1.1}$$

where Re is the Reynolds number, d is the hydraulic diameter of fluid, v is the velocity, ρ is the density, and μ is the viscosity. As the diameter of the microchannel is small, usually Re is well below the transition region. Therefore, under typical flow conditions, the flow in the microchannel is laminar, in which the fluids move in parallel layers without convective mixing between layers. The mixing perpendicular to the flow direction is by diffusion only. When considering mass transfer in a microfluidic device, the effects of diffusion must be taken into account. The average one-dimensional diffusion distance of a molecule, L, is[8]:

$$L = \sqrt{2Dt} \tag{1.2}$$

in which D is the diffusion coefficient and t is the time. In studies relying on the substrate surface to adsorb molecules flowing in the microchannel, the flow rate needs to be slow enough to allow molecules on top of the channel to diffuse to the bottom. In a pressure driven flow, the flow rate in volume, Q, is[8]:

$$Q = \frac{\Delta P}{R} \tag{1.3}$$

in which ΔP is the pressure difference applied across the channel and R is the channel resistance. R in a circular channel can be calculated as[8]:

$$R = \frac{8\mu L}{\pi r^4} \tag{1.4}$$

where μ is the viscosity, L is the channel length, and r is the radius of the channel. As the size of the channel decreases, its resistance increases dramatically. In addition to the fluidic properties mentioned above, surface area also becomes an important factor as the surface area to volume ratio increases with shrinking dimension. Therefore, in the microchannel, the adsorption/absorption of analytes onto the channel wall and the capillary force are usually significant.[8]

Microfluidic devices can be fabricated with a broad array of materials, such as hard materials like silicon and glass. Polymer-based devices have become increasingly popular to biological applications. In particular, polydimethylsiloxane (PDMS), a silicone elastomer, is frequently used because of its optical transparency, flexibility, and gas permeability that allows respiration of cells in contact with PDMS.[9] Moreover, the surface properties of PDMS, such as the hydrophobicity and the capability of adhesion of biomolecules and cells, can be tailored to the requirements of specific applications by treatment with different protocols.[10] Fabrication of PDMS devices is a simple and inexpensive process.[11] Typically, PDMS devices are made by molding on a master with the photoresist pattern on it. The photoresist used with PDMS is usually a negative epoxy-based one, SU-8, due to its rigidity after polymerization. The master is fabricated with photolithography, in which the SU-8 layer spin-coated on a silicon wafer is exposed to UV light (*e.g.* mercury lamp) through a photomask. A large number of PDMS devices can be made from a single master, lowering the cost of fabrication. Due to the advantages of PDMS mentioned above, the microfluidic devices in this dissertation were made of PDMS.

Because of the advantages of this technology, microfluidics has revolutionized the analysis of small amounts of samples and has been adapted for characterizing the contents of single cells[12, 13] and single molecules[14-16]. Particularly, microfluidic systems have already been broadly used in the field of neuroscience, the applications including separation and sensing of neurotransmitters[17], guidance of neuronal growth[18], isolation of axons and somata for manipulation of subcellular regions[19, 20], and studies of neuron-neuron[21] and neuron-glia cells interactions[22]. A neuron culture platform made of extracted PDMS has also been developed for culturing neurons at low densities[23].

1.3 Matrix-Assisted Laser Desorption/Ionization Time of Flight Mass Spectrometry (MALDI-TOF MS) and MALDI Imaging

Mass spectrometry (MS), by definition, is a technique that measures the mass-to-charge ratio (*m/z*) of charged particles. As a detection method, it can provide high information content, including the molecular weight and the chemical structure of analytes. A typical MS instrument mainly consists of an ionization source, a mass analyzer, and a detector.[24] In the ionization source, molecules of interest are vaporized and ionized, which are then introduced into the mass analyzer that separates different ions according to *m/z*. Usually the detector is an electron multiplier that converts the event of ion incidence into a cascade of electrons. A computer records these signals and generates a mass spectrum of peak intensity versus *m/z*. The whole system is maintained in a high vacuum (10^{-6} to 10^{-8} torr) to allow the free movement of the ions in the instrument without collision with other particles.[25] There are various ionization methods and mass analyzers available for specific applications. Nowadays MS has become the technology

of choice for proteomics and peptidomics studies, particularly since the advent of soft ionization methods including matrix-assisted laser desorption/ionization (MALDI)[26] and electrospray ionization (ESI)[27, 28].

The specific instrument used in this dissertation is the combination of MALDI and a time of flight (TOF) analyzer. With MALDI, the sample is co-crystalized with and embedded into a large excessive amount of a UV-absorbing material, named as matrix, on a steel or gold target plate. The matrix is usually a small organic acid, such as 2,5-dihydroxybenzoic acid (DHB), α-cyano-4-hydroxycinnamic acid (alpha-cyano), and 3,5-dimethoxy-4-hydroxycinnamic acid (sinapinic acid). A laser, typically a pulsed nitrogen laser beam (wavelength: 337 nm), is used to illuminate the crystals on the plate, desorbing and ionizing the matrix molecules from the surface. The charged matrix transfers the energy and protons to the analyte molecules so that the analytes also become charged in the gas phase. Because the matrix material absorbs the majority of laser energy, MALDI provides a soft ionization method for studying fragile biopolymers, such as peptides and proteins.[25]

The pulsed nature of generated ions in MALDI makes it well compatible to the TOF mass analyzer which is in a form of a long tube. In TOF, ions are accelerated with a high potential (25 kV in this research) into the drift tube. Because of the same accelerating potential, ions with the same charge possess the same kinetic energy[25]:

$$KE = \frac{1}{2}mv^2 = zU \tag{1.5}$$

where KE, m, v, and z represent the kinetic energy, mass, velocity, charge of the ions respectively, and U is the accelerating potential. In a tube of length L, the time of flight of an ion in the tube, t, is related to its mass-to-charge ratio (*m/z*) by[25]:

$$\frac{m}{z} = \frac{2Ut^2}{L^2} \tag{1.6}$$

Therefore, the ions with larger *m/z* travel slower in the tube and need more time to reach the detector. The computer can record the time and convert it into *m/z* according to the equation (1.6).

In reality, the ions formed in the MALDI source have varied initial kinetic energy. To compensate the spread of initial energy, an extraction delay (80 ns in this study) before ion acceleration is applied. In this way, ions with higher initial kinetic energy moves deeper into the voltage field and thus experience a slightly lower accelerating voltage.[29] To further reduce the spread and increase the mass resolution, an ion mirror, named as reflectron (a voltage of 26.5 kV in this study), is installed at the end of the TOF tube. With the reflectron, charged particles are reflected back to the detector. The ions of the same *m/z* but with higher velocity due to the initial kinetic energy penetrate the electrical field of the reflectron further and thus spend more time on reflection, giving the ions with lower velocity the opportunity to catch up.[24] The whole process of MALDI-TOF MS is depicted in Fig. 1.1.

MALDI mainly produces singly-charged ions, therefore generating mass spectra relatively simple to interpret.[25] It has a low detection limit, able to detect femtomole peptides routinely.[24] In addition, MALDI-TOF can analyze a large mass range up to 300,000 Da.[30] Compared to ESI, MALDI has a higher tolerance towards salts and contaminants and has a lower degree of ion suppression. Because of these advantages, MALDI has been widely used for proteomics and peptidomics studies, including investigations of nervous tissues from different animals[31-34]. On the other hand, MALDI

has its limitations, including that the detection of analytes with mass less than 1000 Da is interfered with matrix peaks and that MALDI is not quantitative[35, 36].

One of the most important advancements of MALDI-MS is the development of MALDI-based MS imaging.[37, 38] MALDI imaging adds the spatial information to characterization by visualizing the distribution of biomolecules, such as peptides, proteins, and metabolites, within a thin slice of sample. To obtain a MALDI image, typically a tissue slice is fixed onto a microscope slide, and a layer of matrix is applied onto the slice. The slide with the sample is then introduced into the MALDI mass spectrometer that can scan the surface of the slide and collect the mass spectrum at each spot. Imaging processing software can then create MS images of analyte distribution from the huge dataset and register the MS images to the optical microscopic images.[37] MALDI imaging does not require prior knowledge of the location and identity of analytes, allowing areas containing the specific or unexpected molecules to be discovered. With MALDI imaging, two-dimensional[39] and even three dimensional[40] maps of analytes can be constructed, providing new insights into biological processes in a tissue sample[41].

1.4 Interfacing Microfluidic Devices with MS

As shown above, microfluidic devices are well suited for sampling and manipulating mass-limited samples; MS can provide detailed information of the analytes of interest. To fully take advantage of these two techniques, it is important to have an efficient interface between the microchip and the mass spectrometer. ESI and MALDI are the two most widely used ionization methods for analysis of biomolecules such as

proteins and peptides. Here we present a short review on the existing technologies that have been developed to couple microfluidics to each of the ionization methods.

1.4.1 ESI Interfaces

In contrast to MALDI, ESI is primarily used for liquid samples. In ESI, the sample is introduced to a capillary needle maintained at a high voltage, where a Taylor cone forms and an aerosol of charged droplets is emitted. With the evaporation of solvents assisted by blowing nitrogen and heat, the charged droplets finally turn into gas-phase ions in a process called Coulombic explosion.[30, 42] The ions formed in ESI usually carry multiple charges. The nature of the ionization process makes ESI-MS readily capable of being coupled with microfluidic devices in an online mode. The interfaces can be fabricated in various ways, in which the liquid is directly sprayed from the chip, a capillary is attached to the end of the channel, or the spray emitter is fabricated as a part of the chip.[43, 44]

In the direct spraying approach, the liquid is sprayed from the open end of a microchannel at a high voltage.[45, 46] The flow can be driven either by pressure[45] or an electrical field[46]. The early devices were made of glass, whose hydrophilic property causes the spreading of liquid around the open outlet on the planar edge of the chip, leading to a large dead volume of the spray and reduced separation resolution.[47] To reduce the liquid spreading, the channel outlet was coated with hydrophobic materials such as alkylsilanes.[45] Alternatively, the devices can be made of hydrophobic polymers, such as PDMS[48] or polyethylenerephthalate (PET)[47]. Porous monolith materials[49] and hydrophobic membranes[50] can also be integrated to the exit, resulting in a more stable

spray. However, because of the planar edge, it is difficult to always form the Taylor cone exactly at the position of the channel outlet.[47] Thus the direct spraying method provides a simple interface between the microfluidic chip and the mass spectrometer, with the cost of performance.

A more sophisticated interface is made by attaching an electrospray capillary to the channel. In an early example, a fused silica capillary was glued to the end of a microchannel and the flow was driven by electroosmotic pumping.[51] With the protruding capillary, the place where the spraying occurred was well defined and the voltage was relatively easily applied at the capillary. A limit of detection in the low fmol/μL range for peptide standards was achieved. However, the alignment was a difficult task and a relatively large dead volume existed in the chip-to-capillary interface. The glues used in the interface could be dissolved in some organic solvents and thus interfere with the sample signals. Alternatively, a liquid junction was integrated into the chip to couple the microfluidic device with removable ESI capillary tips.[52-54] This configuration did not require glues and allowed easy substitution of either the microdevice or the capillary if needed. A low dead volume connection between the chip and the capillary was achieved by a drilling process into the edge of the device with 200-μm tungsten carbide bits.[55] The standard pointed drill bits created a conical shaped-geometry at the end, forming a dead volume of 0.7 nL at the junction when a capillary was inserted into the hole. The dead volume was eliminated effectively by drilling the chip with a flat-tipped bit. However effective, the drilling process is labor-intensive and requires manual implementation, not amenable to automation required by commercial production.

On-chip integrated emitters can essentially overcome the challenge of dead volume associated with coupling the channel with the external emitter, so that the separation efficiency will not be compromised. Fabrication of integrated spray tips on the microchips has been realized in hard materials like silicon[56, 57] and glass[58, 59], as well as various polymer materials, such as PDMS[60, 61], poly(methyl methacrylate) (PMMA)[62], and polycarbonate (PC)[63]. With the excellent fabrication properties of silicon, sharp emitter tips can be made both in the plane[56, 57] and out of the plane[64, 65] of silicon wafers, by using wet etching or deep reactive ion etching. The emitter array was also fabricated in a single silicon chip, enabling high-throughput analysis.[56, 65] For example, the ESI chip, which contains an array of out-of-plane electrospray nozzles and can be coupled to an automated sample delivery system, is already commercialized (by Advion).[64, 66] This chip achieved a high nozzle-to-nozzle reproducibility. But silicon chips can not always be applicable, especially when a high voltage is needed on the chip, such as in electrophoretic separation. In these situations, the use of glass or polymer chips is necessary instead of silicon. For glass emitters, the tips can be made by milling at the end of a microchannel[58], or by patterning a microchannel in such a way that the outlet is directed to a rectangular corner of the chip[59]. However, the processing of glass is relatively slow and tedious. Compared to glass, fabrication with polymers is quicker and simpler. The emitters on a PDMS chip are typically made by cast molding, which are able to produce a stable spray.[61, 67] But PDMS is not compatible to many organic solvents, limiting its use for broader applications. Sharp emitter tips can also be fabricated with micromachining on other materials, for example, out-of-plane emitters were made by micromilling of PMMA[62] and laser ablation of PC[63]. With the PMMA emitters, detection

limits of 10^{-8} mol/L were achieved for standard peptides.[62] In-plane emitter tips can also be made by micromachining.[68, 69] The commercially available Agilent high performance liquid chromatography (HPLC)-Chip contains polyimide separation channels, and an in-plane electrospray tip made by laser ablation of the polyimide.[68] The sensitivity of the HPLC-Chip was archived to be five times that of the conventional nano LC-MS. An alternative way to make a sharp tip at the channel outlet is to manually cut the polymer.[60, 70] Despite of the poor reproducibility, this manual cutting method is very simple to perform and has been used for fabricating emitter tips and tip arrays on PDMS[60], PMMA[70], polyimide[71], and so on. The most accurate and reproducible method for fabricating sharp emitter structures has been achieved with photolithography on devices made of the photoresist SU-8[72, 73] or parylene[74]. For the SU-8 emitters, a relative standard deviation of 14% was achieved between different nozzles.[73] The procedure of photolithography also permits the mass production of accurately-defined emitter tips.

1.4.2 MALDI Interfaces

As another commonly used ionization method, MALDI analyzes samples crystallized on a target plate. Therefore, the most straightforward way for interfacing microfluidic chips with MALDI is through offline coupling. The offline interfaces can be divided into two categories: deposition of eluents from the microfluidic device onto a standard target plate, and direct use of the microfluidic substrate as the MALDI target. Meanwhile, online coupling is also possible with a suitable design of the interface that enables the continuous delivery of samples into the mass spectrometer for real-time detection.[75, 76]

1.4.2.1 Offline Interface to MALDI by Deposition

The simplest approach to deposit samples from the microchannel is direct spotting.[77, 78] In one example, a PMMA microfluidic chip that performed enzymatic digestion of proteins was mounted in a MALDI spotter. A fused silica capillary was attached to the channel outlet on the chip, where the sample was mixed with the matrix introduced from a coaxial tube. The mixture was then directly spotted onto a target plate. A high sequence coverage of protein standards was achieved by this system.[78] However, with mechanical spotting alone, it is difficult to precisely control the volume of liquid to be spotted and the action of spotting may disturb the flow inside the microchannel. To overcome these challenges, samples are deposited onto the MALDI target by a piezoelectric dispenser instead.[79, 80] For example, a microdispenser was used to quickly deposit droplets of protein digestion products from a microfluidic device to a high-density array of nanovials on a silicon target plate.[79] With this method, the volume of the droplet to be spotted can be well defined.

Alternatively, electrospray can be used to deposit the sample from a chip, resulting in a more uniform sample film on the surface.[50, 81] In one electrospray deposition system, a polytetrafluoroethylene (PTFE) membrane was bonded onto the outlet of a PC microfluidic chip to form a hydrophobic electrospray tip. The gap between the tip and the target plate was maintained at 500 μm to 1mm. A syringe pump was used to generate the flow in the channel and a high voltage was applied to the T-junction to introduce electrospray. A detection limit of 3.5 fmol was achieved for a standard peptide, angiotensin II, with this system. An array of three electrospray tips with 150 μm apart

from each other was successfully used for parallel deposition of different analytes without cross-contamination of samples from adjacent spots.[81]

1.4.2.2 Offline Interface to MALDI by Using the Microfluidic Chip as the Target

The substrate used in a microfluidic device is typically flat, allowing it to be directly used as a MALDI target. Compared to the offline deposition described in the previous section, this approach eliminates the deposition step and the need of spotting instruments.

The open channel configuration is one of the ways to make the chip accessible by MALDI characterization.[82, 83] In a simple design of rapid open-access channel electrophoresis (ROACHE)[82], electrophoretic separation was performed in an open microchannel for a certain time before the sample was eluted out of the channel. A matrix was added into the sample before separation. After the solvent in the channel was evaporated, the sample became cocrystallized with the matrix. The chip was then loaded into the MALDI spectrometer to generate a spatial map of separated analytes in the channel area. MALDI has also been interfaced to the on-chip capillary isoelectric focusing (CIEF) in a similar manner.[83] In CIEF, molecules are separated according to their specific isoelectric points. After the separation was completed, a matrix solution was applied onto the chip surface with electrospray for subsequent MALDI imaging. To prevent the solvent evaporation during separation, a pseudo-closed microchannel design was used, which consisted of a base chip and a cover chip, both made of PMMA.[84] The channel features were fabricated in the base chip. During separation, the cover chip was placed on top of the base to form sealed channels. After the completion of separation, the cover was removed to allow the access to the channel area by MALDI interrogation.

Similarly, a resin tape was also used to temporarily cover the separation channels in a microfluidic device.[85] Gel electrophoresis performed in a microfluidic device has also been demonstrated to be readily interfaced to MALDI.[86] The gel electrophoresis device was composed of a PMMA base and a removable PDMS cover. Cross-linked gel was formed inside the microchannel with polymerization after assembly of the device. Following sample migration, the PDMS cover was peeled off and either the base or the cover was characterized with MALDI. In this case, the gel itself was utilized as the matrix and infrared laser was used to enable deeper penetration into the gel.

Besides electrophoresis, the microfluidic devices performing other sample preparation processes can also be directly interfaced to MALDI. For example, a PDMS device was developed to conduct multiple enzyme assays simultaneously on the peptides deposited on the substrate; the substrate was then used as a target for MALDI characterization.[87] More specifically, in this device the substrate of gold was coated with a self-assembled monolayer of alkanethiolate with an end maleimide group designed to adhere peptide molecules. A piece of PDMS with parallel channels was placed on top of the substrate and the different cysteine-terminated peptide solutions were flown through each of the channels, during which the peptides were immobilized onto the surface. The PDMS piece was removed from the substrate, and then was rotated in 90 ° and reapplied. The channels were then infused with various enzyme solutions; in this configuration, each enzyme was allowed to interact with the whole set of the deposited peptides. After that, the PDMS was removed again and the interaction regions of enzymes and peptides were analyzed with MALDI-MS. This system offers the capability for high-throughput analysis of enzyme reactions.

A compact disk (CD) microfluidic device that allows the direct application of MALDI-MS within the chip has been commercialized (from Gyro AB).[88] Multiple microstructures can be fabricated onto the disk, for instance, microcolumns packed with C18 beads are made in the radial direction. After the CD starts to rotate, the centrifugal force pushes the sample in each structure through the column; the sample is retained by the C18 beads but the salts and impurities are drawn into the waste. A matrix solution is then used to elute the sample from the column and the sample is collected onto a gold-coated region, which is to be interrogated with MALDI. The CD chips have been successfully used for parallel analysis of in-gel digestion products of proteins and for enrichment of phosphopeptides.[89, 90]

1.4.2.3 Online Interface to MALDI

With special designs, the microfluidic devices can also be interfaced to MADLI in an online mode. One innovative approach for online interface utilizes the vacuum in the ionization source of the mass spectrometer to continuously pull the solution through the channel.[91, 92] In one microfluidic device, a glass cover contained two sample loading channels that converged into one reaction channel. The glass cover was then bonded onto a silicon wafer to seal the channels, and the entire device was mounted onto a modified MALDI target. The two inlet reservoirs were filled with reactant solutions and then sealed, meanwhile the outlet remained open. After the target was introduced into the vacuum of MALDI, the pressure difference between the inlet and the outlet drew the two reactant solutions into the reaction channel where they were mixed and reacted with each other. The products with any unreacted reactants were dried at the outlet reservoir, which

could be accessed by the MALDI laser. In this way, a chemical reaction can be monitored continuously.[91]

Besides the vacuum approach, online coupling of microfluidics with MALDI has also been realized with mechanical designs that can continuously deliver the analytes at the atmosphere into the vacuum chamber without breaking the vacuum.[93-96] An interesting example is to use a rotating ball. In this example, a PMMA chip was micromilled to have a V shape at the channel exit. The V tip was in contact with a rotating ball; one half of the ball was exposed to the atmosphere while the other was in the vacuum of the mass spectrometer. The eluent from the channel was deposited onto the ball while the matrix was supplied by another capillary. As the ball rotated, the eluent/matrix mixture was then introduced into the vacuum for MALDI analysis. This cycle of deposition and ionization was repeated so that a continuous delivery of the sample into MALDI was achieved.[95]

In the microfluidic systems presented in this dissertation, we used the offline interface by collecting the neuropeptides onto a derivatized substrate, which was then directly used as a target plate for MALDI imaging analysis. Such an interface, as mentioned before, is simple to operate and does not require any special instrument. The imaging capability of MALDI allows the analytes, expected or unexpected, to be identified on the surface without the need to know their exact locations in advance.

1.5 Dissertation Overview

This dissertation demonstrates several PDMS microfluidic chips that can control and sample the microenvironments of the small areas around neurons. With a suitable

sample collection method, neuropeptide release from neurons of the model system, *Aplysia*, can be investigated with a temporal and spatial resolution, down to single cell sampling.

In Chapter 2[97], a sampling method by functionalizing a silicon or glass surface with a self-assembled monolayer of octadecyl alkyl chains (C18) is demonstrated. Comparing to other surfaces modified with different reagents, C18 was shown to be the optimal and the most universal way to collect peptides. A PDMS microfluidic device containing an octadecyltrichlorosilane (OTS)-derivatized silicon substrate was developed for temporal analysis of peptide release from a small number of neurons. The design consists of a reservoir for placing cells, and three branching channels that can sample the environment in the reservoir before, during, and after neuronal stimulation. Multiple released peptides were detected only in the middle channel and they were separated as in thin layer chromatography. This chapter also describes a modified microfluidic device that has a single neuron loaded into the channel and a functionalized glass substrate to facilitate microscope monitoring. The results indicate that the microfluidics is well suited for single cell measurements. In addition, the surface coverage of various peptides was studied with scintillation measurements of radiolabeled peptides adsorbed onto substrates as well as by flowing increasing amounts of standard peptides through a microfluidic device with a serpentine channel. The results from the serpentine channel show the potential to use adsorption length to quantify the amount of a peptide, which is the focus of the next chapter.

Chapter 3[98] describes a novel method to quantify peptide release from a small number of neurons by measuring the adsorption length of each peptide. The PDMS

microfluidic device used here is an enhancement to the device with a serpentine channel shown in Chapter 2. Flow rate in the new device can be precisely controlled with a syringe pump. The silicon substrate is patterned with OTS and oligo(ethylene glycol) that significantly reduces the loss of peptides to the reservoir area. The PDMS surface is also modified with oligo(ethylene glycol) to reduce the absorption of analytes into PDMS, the effectiveness of which was demonstrated by scintillation measurements of peptide recovery from incubation with PDMS treated with different protocols. A simplified mathematical model supports the concept of quantitation based on adsorption length and separation of multiple peptides according to the adsorption capability. The calibration experiments on a single peptide, acidic peptide, demonstrate the expected linear relationship between length and amount. The experiments on multiple peptides, acidic peptide and α-bag cell peptide, show that the two peptides are separated and that the length-to-amount relationship for individual peptide remains to be linear. The variance of length measurements between devices is as low as 3%. By applying this quantitation approach on *Aplysia* bag cell neurons stimulated with elevated potassium, the measured peptide amounts are comparable to the measures using other methods. Our method based on adsorption length provides a simple, label-free, and robust way for quantifying small amounts of samples within microfluidic devices.

To add a spatial resolution to peptide release studies, Chapter 4 demonstrates a compartmentalized microfluidic device that can separate the cell body (soma) of a neuron from its processes. The device contains one main channel and two secondary channels; they were connected with a number of small interconnects. Glass coverslips were used as the substrates to permit continuous monitoring of cells inside the microchannel with

optical microscopy. Under appropriate conditions, the process growth from neurons loaded into the main channel can potentially penetrate the interconnects into the adjacent secondary channels. The high resistance of interconnects, combined with hydrostatic pressure manipulation, allows the flow in each channel to be separately controlled. Using a pipette to pull the cell solution through the channel was demonstrated to be the most effective way for loading cells into the microchannel. Neuron viability in the microchannel was increased by introducing a perfusion flow in the system and by serial solvent extraction of PDMS to remove toxic materials in the cured polymer. The glass surface is patterned with repeated lines of poly-L-lysine (PLL) and bovine serum albumin (BSA) to guide the direction of process growth.

Chapter 5 concludes the previous chapters and describes the future directions of this research project. One area for future endeavor is to continue working on the compartmentalized microfluidic device by applying the PLL/BSA patterning to cell culturing in the device to guide the neurites through the interconnects and by combining the OTS collection method with this device to sample local peptide release from subcellular regions of individual neurons. Microfluidic devices that can compare the components and quantities of released peptides under different physiological conditions are to be developed. Moreover, to gain insights into important chemical signals during neuronal network formation, the development of microfluidic systems that allow neuronal wiring within the device and collection of local microenvironment during this event is an important area to be explored in the future.

1.6 Figures

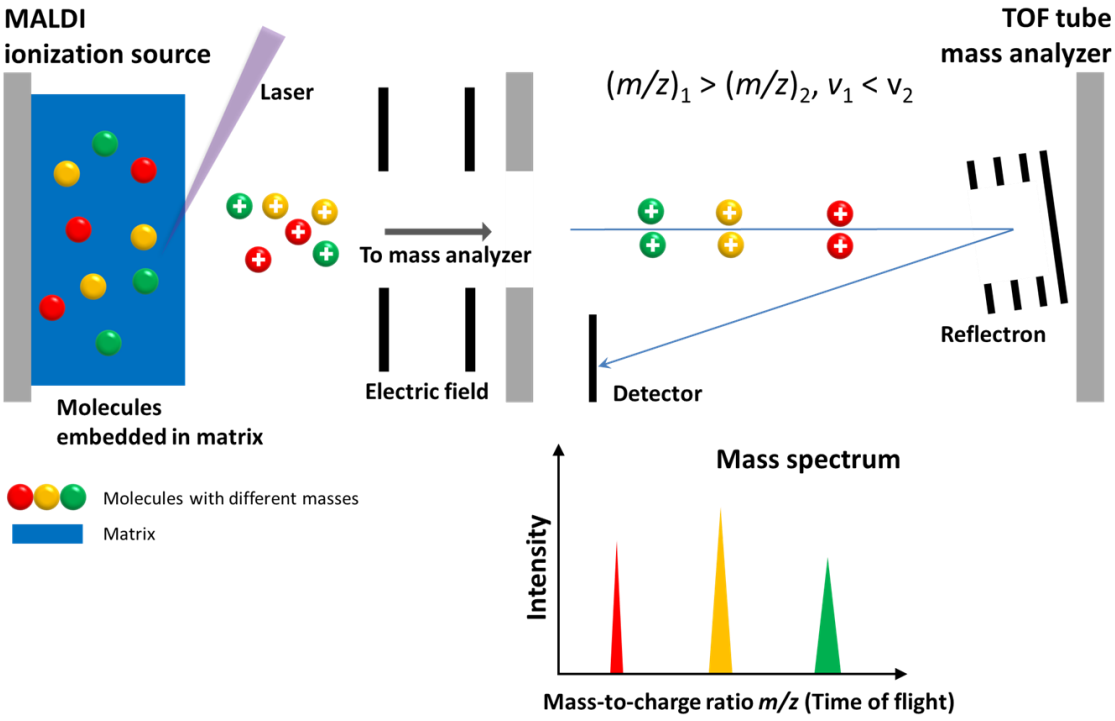

Figure 1.1 Schematics of MALDI-TOF MS. In the MALDI ionization source, the analyte molecules are embedded into a UV absorbing material, matrix. A laser beam desorbs and ionizes the matrix and analyte molecules, and the charged particles are pushed into a TOF mass analyzer by an electrical field. The mass analyzer is a long drift tube, in which ions with higher *m/z* travel slower. An ion mirror, reflectron, is installed at the end of the tube to reflect the ions back. Because of the difference in flight velocity, ions with increasing *m/z* reach the detector sequentially. A computer records the signals and converts the time of flight into *m/z*, generating a mass spectrum we can read. MALDI: matrix-assisted laser desorption/ionization, TOF: time of flight, *m/z*: mass-to-charge ratio, and v: velocity.

1.7 References

1. S. S. Millard and S. L. Zipursky, *Curr. Opin. Neurobiol.*, 2008, **18**, 84-89.
2. R. H. Scheller, R. R. Kaldany, T. Kreiner, A. C. Mahon, Nambu, M. Schaefer and R. Taussig, *Science*, 1984, **225**, 1300-1308.
3. L. J. Jung and R. H. Scheller, *Science*, 1991, **251**, 1330-1335.
4. P. Conn and L. Kaczmarek, *Mol. Neurobiol.*, 1989, **3**, 237-273.
5. A. Manz, D. J. Harrison, E. M. J. Verpoorte, J. C. Fettinger, A. Paulus, H. Lüdi and H. M. Widmer, *J. Chromatogr., A*, 1992, **593**, 253-258.
6. G. M. Whitesides, *Nature*, 2006, **442**, 368-373.
7. M. A. Burns, B. N. Johnson, S. N. Brahmasandra, K. Handique, J. R. Webster, M. Krishnan, T. S. Sammarco, P. M. Man, D. Jones, D. Heldsinger, C. H. Mastrangelo and D. T. Burke, *Science*, 1998, **282**, 484-487.
8. S. E. Ong, S. Zhang, H. J. Du and Y. Q. Fu, *Frontiers Biosci.*, 2008, **13**, 2757-2773.
9. K. J. Regehr, M. Domenech, J. T. Koepsel, K. C. Carver, S. J. Ellison-Zelski, W. L. Murphy, L. A. Schuler, E. T. Alarid and D. J. Beebe, *Lab Chip*, 2009, **9**, 2132-2139.
10. J. Zhou, A. V. Ellis and N. H. Voelcker, *Electrophoresis*, 2010, **31**, 2-16.
11. D. C. Duffy, J. C. McDonald, O. J. A. Schueller and G. M. Whitesides, *Anal. Chem.*, 1998, **70**, 4974-4984.
12. L. Cai, N. Friedman and X. S. Xie, *Nature*, 2006, **440**, 358-362.
13. B. Huang, H. Wu, D. Bhaya, A. Grossman, S. Granier, B. K. Kobilka and R. N. Zare, *Science*, 2007, **315**, 81-84.
14. T. T. Perkins, D. E. Smith and S. Chu, *Science*, 1997, **276**, 2016-2021.
15. S. Zhou, A. Kile, M. Bechner, M. Place, E. Kvikstad, W. Deng, J. Wei, J. Severin, R. Runnheim, C. Churas, D. Forrest, E. T. Dimalanta, C. Lamers, V. Burland, F. R. Blattner and D. C. Schwartz, *J. Bacteriol.*, 2004, **186**, 7773-7782.
16. J. O. Tegenfeldt, C. Prinz, H. Cao, S. Chou, W. W. Reisner, R. Riehn, Y. M. Wang, E. C. Cox, J. C. Sturm, P. Silberzan and R. H. Austin, *Proc. Natl. Acad. Sci. U. S. A.*, 2004, **101**, 10979-10983.
17. N. A. Cellar and R. T. Kennedy, *Lab Chip*, 2006, **6**, 1205-1212.

18. L. J. Millet, M. E. Stewart, R. G. Nuzzo and M. U. Gillette, *Lab Chip*, 2010, **10**, 1525-1535.
19. A. M. Taylor, M. Blurton-Jones, S. W. Rhee, D. H. Cribbs, C. W. Cotman and N. L. Jeon, *Nat. Methods*, 2005, **2**, 599-605.
20. S. Hosmane, I. H. Yang, A. Ruffin, N. Thakor and A. Venkatesan, *Lab Chip*, 2010, **10**, 741-747.
21. A. M. Taylor, D. C. Dieterich, H. T. Ito, S. A. Kim and E. M. Schuman, *Neuron*, 2010, **66**, 57-68.
22. D. Majumdar, Y. Gao, D. Li and D. J. Webb, *J. Neurosci. Methods.*, 2011, **196**, 38-44.
23. L. J. Millet, M. E. Stewart, J. V. Sweedler, R. G. Nuzzo and M. U. Gillette, *Lab Chip*, 2007, **7**, 987-994.
24. G. L. Glish and R. W. Vachet, *Nat. Rev. Drug Discov.*, 2003, **2**, 140-150.
25. E. J. Finehout and K. H. Lee, *Biochem. Mol. Biol. Educ.*, 2004, **32**, 93-100.
26. M. Yamashita and J. B. Fenn, *J. Phys. Chem.*, 1984, **88**, 4451-4459.
27. K. Tanaka, H. Waki, Y. Ido, S. Akita, Y. Yoshida, T. Yoshida and T. Matsuo, *Rapid Commun. Mass Spectrom.*, 1988, **2**, 151-153.
28. M. Karas and F. Hillenkamp, *Anal. Chem.*, 1988, **60**, 2299-2301.
29. M. L. Vestal, P. Juhasz and S. A. Martin, *Rapid Commun. Mass Spectrom.*, 1995, **9**, 1044-1050.
30. C. E. C. A. Hop and R. Bakhtiar, *Biospectroscopy*, 1997, **3**, 259-280.
31. R. Predel, S. Neupert, S. F. Garczynski, J. W. Crim, M. R. Brown, W. K. Russell, J. Kahnt, D. H. Russell and R. J. Nachman, *J. Proteome Res.*, 2010, **9**, 2006-2015.
32. S. S. Rubakhin and J. V. Sweedler, *Nat. Protoc.*, 2007, **2**, 1987-1997.
33. N. G. Hatcher, T. A. Richmond, S. S. Rubakhin and J. V. Sweedler, *Anal. Chem.*, 2005, **77**, 1580-1587.
34. L. Li, R. W. Garden and J. V. Sweedler, *Trends Biotechnol.*, 2000, **18**, 151-160.
35. E. Szájli, T. Fehér and K. F. Medzihradszky, *Mol. Cell. Proteomics*, 2008, **7**, 2410-2418.
36. R. Knochenmuss, *Anal. Chem.*, 2003, **75**, 2199-2207.

37. P. Chaurand, S. A. Schwartz and R. M. Caprioli, *Curr. Opin. Chem. Biol.*, 2002, **6**, 676-681.
38. S. S. Rubakhin, J. C. Jurchen, E. B. Monroe and J. V. Sweedler, *Drug Discovery Today*, 2005, **10**, 823-837.
39. T. A. Zimmerman, S. S. Rubakhin, E. V. Romanova, K. R. Tucker and J. V. Sweedler, *Anal. Chem.*, 2009, **81**, 9402-9409.
40. A. Crecelius, D. Cornett, R. Caprioli, B. Williams, B. Dawant and B. Bodenheimer, *J. Am. Soc. Mass Spectrom.*, 2005, **16**, 1093-1099.
41. J. Pierson, J. L. Norris, H.-R. Aerni, P. Svenningsson, R. M. Caprioli and P. E. Andren, *J. Proteome Res.*, 2004, **3**, 289-295.
42. N. B. Cech and C. G. Enke, *Mass Spectrom. Rev.*, 2001, **20**, 362-387.
43. J. Lee, S. A. Soper and K. K. Murray, *J. Mass. Spectrom.*, 2009, **44**, 579-593.
44. T. Sikanen, S. Franssila, T. J. Kauppila, R. Kostiainen, T. Kotiaho and R. A. Ketola, *Mass Spectrom Rev.*, 2010, **29**, 351-391.
45. Q. Xue, F. Foret, Y. M. Dunayevskiy, P. M. Zavracky, N. E. McGruer and B. L. Karger, *Anal. Chem.*, 1997, **69**, 426-430.
46. R. S. Ramsey and J. M. Ramsey, *Anal. Chem.*, 1997, **69**, 1174-1178.
47. T. C. Rohner, J. S. Rossier and H. H. Girault, *Anal. Chem.*, 2001, **73**, 5353-5357.
48. K. Huikko, P. Ostman, K. Grigoras, S. Tuomikoski, V. M. Tiainen, A. Soininen, K. Puolanne, A. Manz, S. Franssila, R. Kostiainen and T. Kotiaho, *Lab Chip*, 2003, **3**, 67-72.
49. M. F. Bedair and R. D. Oleschuk, *Anal. Chem.*, 2006, **78**, 1130-1138.
50. Y.-X. Wang, J. W. Cooper, C. S. Lee and D. L. DeVoe, *Lab Chip*, 2004, **4**, 363-367.
51. D. Figeys, Y. Ning and R. Aebersold, *Anal. Chem.*, 1997, **69**, 3153-3160.
52. B. Zhang, F. Foret and B. L. Karger, *Anal. Chem.*, 2000, **72**, 1015-1022.
53. T. Wachs and J. Henion, *Anal. Chem.*, 2001, **73**, 632-638.
54. B. Zhang, H. Liu, B. L. Karger and F. Foret, *Anal. Chem.*, 1999, **71**, 3258-3264.
55. N. H. Bings, C. Wang, C. D. Skinner, C. L. Colyer, P. Thibault and D. J. Harrison, *Anal. Chem.*, 1999, **71**, 3292-3296.
56. W. Kim, M. Guo, P. Yang and D. Wang, *Anal. Chem.*, 2007, **79**, 3703-3707.

57. T. Nissilä, L. Sainiemi, T. Sikanen, T. Kotiaho, S. Franssila, R. Kostiainen and R. A. Ketola, *Rapid Commun. Mass Spectrom.*, 2007, **21**, 3677-3682.
58. P. Hoffmann, U. Häusig, P. Schulze and D. Belder, *Angew. Chem., Int. Ed.*, 2007, **46**, 4913-4916.
59. J. S. Mellors, V. Gorbounov, R. S. Ramsey and J. M. Ramsey, *Anal. Chem.*, 2008, **80**, 6881-6887.
60. J. M. Iannacone, J. A. Jakubowski, P. W. Bohn and J. V. Sweedler, *Electrophoresis*, 2005, **26**, 4684-4690.
61. J.-S. Kim and D. R. Knapp, *J. Chromatogr., A*, 2001, **924**, 137-145.
62. M. Schilling, W. Nigge, A. Rudzinski, A. Neyer and R. Hergenroder, *Lab Chip*, 2004, **4**, 220-224.
63. K. Tang, Y. Lin, D. W. Matson, T. Kim and R. D. Smith, *Anal. Chem.*, 2001, **73**, 1658-1663.
64. G. A. Schultz, T. N. Corso, S. J. Prosser and S. Zhang, *Anal. Chem.*, 2000, **72**, 4058-4063.
65. W. Deng, J. F. Klemic, X. Li, M. A. Reed and A. Gomez, *J. Aerosol Sci.*, 2006, **37**, 696-714.
66. J.-M. Dethy, B. L. Ackermann, C. Delatour, J. D. Henion and G. A. Schultz, *Anal. Chem.*, 2003, **75**, 805-811.
67. M. Svedberg, M. Veszelei, J. Axelsson, M. Vangbo and F. Nikolajeff, *Lab Chip*, 2004, **4**, 322-327.
68. H. Yin, K. Killeen, R. Brennen, D. Sobek, M. Werlich and T. van de Goor, *Anal. Chem.*, 2004, **77**, 527-533.
69. M. Svedberg, A. Pettersson, S. Nilsson, J. Bergquist, L. Nyholm, F. Nikolajeff and K. Markides, *Anal. Chem.*, 2003, **75**, 3934-3940.
70. A. Muck and A. Svatoš, *Rapid Commun. Mass Spectrom.*, 2004, **18**, 1459-1464.
71. V. Gobry, J. van Oostrum, M. Martinelli, T. C. Rohner, F. Reymond, J. S. Rossier and H. H. Girault, *Proteomics*, 2002, **2**, 405-412.
72. S. Tuomikoski, T. Sikanen, R. A. Ketola, R. Kostiainen, T. Kotiaho and S. Franssila, *Electrophoresis*, 2005, **26**, 4691-4702.

73. T. Sikanen, S. Tuomikoski, R. A. Ketola, R. Kostiainen, S. Franssila and T. Kotiaho, *J. Mass. Spectrom.*, 2008, **43**, 726-735.
74. J. Kameoka, R. Orth, B. Ilic, D. Czaplewski, T. Wachs and H. G. Craighead, *Anal. Chem.*, 2002, **74**, 5897-5901.
75. D. L. DeVoe and C. S. Lee, *Electrophoresis*, 2006, **27**, 3559-3568.
76. J. Lee, S. A. Soper and K. K. Murray, *Anal. Chim. Acta*, 2009, **649**, 180-190.
77. S. Hsieh, K. Dreisewerd, R. C. van der Schors, C. R. Jiménez, J. Stahl-Zeng, F. Hillenkamp, J. W. Jorgenson, W. P. M. Geraerts and K. W. Li, *Anal. Chem.*, 1998, **70**, 1847-1852.
78. J. Lee, H. K. Musyimi, S. A. Soper and K. K. Murray, *J. Am. Soc. Mass Spectrom.*, 2008, **19**, 964-972.
79. S. Ekström, P. Önnerfjord, J. Nilsson, M. Bengtsson, T. Laurell and G. Marko-Varga, *Anal. Chem.*, 1999, **72**, 286-293.
80. L. Wallman, S. Ekström, G. Marko-Varga, T. Laurell and J. Nilsson, *Electrophoresis*, 2004, **25**, 3778-3787.
81. Y.-X. Wang, Y. Zhou, B. M. Balgley, J. W. Cooper, C. S. Lee and D. L. DeVoe, *Electrophoresis*, 2005, **26**, 3631-3640.
82. J. Liu, K. Tseng, B. Garcia, C. B. Lebrilla, E. Mukerjee, S. Collins and R. Smith, *Anal. Chem.*, 2001, **73**, 2147-2151.
83. X. Guo, M. B. Chan-Park, S. F. Yoon, J.-h. Chun, L. Hua and N. S. K. Sze, *Anal. Chem.*, 2006, **78**, 3249-3256.
84. M. L. S. Mok, L. Hua, J. B. C. Phua, M. K. T. Wee and N. S. K. Sze, *Analyst*, 2004, **129**, 109-110.
85. M. Fujita, W. Hattori, T. Sano, M. Baba, H. Someya, K. Miyazaki, K. c. Kamijo, K. Takahashi and H. Kawaura, *J. Chromatogr., A*, 2006, **1111**, 200-205.
86. Y. Xu, M. W. Little and K. K. Murray, *J. Am. Soc. Mass Spectrom.*, 2006, **17**, 469-474.
87. J. Su, M. R. Bringer, R. F. Ismagilov and M. Mrksich, *J. Am. Chem. Soc.*, 2005, **127**, 7280-7281.
88. M. Gustafsson, D. Hirschberg, C. Palmberg, H. Jörnvall and T. Bergman, *Anal. Chem.*, 2003, **76**, 345-350.

89. D. Hirschberg, S. Tryggvason, M. Gustafsson, T. Bergman, J. Swedenborg, U. Hedin and H. Jörnvall, *Protein J.*, 2004, **23**, 263-271.
90. D. Hirschberg, T. Jägerbrink, J. Samskog, M. Gustafsson, M. Ståhlberg, G. Alvelius, B. Husman, M. Carlquist, H. Jörnvall and T. Bergman, *Anal. Chem.*, 2004, **76**, 5864-5871.
91. M. Brivio, R. H. Fokkens, W. Verboom, D. N. Reinhoudt, N. R. Tas, M. Goedbloed and A. van den Berg, *Anal. Chem.*, 2002, **74**, 3972-3976.
92. M. Brivio, N. R. Tas, M. H. Goedbloed, H. J. G. E. Gardeniers, W. Verboom, A. van den Berg and D. N. Reinhoudt, *Lab Chip*, 2005, **5**, 378-381.
93. J. Preisler, F. Foret and B. L. Karger, *Anal. Chem.*, 1998, **70**, 5278-5287.
94. H. Ørsnes, T. Graf, H. Degn and K. K. Murray, *Anal. Chem.*, 1999, **72**, 251-254.
95. H. K. Musyimi, J. Guy, D. A. Narcisse, S. A. Soper and K. K. Murray, *Electrophoresis*, 2005, **26**, 4703-4710.
96. H. K. Musyimi, D. A. Narcisse, X. Zhang, W. Stryjewski, S. A. Soper and K. K. Murray, *Anal. Chem.*, 2004, **76**, 5968-5973.
97. K. Jo, M. L. Heien, L. B. Thompson, M. Zhong, R. G. Nuzzo and J. V. Sweedler, *Lab Chip*, 2007, **7**, 1454-1460.
98. M. Zhong, C. Y. Lee, C. Croushore and J. V. Sweedler, *Submitted to Lab Chip*, 2011.

CHAPTER 2

MASS SPECTROMETRIC IMAGING OF PEPTIDE RELEASE FROM NEURONAL CELLS WITHIN MICROFLUIDIC DEVICES

2.1 Notes and Acknowledgements

This chapter was modified from a manuscript published in *Lab on a Chip* in 2007 (DOI: 10.1039/B706940E. Kyubong Jo, Michael L. Heien, Lucas B. Thompson, Ming Zhong, Ralph G. Nuzzo and Jonathan V. Sweedler, "Mass spectrometric imaging of peptide release from neuronal cells within microfluidic devices," *Lab Chip*, 2007, **7**, 1454-1460. http://pubs.rsc.org/en/Content/ArticleLanding/2007/LC/b706940e. Reproduced by permission of The Royal Society of Chemistry.) This work focused on interfacing microfluidics and mass spectrometry imaging to interrogate peptides released from neuronal cells. Several device formats were developed for this purpose. In this work, Dr. Kyubong Jo performed the experiments on sampling efficiency from the octadecyltrichlorosilane (OTS)-modified surface, surface coverage of angiotensin II by using a microfluidic device with a serpentine channel, and neuropeptide release by using a device with three branching channels. Dr. Michael L. Heien and Dr. Lucas B. Thompson meaured surface coverage using radioisotope labeled molecules and conducted single cell analysis. I applied the serpentine channel design to another peptide, substance P, and compared the OTS surface with other modified surfaces in terms of sampling efficiency. The work is reproduced here for completeness. This study was

supported by the W.M. Keck Foundation and the National Science Foundation through Awards CHE-05-26692 and CHE-04-02420.

2.2 Introduction

Microfluidics offer promise as a revolutionary technology in analytical chemistry.[1] Microfluidic technology provides advantages such as small reaction volumes, minimal reagent consumption, portability, disposability, and local control of the microenvironment. These advantages directly contribute to enhancing analytical performance in a number of applications. Moreover, integrated components facilitate a variety of functions such as sample clean-up, concentration, separation, and detection.[2] As a result, microfluidics have revolutionized the analysis of small amounts of analytes and have been adapted for characterizing the contents of single cells[3, 4] and single molecules.[5-8]

For microfluidic applications, analyte detection remains an important issue given the small sample-volumes typically available. Accordingly, many analyses have been conducted using laser-induced fluorescence, by which small sample-volumes are easily probed with unparalleled mass detection limits.[9-11] Even single molecules have been effectively analyzed using fluorescence techniques in microfluidic devices.[5-8]

Fluorescence imaging (microscopy) is particularly beneficial because large areas of the device can be probed, and the field of view of many microscopes matches typical microfluidic device dimensions. Because of the ease of adapting fluorescence imaging to such devices, and its high sensitivity, it is among the most commonly employed detection schemes for microfluidics. Although fluorescent technology has many advantages, it is

limited to analyzing previously labeled target molecules or those that have specific reactive groups, and can be difficult to adapt when characterizing unknown molecules.

Mass spectrometry (MS), on the other hand, offers unparalleled information content. The high sensitivity of MS is an essential component for the identification of low-abundance species from mass-limited samples. The integration of microfluidic systems with MS has received substantial attention following early demonstrations of microfluidic electrospray (ESI)-MS interfaces.[12, 13] On-line ESI-MS offers a simple approach for directly interfacing the mass spectrometer to a microfluidic device. These systems allow reproducible quantitation with high sensitivity, and are now commercially available.[14] As opposed to on-line ESI-MS, matrix-assisted laser desorption/ionization (MALDI)-MS can measure the eluant from a microdevice with off-line coupling.[15] This off-line approach offers the advantages of parallel sample deposition and on-chip sample processing such as sample desalting prior to MS analysis. As an alternative to off-line coupling, a section of the microfluidic device can also be utilized as the MALDI target. For example, open-top microchannels have been used as MALDI targets to analyze molecules that are dried after electrophoresis or isoelectric focusing.[16, 17] In another recent study, an alkane-thiol coated gold surface was used as a MALDI target after parallel enzyme reactions within a microfluidic network.[18]

One of the most intriguing recent advances in MALDI-MS has been the development of MALDI-based mass spectrometric imaging (MSI).[19-21] Building upon the early application of MALDI-MS to create molecular images from a variety of surfaces,[21-23] MSI has been used to measure the distribution of biomolecules in tissue sections.[19-21] Two-dimensional, or sometimes three-dimensional,[24] intensity maps have

been reconstructed to create molecular images; these images provide molecular information with relative abundance and spatial distribution, allowing for better understanding of the biological processes in a tissue sample.[25] Although microfluidic devices are amenable to MALDI-MSI, to the best of our knowledge, molecular imaging has not been demonstrated from a microfluidic device. Imaging of the compounds from a functionalized surface coupled to a microfluidic device yields a wealth of information concerning the detailed spatial arrangement of analytes within that device. In many ways, the advantages of this approach may mimic the benefits of using fluorescence microscopy from microfluidic devices as opposed to single-point fluorescence detection. In other words, by probing a device with MSI, areas of interest that contain specific analytes or unexpected compounds can be discovered, even if the precise location is not known in advance.

Here we present an approach whereby we interface microfluidics with MSI. The goal is to create a system that allows neurons to be stimulated and neuronal release to be collected and monitored. Several elegant chip-based designs for characterizing peptide secretion have appeared that use laser-based fluorescence detection.[26, 27] Peptide profiling of neurons has often used MS due to the sensitivity and structural information that can be acquired.[28, 29] Our goal here is to develop microfluidic devices that can be used to manipulate the extracellular environment of neurons, collect the resulting neuropeptide release, and examine the releasate with spatial, temporal and chemically selective analyses. We demonstrate this approach by analyzing peptide release using *Aplysia* bag cell neurons as a model. *Aplysia* is a well-known neurobiological model with a well-characterized physiology and biochemistry;[30, 31] the bag cell neurons are ideal

for validating the measurements because of their equally well-known neuropeptide complement.[32, 33]

2.3 Experimental

Appendix A contains a master list of all abbreviations used in this chapter.

2.3.1 Materials and Reagents

Unless noted, all chemicals were obtained from Sigma-Aldrich (St. Louis, MO) and used as received. Silicon wafers were from Montco Silicon Technologies, Inc (Royersford, PA). Photoresist SU-8 100 and SU-8 2010, and developer were obtained from MicroChem Corp. (Newton, MA). Glass coverslips (24 × 60 mm No. 1 thickness) were obtained from Fisher Scientific (Pittsburgh, PA). Radiolabeled [^{14}C] cytochrome *c* was obtained from American Radiolabeled Chemicals Inc. (St. Louis, MO). Artificial seawater (ASW), pH 7.8 (460 mM NaCl, 10 mM KCl, 10 mM $CaCl_2$, 22 mM $MgCl_2$, 6 mM $MgSO_4$, 10 mM HEPES) was used in all experiments involving *Aplysia*.

2.3.2 Device Fabrication

Microfluidic devices were formed by molding poly(dimethylsiloxane) (PDMS), Sylgard 184, (Dow Corning, Midland, MI) onto a photolithographic master as described previously.[34, 35] Briefly, negative SU-8 photoresist was used to fabricate a master by exposure through a pattern mask. Small pieces of tubing were glued to the master prior to pouring PDMS over the master. PDMS devices were cured at 65 ℃ for several hours and removed from the master. The tubing pieces were pulled from the PDMS creating voids where the full-length tubing was inserted. For a reservoir, a hole was punched at

the inlet using a 5-mm-diameter biopsy punch, or a piece of wide tubing (2 mm outer diameter) was used as a mold to create the reservoir. The fabrication procedure is illustrated in Fig. 2.1.

2.3.3 Surface Derivatization

Silicon surfaces were derivatized with octadecyltrichlorosilane (OTS) in organic solvent.[36] A wafer was dipped in a 100 mL solution of chloroform (30 mL) and hexane (70 mL) containing OTS (0.8 % v/v) for 5 min and then transferred to hexane solution for 10 min. A derivatized silicon wafer was washed with acetone and dried at 65 ℃ for at least 6 h. To test if OTS offers optimal ability of collecting peptides, silicon wafers were also treated with (N,N-Dimethylaminopropyl)trimethoxysilane (DMAPTS), (3-aminopropyl)trimethoxysilane (APTS), and dimethyloctadecyl[3-(trimethoxysilyl)propyl]ammonium chloride (DMOPAC) for comparison. The derivatization process and condition of DMAPTS and APTS is the same as OTS. While DMOPAC was dissolved in DI water (0.1% v/v) and the silicon wafer was dipped into the solution for 5 min. The substrate was then rinsed with DI water to remove excess DMOPAC and dried with nitrogen. The derivatized wafer was cured at 110 ℃ for 1 h. Before use, surfaces were rinsed with methanol and water. For cell plating, a droplet (1 μL, ~1–2 mm diameter) of 1% poly-L-lysine solution was placed and dried on the functionalized surface. A reservoir in a PDMS device was aligned with the poly-L-lysine coated area.

Alternatively, octadecanethiol (C18) derivatized gold strips were fabricated on glass coverslips.[37] For this derivatization, glass coverslips were cleaned in piranha

solution (**Caution!** Piranha is a strong oxidant. It may explode on contact with organic residues), rinsed, and dried with N_2. PDMS was then conformally sealed to the coverslips to create a stencil mask for the subsequent deposition of gold using a Temescal FC-1800 e-beam evaporator. The coverslips with the deposited gold were then immersed into a 2% v/v solution of octadecanethiol in ethanol for 30 min, and then rinsed with ethanol and water. The coating of poly-L-lysine was done by applying poly-L-lysine to the glass slide prior to sealing with the channel. The poly-L-lysine solution was placed on the glass surface for ~1 h.

2.3.4 Biological Experiments

Aplysia californica (100–300 g) were supplied by Vivida Biological (Santa Barbara, CA) and kept in a tank with aerated and circulated seawater at 14 ℃. For dissection, animals were anesthetized by injection of isotonic magnesium chloride solution (~30 to 50% of body weight) into the body cavity. Individual *Aplysia* bag cells were isolated after incubation in ASW with proteases (1% type IX and 1% type XIV, Sigma-Aldrich) at 35 ℃ for between 60–120 min as described previously.[38, 39] The cells were then transferred onto a poly-L-lysine coated area on the surface in a microfluidic device. For the potassium stimulation experiments, elevated potassium chloride solution (final concentration 60 mM) was added to stimulate neurons to release peptides, which were transported and collected on an OTS coated surface. Fig. 2.2 shows an overview of these procedures.

2.3.5 Mass Spectrometric Imaging

After completing the biological experiments, as much solution was removed from the device as feasible, and the PDMS device was peeled off from the surface. The surface was briefly washed with DI water to remove salts from the cell media. MALDI matrix was applied to surfaces using a commercial airbrush (Badger, Franklin Park, IL).[40] The airbrush nozzle was positioned at a distance of ~10 cm from the surface, and 2,5-dihydroxybenzoic acid (10 mg/mL in acetone) was sprayed onto the surface.

MALDI-MS detection was performed with a Bruker Ultraflex II mass spectrometer (Bruker Daltonics Inc., Billerica, MA) with a solid-state UV laser. Mass spectra were obtained as sums of 100 laser shots at 50 Hz in the reflectron mode with an acceleration voltage of +25 kV. Imaging resolution ranged from 100 μm to 200 μm. All mass spectra were externally calibrated and MS image analysis was performed with Bruker FlexImaging, Biomap imaging software (http://www.maldi-msi.org/), and homemade software written in Microsoft Visual C# 2005, Express Edition (http://www.microsoft.com).

2.3.6 Surface Coverage Measurement Using Radioisotope Labeled Molecules

The quantity of radiolabeled molecules was measured by using a phosphorimager as described previously.[41] Briefly, radioactive stock solution was diluted with ASW to a volume of 86 μL, giving a final concentration of 2 μM. The samples were covered with Reynolds Film 910 (Grottoes, VA) and placed face down on a Fuji BAS III imaging plate (48-h exposure). The decay intensities from individual channels were summed and background-subtracted with a Fujix BAS 1000 phosphorimager (Fuji Photo Film Co.

Tokyo, Japan). The radioactivity for each spot corresponds to the image intensity, and was converted to a mass by comparison with intensity values acquired from a calibration strip.

2.4 Results and Discussion

2.4.1 Sampling from a Functionalized Surface

We previously reported monitoring peptide release from the nervous system by using single-bead solid-phase extraction and MALDI-MS.[41] Single-bead solid-phase extraction uses the bead surface to adsorb hydrophobic molecules to monitor peptide release from a neuronal sample. The peptides are then eluted from the beads onto a MALDI target using the appropriate organic solvents. This system has proven to be a robust sampling strategy for measuring neuropeptide release.[42, 43] However, the approach requires the manual placement of the beads onto the brain slice or neuronal culture, followed by their removal after the neuronal stimulation; additional steps include a manual wash step and placement of the beads on the MALDI target.

Here we adapt this approach to function on flat surfaces by forming a self-assembled monolayer of octadecyl alkyl chains.[36, 44] This platform employs a PDMS microfluidic device mounted on a functionalized surface, and subsequent MS imaging for monitoring peptide release from the nervous system. The surface-supported, self-assembled octadecyl alkyl chains not only adsorb molecules through hydrophobic interactions, but they also allow direct MALDI-MS measurement. Direct MS measurement on a flat surface facilitates MS imaging because in this two-dimensional plane, the positional information on the location of collected peptides is retained.

Advantages of this approach include the reduction of manual manipulations and ease of sampling the releasates. MS imaging is an efficient way to obtain mass spectra by scanning the surface, which is especially useful when the exact location(s) of peptides are not known. Of course, such visualization yields insights about the phenomena occurring within microfluidic devices such as the collection efficiency for different analytes onto the surfaces.

Before applying this approach to biological measurements, we validate the performance of the functionalized surface for sampling peptides from the channels in concentrations equivalent to those previously reported in neuronal release studies from single, chemically stimulated neurons, (e.g., the low femtomole amount of egg laying hormone expected to be released from an individual *Aplysia californica* bag cell neuron).[45] MSI of these peptides should also possess comparable sensitivity to conventional MALDI techniques. Fig. 2.3 illustrates the microfluidic device used for sampling peptides visualized by MSI. An OTS coated silicon surface collected four different standard peptides (0.5 μL of 1.0 pmol/μL), each introduced through simple parallel microchannels as seen in Fig. 2.3A. The MS image shown in Fig. 2.3B depicts the parallel microchannel pattern of these peptides whose mass spectra are represented in Fig. 2.3C.

Although glass surfaces are widely used in many biological applications,[39] to ensure high-quality mass spectra are obtained, we have used silicon surfaces for these experiments. The primary reason for choosing silicon is that the insulating properties of the glass may cause space charge effects, which can reduce the resulting signal-to-noise ratio (SNR).[46] The semiconductor nature of silicon wafers avoids this charging problem.

We observe that low femtomole standard peptides are detected on silicon surfaces with high SNR, comparable to those on conventional targets. Moreover, silicon surfaces have some of the same properties as glass, derivatization of silicon surfaces is common,[36] and silicon has been investigated and optimized for cell biology and cell culture.[47]

2.4.2 Surface Coverage

The ability of functionalized surfaces to concentrate peptides has been characterized by using ^{14}C-labeled cytochrome *c*; this radionuclide detection approach allows verification of performance independently from the MALDI MS performance. For these experiments, the PDMS channels were sealed on C18 coated surfaces to create separate channels measuring 200 μm × 300 μm × 1 cm. The surfaces were activated by rinsing them with a 50% acetonitrile/water solution (for 30 min) prior to equilibration with ASW. In order to quantitate surface coverage at low concentrations, a 1 μM solution of ^{14}C-labeled cytochrome *c* was then introduced to each channel, and 1 μL of solution was allowed to interact with the surface. A volumetric flow rate of 500 nL/min (linear flow rate = 0.014 cm/s) was used, which (on average) allows all analyte molecules to interact with the functionalized surface. After the peptides were introduced, each channel was rinsed with 0.1 % trifluoroacetic acid to remove salts. The PDMS channel system was then removed and the amount of ^{14}C cytochrome *c* retained by the C18 modified substrate measured. Each channel contained 370 ± 50 fmol of material (n = 8 channels), which corresponds to a surface coverage of 19 ± 3 pmol/cm^2.

In a separate experiment, the concentration of ^{14}C cytochrome *c* was varied to introduce differing amounts of peptide ranging from 75–2000 fmol into the channel. The

channel dimensions and flow rates are the same as those described above. The measured amount of ^{14}C cytochrome *c* on the surface in each case is given in Table 2.1. At the lowest concentration tested, the entire solution was depleted over the length of the channel and deposited on the surface. In addition, the high recovery rate at the lowest concentration implies that a major portion of the peptides were deposited on the functionalized surface rather than the PDMS walls.

Although isotope labeling experiments provide quantitative surface coverage information, these values vary with channel dimension, flow rate, molecular weight, and chemical structure;[48] for example, large hydrophilic molecules will have lower surface coverage than small hydrophobic molecules. Perhaps the optimum method of measuring sampling efficiency is to make the measurements using the specific molecules of interest under identical conditions; in this case however, we do not have the appropriate radiolabeled peptides from *Aplysia* bag cell neurons. Here we measure sample collection efficiency using the approach shown in Fig. 2.4 for a range of peptides. In this method, molecules flow along a serpentine channel until they become depleted by interacting with the OTS coated surface. As shown in Fig. 2.4, different amounts of angiotensin II (1.0 ng, 2.5 ng and 4.0 ng) loaded in a reservoir and drawn by the negative pressure through a long serpentine channel are depleted at different locations along the channel: after a length of 12 mm for 1.0 ng, 40 mm for 2.5 ng, and 54 mm for 4.0 ng, respectively. Given the 200 μm channel width, the surface coverage is 33 pmol/cm^2 calculated from the rate of the increase in area covered by the peptide compared to the amount of peptide initially present in the solution. The increase of adsorption length with amount was also observed with another standard peptide, substance P, as illustrated in Fig. 2.5. These results imply

that one can estimate peptide amounts from the area on the surface covered by the peptide. Follow-up investigations on the quantitation of peptides based on adsorption length are included in Chapter 3.

Our results show a surface coverage of 19 pmol/cm^2 for cytochrome *c* (12 kDa) and 33 pmol/cm^2 for angiotensin II (1046.5 Da). Why is there a difference between the two? From a simple geometrical calculation, assuming that molecules form a well-packed square lattice monolayer, surface coverage should range from 166 pmol/cm^2 for the molecules of 1 nm diameter to 7 pmol/cm^2 for molecules of 5 nm diameter. Experimentally, Margel *et al.*[48] reported ~17–22 pmol/cm^2 for synthetic peptides containing multiple lysine residues and 0.4 pmol/cm^2 for human serum albumin (65 kDa) on OTS coated surfaces. Fragneto *et al.*[49] reported 7.9 pmol/cm^2 surface coverage for β-casein (24 kDa) adsorbed on OTS coated surfaces. Our measurements are consistent both with geometrical considerations and prior measurements.

2.4.3 Comparison of Different Derivatized Surfaces

Before the microfluidic system containing OTS surfaces was applied to neuron release experiments, we also tested if OTS offers optimal capability to adsorb peptide molecules compared to other derivatization reagents. For this purpose, silicon wafers were treated with DMAPTS, APTS, and DMOPAC respectively. The molecule of DMAPTS contains a $N(CH_3)_2$ group at the end, and APTS contains an end group of NH_2. DMOPAC has a quaternary ammonium end group with a positively charged N and an octadecyl alkyl chain. A PDMS piece with the serpentine channel was placed on top of each derivatized surface and 5 ng substance P was flown through the microchannel. Fig.

2.6 shows the MS images from DMAPTS, APTS, and OTS surfaces. On DMAPTS, the peptide signals were only detected in the reservoir (Fig 2.6A). The APTS surface provided better adsorption capability but still only contained sparse signal dots in both the reservoir and channel areas (Fig. 2.6B). In both cases, the signal intensity was low. Meanwhile, OTS surface produced a continuous peptide band with strong intensity (Fig. 2.6C). The results here clearly demonstrate that OTS is superior to DMAPTS and APTS in terms of sample collection ability.

The surface of DMOPAC is positively charged with a long alkyl chain, therefore it can adsorb peptides through both electrical and hydrophobic interactions. As the isoelectric point (pI) of substance P is 11.5, the peptide possesses negative charge in DI water. A buffer containing 0.1 M Na_3PO_4/Na_2HPO_4 (pH = 12.5) needs to be added to the substance P solution to convert it negatively charged. 5 ng substance P either in DI water or the buffer was introduced into the microfluidic device with the serpentine channel, and the MS imaging results are shown in Fig. 2.7. Although it has been demonstrated with OTS that the hydrophobic alkyl chain can capture substance P, the positively charged peptide did not adsorb well on DMOPAC as no significant signals were observed in the channel (Fig. 2.7A). In contrast, the negatively charged peptide in the buffer solution was collected on the same surface, indicated by strong peaks in the channel (Fig. 2.7B). The difference in MS profiles demonstrates that electrical force played a stronger role than hydrophobic interaction in capturing molecules from the solution. This conclusion was further supported by the fact that negatively charged acidic peptide (pI = 4.3) in DI water were successfully collected on DMOPAC (Fig. 2.7C). Charges on this surface limit its use for cell experiments, since peptide molecules

released by neurons can have both negative and positive charges in ASW. Therefore, the OTS surface offers a more universal method for sample collection and was used for the following biological experiments.

2.4.4 Neuropeptide Release

Our overarching goal is to develop a platform for collecting neuropeptide releasates from neurons and correlate this approach with stimulation protocols along with temporal and chemical information. Fig. 2.8A shows the design of a device for the temporal analysis of peptides released from neuronal cells mounted onto a poly-L-lysine coated silicon surface in an open-top reservoir. This open-top design allows for the manipulation of cells as well as electrophysiological recording from those cells. We have designed our initial collection system with three time-points, corresponding to before, during, and after chemical stimulation. For pre-stimulation monitoring, the solution in the reservoir is transported through the first channel by negative pressure. Next a secretagogue, potassium chloride, is added. This depolarizes the cell membrane and causes neuropeptide release. The solution putatively containing peptide releasates is transported through the second channel. For the post-stimulation collection, the solution in the reservoir is exchanged with fresh ASW and then transported through the third channel. After the stimulation experiment, the PDMS is removed and the exposed OTS coated surface is sprayed with the appropriate matrix and then imaged using MSI.

In order to validate this design, we simulated a peptide release experiment by manual injection of angiotensin II (1.0 pmol) and substance P (0.5 pmol, 1347.7 Da) before transportation to the second channel. As expected, angiotensin II and substance P

were detected in the second channel and traces (from carryover) of the peptides were detected in the third channel (Fig. 2.8C). Intriguingly, substance P deposited first and angiotensin II deposited afterward. This phenomenon appears to be due to the differential partitioning of these materials onto the OTS surface in a process analogous to thin layer chromatography (TLC). We observed a similar effect in another trial that used 1.0 pmol substance P and 1.0 pmol angiotensin II; in this case, the entire channel was covered by substance P without angiotensin II; we suspect that the angiotensin II eluted from the device (data not shown).

The MS image shown in Fig. 2.8D demonstrates the selective sampling of secreted neuropeptides from neurons. As shown in Fig. 2.8B, five *Aplysia* bag cell neurons placed into the reservoir were stimulated by elevated potassium chloride (final concentration 60 mM). As a result, two well-characterized peptides from bag cell neurons were detected:[33, 41] acidic peptide (AP), with a protonated mass-to-charge ratio (*m/z*) of 2961.3, and egg laying hormone (ELH), with a protonated *m/z* of 4385.2. We also observed the "TLC-like" separation between AP and ELH as shown in Fig. 2.8D.

2.4.5 Single Cell Analysis

Can this approach be adapted for single cell measurements? In order to maximize releasate collection and control stimulation protocols, we modified the first device so that the cell is loaded and located in a channel rather than a larger-volume reservoir, and combined this set up with optical microscopy. The latter is problematic when using silicon substrates; silicon surfaces do not facilitate optical microscopy because they are not transparent at these wavelengths. We therefore modified the device design as

illustrated in Fig. 2.9A. In this case, the surface is a glass slide with a C18 functionalized gold strip (yellow band in Fig. 2.9A) that collects releasate from a single cell. This PDMS device consists of a main channel, in which cells can be loaded, and a collection area. Similar to our prior device, the collection area contains three channels branching off from the main channel area overlapping the C18 functionalized surfaces. The channels can be used to collect analyte from cells and allow the temporal isolation of peptide release. Here a single *Aplysia* bag cell neuron was loaded into the main channel (see Fig. 2.9B). The solution was then collected from the cell for 15 min before elevated KCl (60 mM) was added to the first solution cell channel as our pre-stimulation control; next, the flow was redirected to the middle channel for 15 min using pressure-driven flow. After the releasate was collected, 15 min post-stimulation solution was collected in the third channel. The MS image is shown in Fig. 2.9C, with each channel defined with a rectangular box. The peak for AP is shown in blue, and is localized in the channel that collected the stimulated material. Mass spectra for the channel pre-stimulation (Fig. 2.9D, upper) and during stimulations (Fig. 2.9D, lower) show released peptides including AP and alpha bag cell peptide (α-BCP_{1-9}), *m/z* 1122.6. If greater temporal information is desired, additional collection channels can be added to this device.

2.5 Conclusions

The ability of MS to characterize peptide and proteins ensures its use in an increasingly wider range of applications. Mass limited samples are becoming more common, requiring the development of enhanced small-volume measurement technologies. To meet this challenge, MS, in combination with a microfluidic sampling

and manipulation system, is used here to create a flexible scheme for monitoring neuronal release. The use of microfluidics with a functionalized surface, interfaced with MSI, provides molecular maps of neuropeptide release. This approach allows for the study of the modulation of neurotransmission within engineered neuronal circuits inside a microfluidic device. Because MSI allows a larger surface device to be probed, it allows devices with multiple collection areas containing different collection materials to be probed via MS.

The surface coverage experiments on the microfluidic device with a serpentine channel showed promising results that the channel length covered by a peptide increased with the amount of that peptide, indicating that the adsorption length could be used as a measure for the sample amount. This quantitation approach was not completely validated here, for example, the device-to-device reproducibility needed to be tested, the influence of experimental parameters such as sample concentration and flow rate on the length measurements was not studied, and the nonspecific adsorption/absorption of peptides onto the reservoir area and PDMS was not controlled. Also a mathematical model explaining this approach needed to be developed. The next chapter will address these issues and describe the details of the fully established length-based quantitation approach.

2.6 Tables and Figures

Table 2.1 Adsorption of radiolabeled cytochrome *c* onto a hydrophobic surface. Reproduced by permission of The Royal Society of Chemistry.

Amount in solution (fmol)	Amount on surface (fmol)	Percent recovery
75	80 ± 10	110 ± 10
125	90 ± 30	70 ± 20
250	110 ± 40	40 ± 20
500	180 ± 60	40 ± 10
1000	410 ± 70	40 ± 10
2000	700 ± 100	35 ± 5

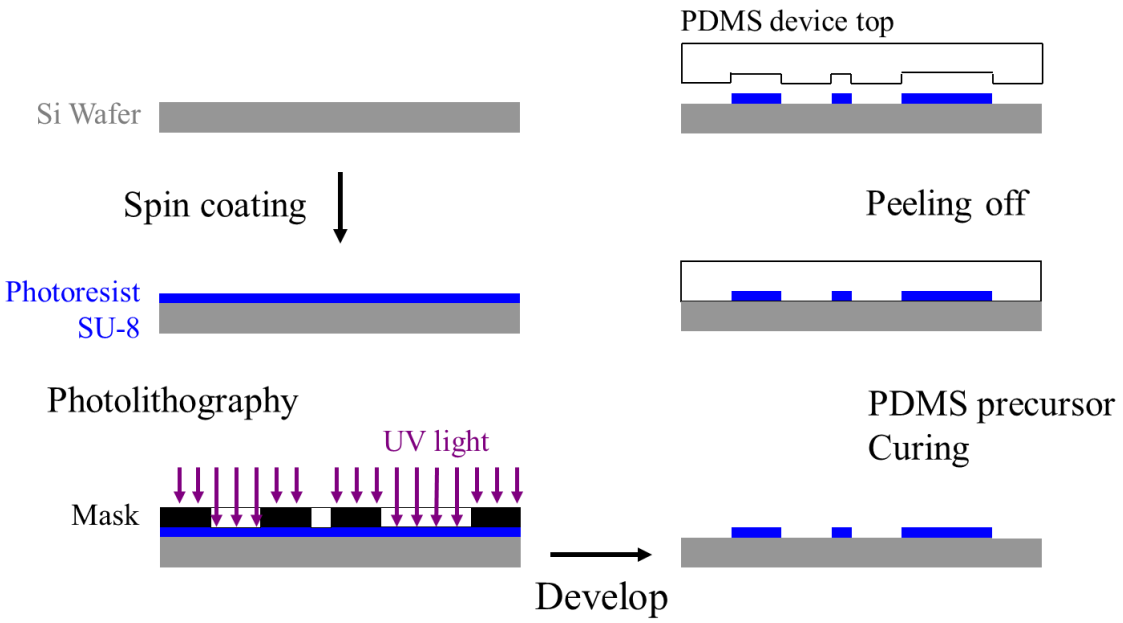

Figure 2.1 Fabrication process of PDMS microfluidic device. A negative photoresist SU-8 is used. The patterned photoresist on the silicon wafer is used as a master for molding PDMS devices.

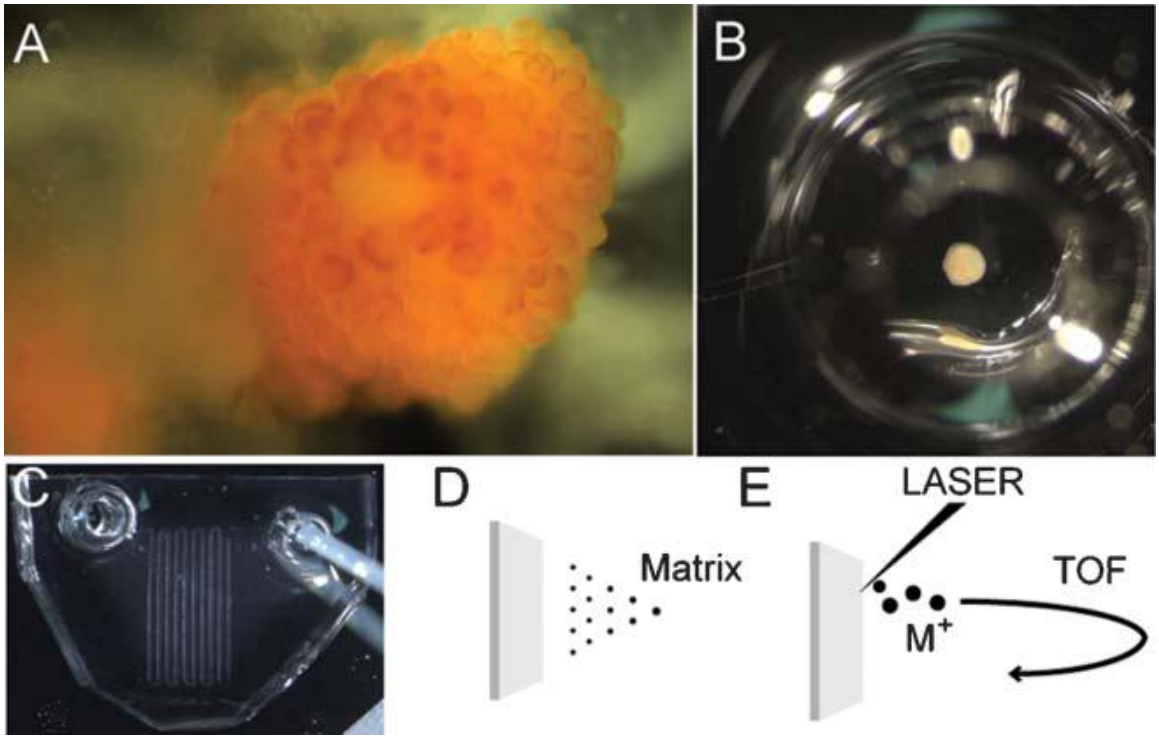

Figure 2.2 Experimental overview of the process of collecting and measuring neuronal analysis using a microfluidic device. (A) Isolated neuronal tissue is digested by proteases and desheathed. The image shows a desheathed *Aplysia* ganglion. (B) Individual neurons are loaded into the sampling chamber of the microfluidic device. (C) Neurons are chemically stimulated and their releasate transported through microfluidic channels and collected on the functionalized surface. (D) The microfluidic device is peeled off from the surface, and the appropriate matrix-assisted laser desorption/ionization matrix solution is sprayed. (E) The matrix coated surface is inserted into a MALDI time-of-flight (TOF) instrument and mass spectra acquired in a spatially resolved manner from the surface. Reproduced by permission of The Royal Society of Chemistry.

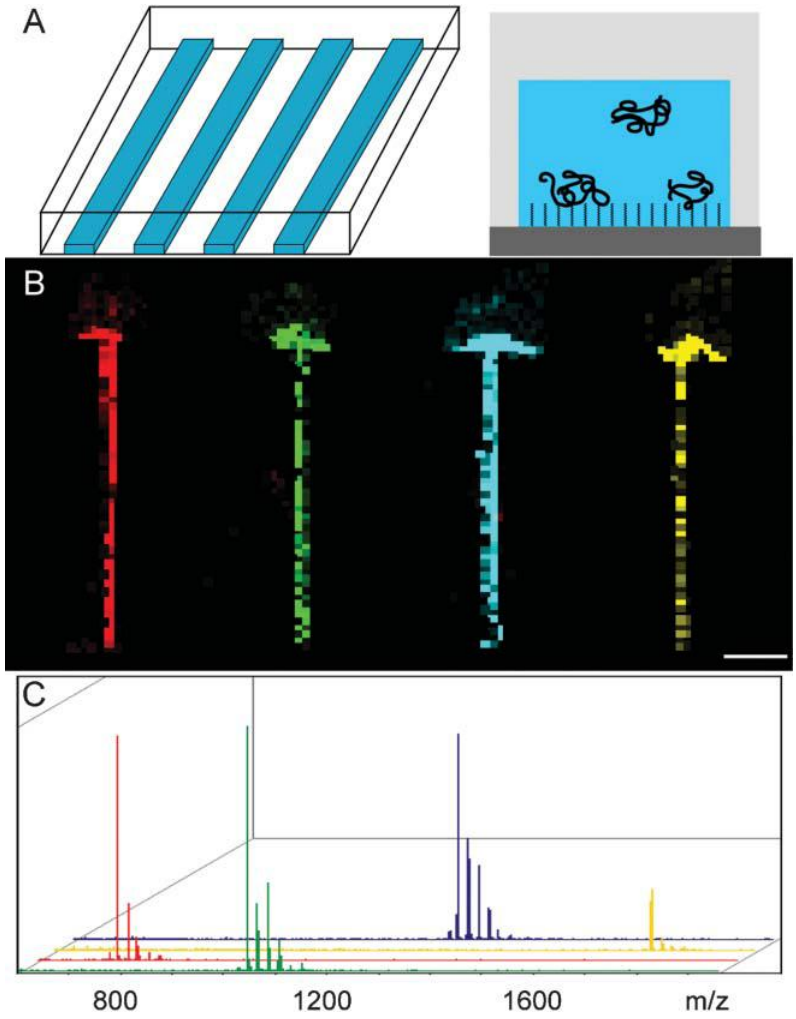

Figure 2.3 Sampling peptides on a functionalized surface using a microfluidic device. (A) Schematic illustration of four channels (0.2 mm × 0.01mm × 4.5 mm) and a cartoon showing peptide sampling on an OTS surface in a microchannel. (B) MS image of four different peptides at 0.5 pmol: bradykinin, 757.4 Da (red), angiotensin II, 1046.5 Da (green), substance P, 1347.7 Da (blue), renin substrate, 1758.9 Da (yellow). Scale bar = 1 mm. (C) Mass spectra of the four different peptides; spectrum colors correspond to those used in the MS image. Reproduced by permission of The Royal Society of Chemistry.

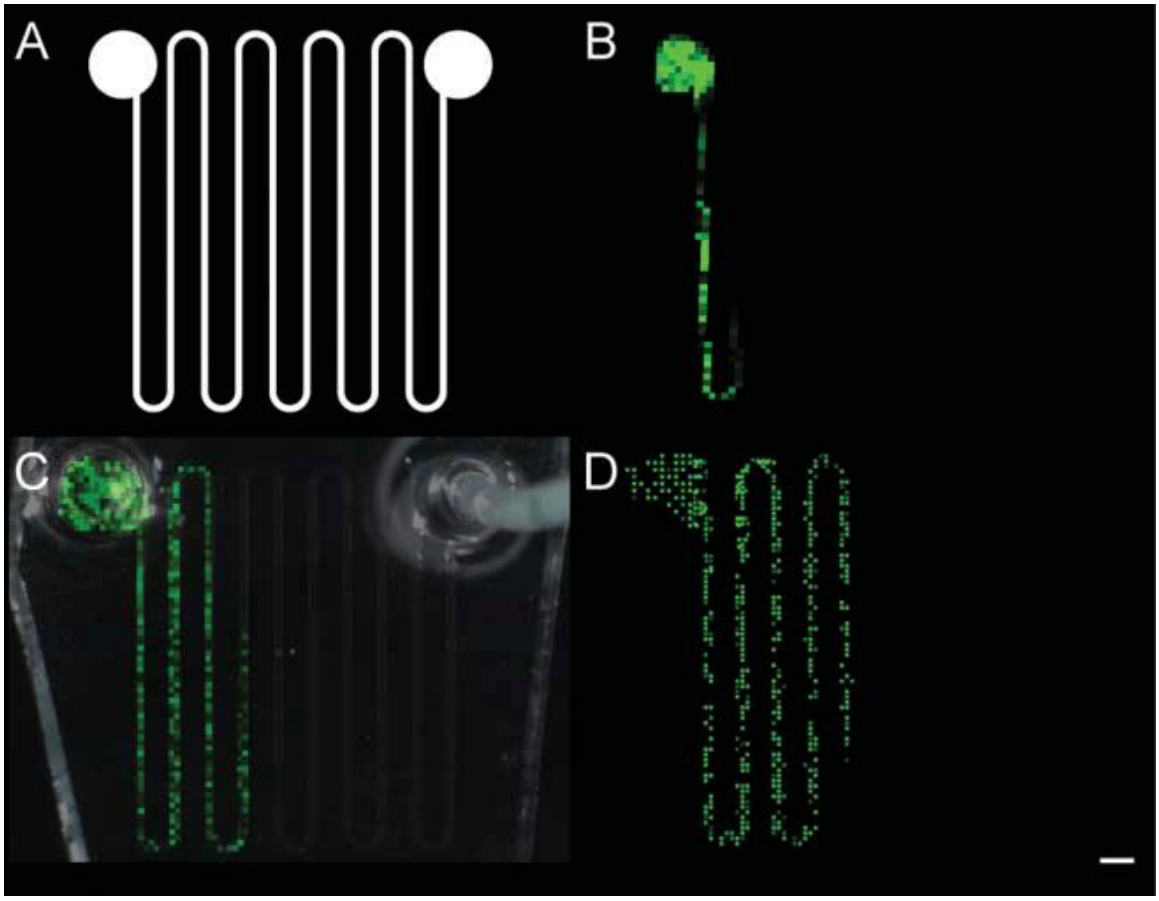

Figure 2.4 Depletion of angiotensin II along a serpentine channel. (A) Schematic of the design of the PDMS device consisting of a 114-mm-long serpentine microchannel (200 μm wide × 10 μm high) and two reservoirs, each 2 mm in diameter; one is a loading reservoir and the other is connected to a piece of tubing for flow control. (B) MS image of 1.0 ng angiotensin II; (C) MS image of 2.5 ng angiotensin II with an overlay of an image of the PDMS device; and (D) MS image of 4.0 ng angiotensin II. Scale bar = 1 mm. Reproduced by permission of The Royal Society of Chemistry.

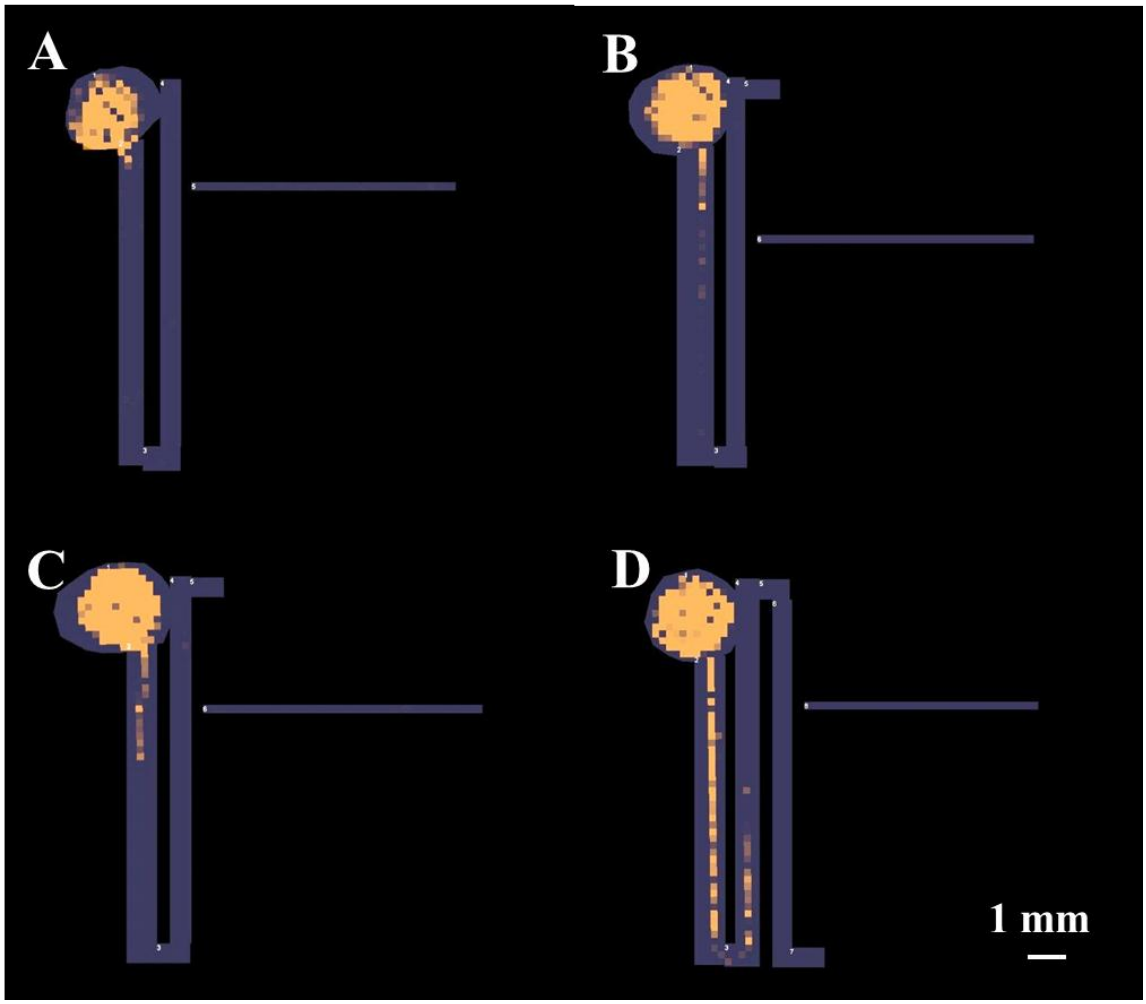

Figure 2.5 MS images of substance P drawn through the serpentine channel illustrated in Fig. 2.4. Substance P is visualized in orange color. Grey color indicates the imaging areas. (A) 1.0 ng substance P, (B) 2.0 ng, (C) 4.0 ng, and (D) 6.0 ng.

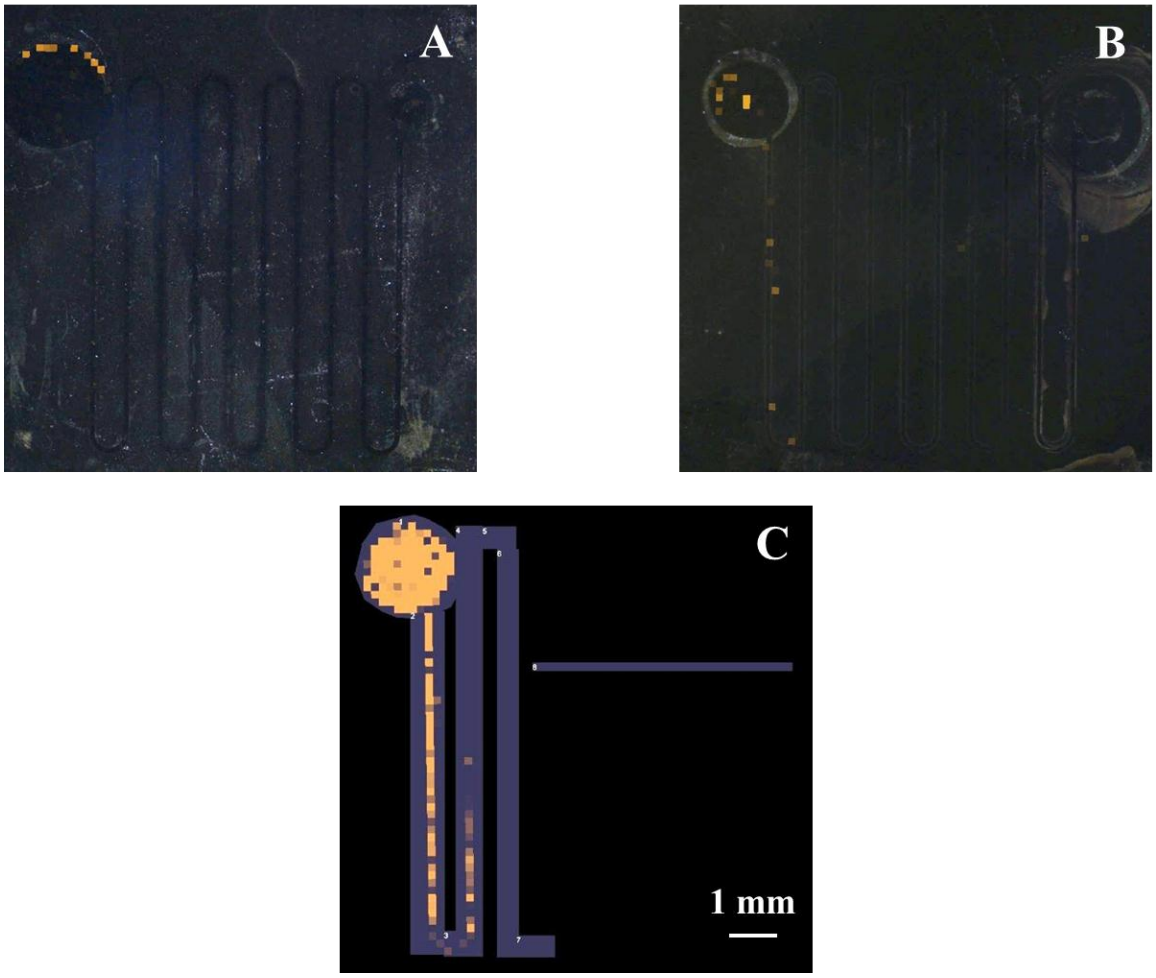

Figure 2.6 MS images of 5 ng substance P on silicon surfaces derivatized with different reagents. Substance P is visualized in orange color. (A) Silicon surface treated with DMAPTS, (B) APTS, and (C) OTS.

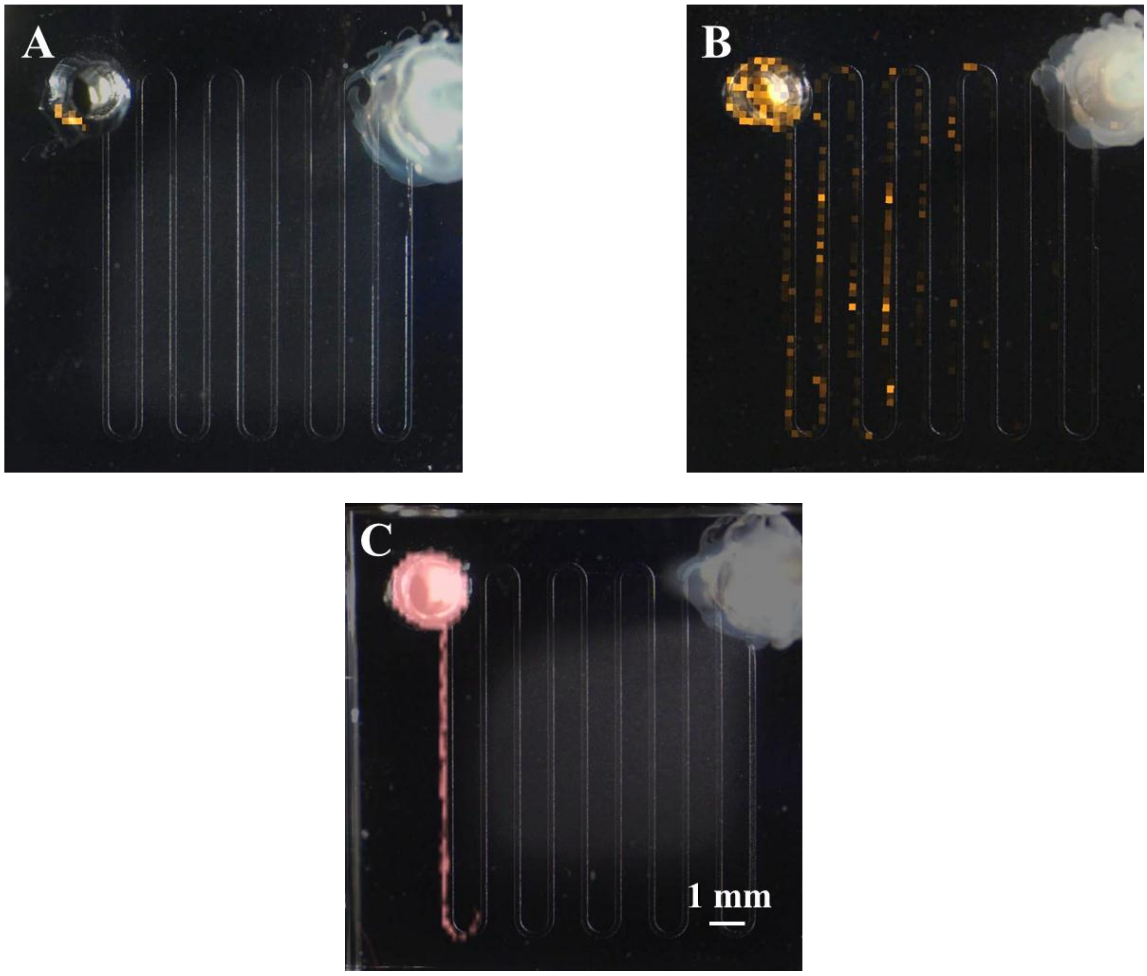

Figure 2.7 MS images of peptides on silicon surfaces derivatized with DMOPAC. (A) 5 ng substance P in DI water was dragged through the serpentine channel. (B) 5 ng substance P in a pH = 12.5 buffer, and (C) 5 pmol acidic peptide in DI water. Yellow represents substance P and pink, acidic peptide.

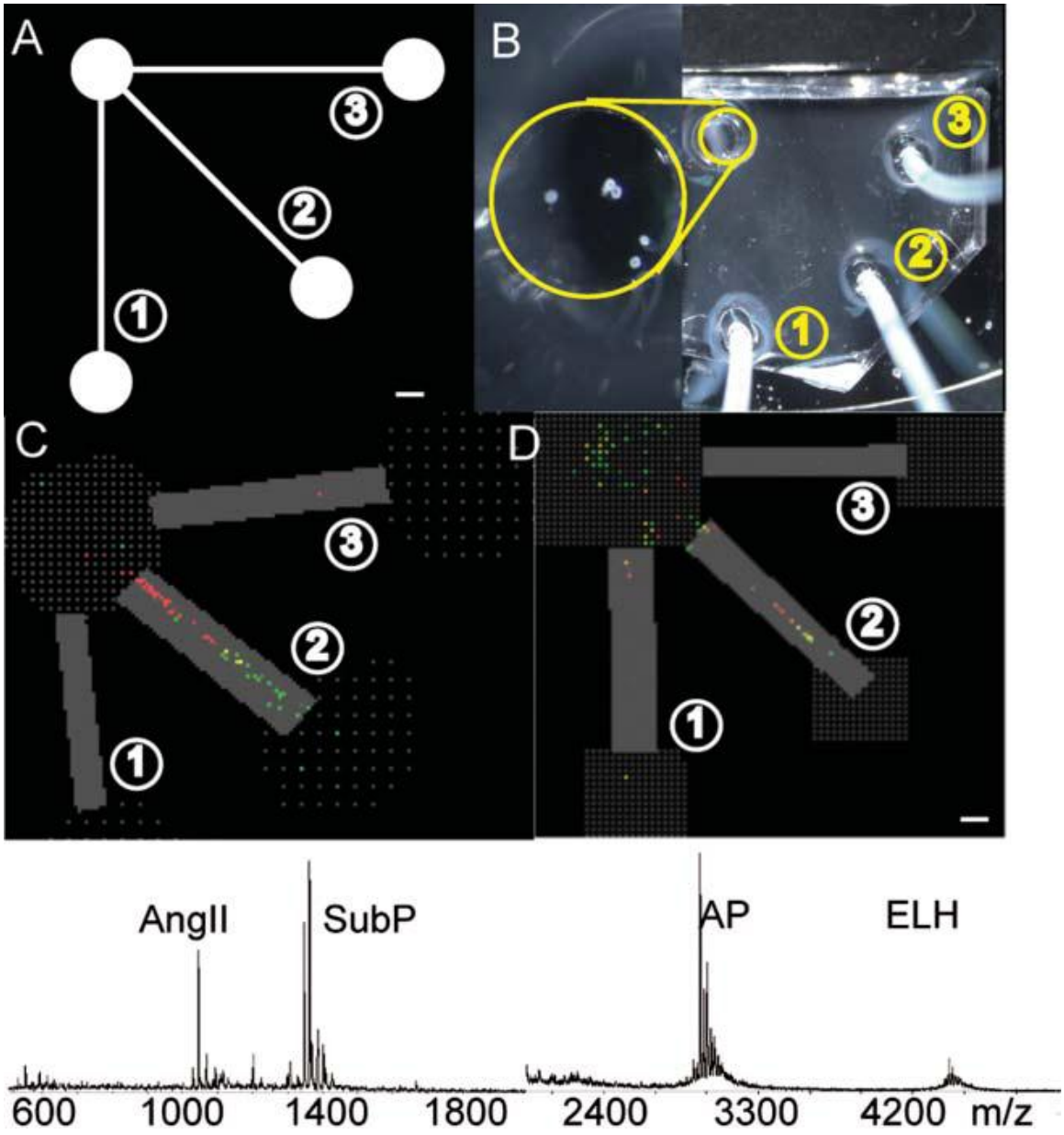

Figure 2.8 Temporal analysis of released neuropeptides from five *Aplysia* bag cell neurons stimulated using potassium. (A) Schematic of the design of the PDMS device with three sampling channels and a reservoir. Circled numbers outline the releasate sampling procedure: (1) pre-stimulation, (2) during stimulation and (3) post-stimulation. Scale bars = 1 mm. (B) Photograph of the PDMS device filled with ASW. Each

sampling channel is connected to a piece of tubing for external flow control. Left photograph is a magnified image of the reservoir containing five bag cell neurons. (C) MS image of experimental simulation of peptide release using angiotensin II (AngII), *m/z* 1046.5 (green), and substance P (SubP), *m/z* 1347.7 (red): yellow represents the presence of both AngII and SubP. A representative mass spectrum of the middle channel is shown. (D) MS image of *Aplysia* bag cell neuron release stimulated using elevated potassium: AP, m/z 2961.3 (red) and ELH, *m/z* 4385.2 (green). Yellow represents the presence of both AP and ELH. A representative mass spectrum from the middle channel surface is shown at the bottom. Reproduced by permission of The Royal Society of Chemistry.

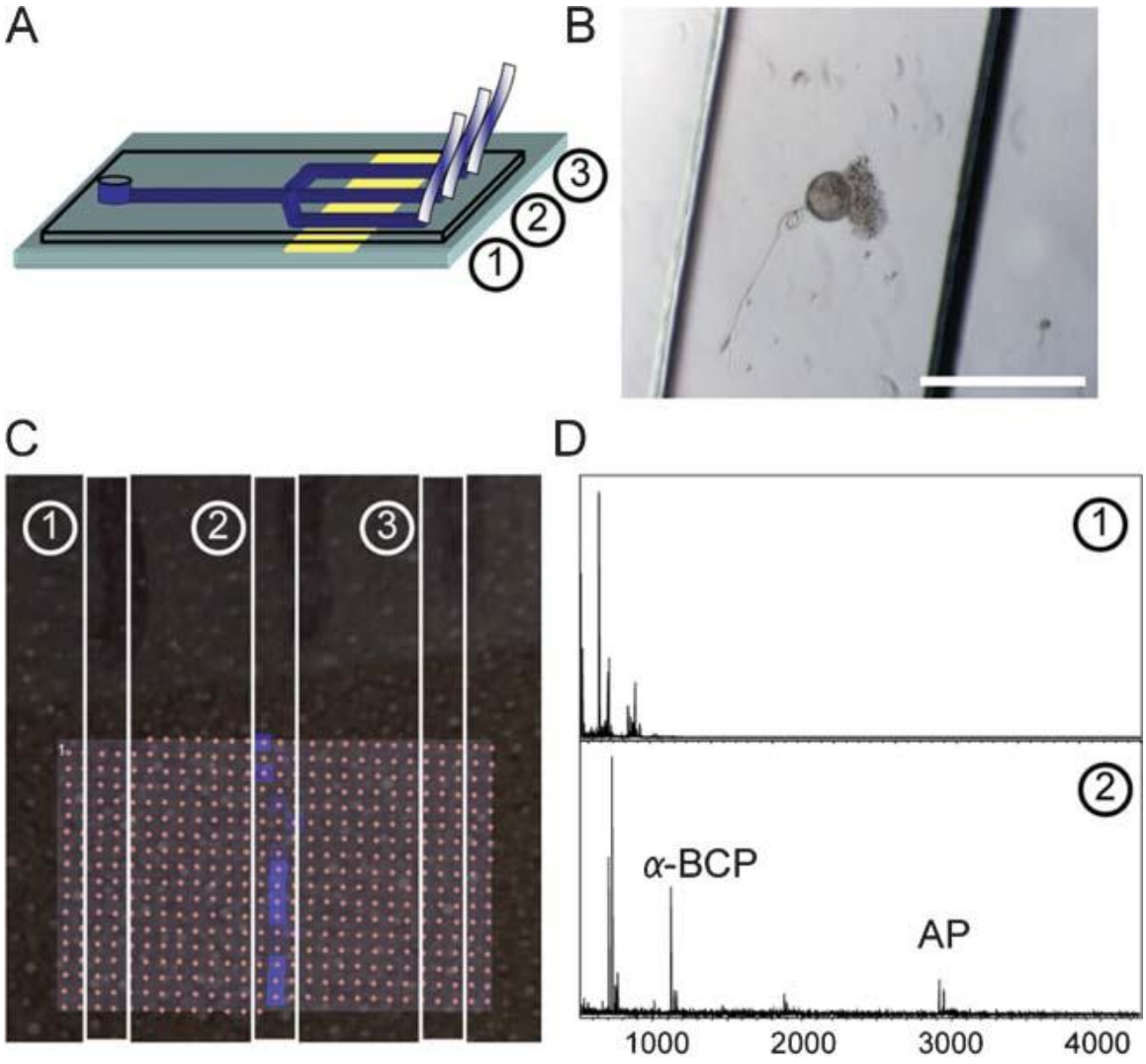

Figure 2.9 Analysis of release from a single *Aplysia* bag cell neuron. (A) Schematic of the device containing a channel for cell placement, and three channels for peptide collection. The functionalized gold surface is indicated. (B) Image of a cell in the microchannel prior to stimulation. Scale bar = 100 μm. (C) MS image of neuronal releasate from the surface collected after the experiment. AP is shown in blue. (D) Representative mass spectra of an area with (1) only matrix peaks and (2) a region with bag cell neuron releasate. Shown are AP and alpha bag cell peptide (α-BCP_{1-9}), *m/z* 1122.6. Reproduced by permission of The Royal Society of Chemistry.

2.7 References

1. G. M. Whitesides, *Nature*, 2006, **442**, 368-373.
2. M. A. Burns, B. N. Johnson, S. N. Brahmasandra, K. Handique, J. R. Webster, M. Krishnan, T. S. Sammarco, P. M. Man, D. Jones, D. Heldsinger, C. H. Mastrangelo and D. T. Burke, *Science*, 1998, **282**, 484-487.
3. L. Cai, N. Friedman and X. S. Xie, *Nature*, 2006, **440**, 358-362.
4. B. Huang, H. K. Wu, D. Bhaya, A. Grossman, S. Granier, B. K. Kobilka and R. N. Zare, *Science*, 2007, **315**, 81-84.
5. T. T. Perkins, D. E. Smith and S. Chu, *Science*, 1997, **276**, 2016-2021.
6. J. O. Tegenfeldt, C. Prinz, H. Cao, S. Chou, W. W. Reisner, R. Riehn, Y. M. Wang, E. C. Cox, J. C. Sturm, P. Silberzan and R. H. Austin, *Proc. Natl. Acad. Sci. U. S. A.*, 2004, **101**, 10979-10983.
7. E. T. Dimalanta, A. Lim, R. Runnheim, C. Lamers, C. Churas, D. K. Forrest, J. J. de Pablo, M. D. Graham, S. N. Coppersmith, S. Goldstein and D. C. Schwartz, *Anal. Chem.*, 2004, **76**, 5293-5301.
8. K. Jo, D. M. Dhingra, T. Odijk, J. J. de Pablo, M. D. Graham, R. Runnheim, D. Forrest and D. C. Schwartz, *Proc. Natl. Acad. Sci. U. S. A.*, 2007, **104**, 2673-2678.
9. Y. F. Cheng and N. J. Dovichi, *Science*, 1988, **242**, 562-564.
10. J. V. Sweedler, J. B. Shear, H. A. Fishman, R. N. Zare and R. H. Scheller, *Anal. Chem.*, 1991, **63**, 496-502.
11. A. T. Woolley and R. A. Mathies, *Proc. Natl. Acad. Sci. U. S. A.*, 1994, **91**, 11348-11352.
12. Q. F. Xue, F. Foret, Y. M. Dunayevskiy, P. M. Zavracky, N. E. McGruer and B. L. Karger, *Anal. Chem.*, 1997, **69**, 426-430.
13. R. S. Ramsey and J. M. Ramsey, *Anal. Chem.*, 1997, **69**, 1174-1178.
14. I. M. Lazar, J. Grym and F. Foret, *Mass Spectrom. Rev.*, 2006, **25**, 573-594.
15. P. Onnerfjord, J. Nilsson, L. Wallman, T. Laurell and G. Marko-Varga, *Anal. Chem.*, 1998, **70**, 4755-4760.
16. J. Liu, K. Tseng, B. Garcia, C. B. Lebrilla, E. Mukerjee, S. Collins and R. Smith, *Anal. Chem.*, 2001, **73**, 2147-2151.

17. M. L. S. Mok, L. Hua, J. B. C. Phua, M. K. T. Wee and N. S. K. Sze, *Analyst*, 2004, **129**, 109-110.
18. J. Su, M. R. Bringer, R. F. Ismagilov and M. Mrksich, *J. Am. Chem. Soc.* , 2005, **127**, 7280-7281.
19. S. S. Rubakhin, J. C. Jurchen, E. B. Monroe and J. V. Sweedler, *Drug Discov. Today*, 2005, **10**, 823-837.
20. M. L. Reyzer and R. M. Caprioli, *Curr. Opin. Chem. Biol.*, 2007, **11**, 29-35.
21. R. M. Caprioli, T. B. Farmer and J. Gile, *Anal. Chem.*, 1997, **69**, 4751-4760.
22. B. Spengler, M. Hubert and R. Kaufmann, *42nd ASMS Conference Mass Spectrom.*, 1994.
23. A. I. Gusev, O. J. Vasseur, A. Proctor, A. G. Sharkey and D. M. Hercules, *Anal. Chem.*, 1995, **67**, 4565-4570.
24. A. C. Crecelius, D. S. Cornett, R. M. Caprioli, B. Williams, B. M. Dawant and B. Bodenheimer, *J. Am. Soc. Mass Spectrom.*, 2005, **16**, 1093-1099.
25. J. Pierson, J. L. Norris, H. R. Aerni, P. Svenningsson, R. M. Caprioli and P. E. Andren, *J. Proteome Res.*, 2004, **3**, 289-295.
26. J. F. Dishinger and R. T. Kennedy, *Anal. Chem.*, 2007, **79**, 947-954.
27. J. G. Shackman, G. M. Dahlgren, J. L. Peters and R. T. Kennedy, *Lab Chip*, 2005, **5**, 56-63.
28. A. B. Hummon, A. Amare and J. V. Sweedler, *Mass Spectrom. Rev.*, 2006, **25**, 77-98.
29. J. N. Stuart, A. B. Hummon and J. V. Sweedler, *Anal. Chem.*, 2004, **76**, 121A-128A.
30. E. R. Kandel, *Behavioural Biology of Aplysia*, W. H. Freeman & Co., 1979.
31. V. F. Castellucci, E. R. Kandel, J. H. Schwartz, F. D. Wilson, A. C. Nairn and P. Greengard, *Proc. Natl. Acad. Sci. U. S. A.*, 1980, **77**, 7492-7496.
32. W. S. Sossin, J. M. Fisher and R. H. Scheller, *Neuron*, 1989, **2**, 1407-1417.
33. R. W. Garden, S. A. Shippy, L. J. Li, T. P. Moroz and J. V. Sweedler, *Proc. Natl. Acad. Sci. U. S. A.*, 1998, **95**, 3972-3977.
34. C. S. Effenhauser, G. J. M. Bruin, A. Paulus and M. Ehrat, *Anal. Chem.*, 1997, **69**, 3451-3457.

35. D. C. Duffy, J. C. McDonald, O. J. A. Schueller and G. M. Whitesides, *Anal. Chem.*, 1998, **70**, 4974-4984.
36. J. Sagiv, *J. Am. Chem. Soc.* , 1980, **102**, 92-98.
37. C. D. Bain, E. B. Troughton, Y. T. Tao, J. Evall, G. M. Whitesides and R. G. Nuzzo, *J. Am. Chem. Soc.*, 1989, **111**, 321-335.
38. D. Dagan and I. B. Levitan, *J. Neurosci.*, 1981, **1**, 736-740.
39. G. Banker and K. Goslin, *Culturing Nerve Cells*, 2nd edn., The MIT Press, 1998.
40. S. A. Schwartz, M. L. Reyzer and R. M. Caprioli, *J. Mass Spectrom.*, 2003, **38**, 699-708.
41. N. G. Hatcher, T. A. Richmond, S. S. Rubakhin and J. V. Sweedler, *Anal. Chem.*, 2005, **77**, 1580-1587.
42. J. Jing, F. S. Vilim, C. C. Horn, V. Alexeeva, N. G. Hatcher, K. Sasaki, I. Yashina, Y. Zhurov, I. Kupfermann, J. V. Sweedler and K. R. Weiss, *J. Neurosci.*, 2007, **27**, 3490-3502.
43. J. A. Jakubowski, N. G. Hatcher, F. Xie and J. V. Sweedler, *Neurochem. Int.*, 2006, **49**, 223-229.
44. K. L. Prime and G. M. Whitesides, *Science*, 1991, **252**, 1164-1167.
45. N. L. Wayne, J. Kim and E. Lee, *J. Neuroendocrinol.*, 1998, **10**, 529-537.
46. A. Scherl, C. G. Zimmermann-Ivol, J. Di Dio, A. R. Vaezzadehl, P. A. Binz, M. Amez-Droz, R. Cochard, J. C. Sanchez, M. Gluckmann and D. F. Hochstrasser, *Rapid Commun. Mass Spectrom.*, 2005, **19**, 605-610.
47. P. Fromherz, A. Offenhausser, T. Vetter and J. Weis, *Science*, 1991, **252**, 1290-1293.
48. S. Margel, E. A. Vogler, L. Firment, T. Watt, S. Haynie and D. Y. Sogah, *J. Biomed. Mater. Res.*, 1993, **27**, 1463-1476.
49. G. Fragneto, R. K. Thomas, A. R. Rennie and J. Penfold, *Science*, 1995, **267**, 657-660.

CHAPTER 3

QUANTITATION OF PEPTIDE RELEASE FROM NEURONS

3.1 Notes and Acknowledgements

This chapter was mainly adapted from a manuscript submitted to *Lab on a Chip* (Ming Zhong, Chang Young Lee, Callie Croushore and Jonathan V. Sweedler, "Label-free quantitation of peptide release from neurons in a microfluidic device with mass spectrometry imaging," submitted on November 8, 2011) The main objective here was to develop a unique method to quantify released neuropeptides in microfluidic devices based on the adsorption length measured with mass spectrometry imaging. This work was performed by several individuals and is included here for completeness. The experiments and section "Modeling the molecular adsorption and separation in microchannels" were performed by Dr. Chang Young Lee. The experiments of scintillation measurements of peptide absorption were performed by Callie Croushore. The preparation of the manuscript involved all coauthors but I took the lead in manuscript preparation. This work was supported by the National Science Foundation, Award No. DMI-0328162, the National Institute on Drug Abuse, Award No. P30DA018310, and the National Institute of Neurological Disease and Stroke, Award No. R01NS031609.

3.2 Introduction

As mentioned in Chapter 2, microfluidics has made significant contributions to analytical chemistry since the technology was first introduced.[1,2] The microfluidic devices described in the previous chapter are good examples of how the small volumes in microdevices enable handling of mass-limited samples with minimal reagent consumption, control of local microenvironments, and integration of multiple processing steps into a single system. It is not surprising that microfluidics has been broadly used to investigate low-amount analytes[3-6] and to provide promising platforms that mimic *in vivo* environments for cell-based biological studies.[7-9]

One of the challenges in this field has been the integration of microfluidic devices with information-rich detection modalities. As a detection scheme, mass spectrometry (MS) can unambiguously identify multiple analytes simultaneously from a small-volume biological sample without prior preselection. In particular, matrix-assisted laser desorption/ionization (MALDI) MS offers several advantages, such as tolerance to salts and other contaminants and spectra that are easy to interpret, making it quite useful for proteomic and peptidomic studies, including investigations of nervous system tissues.[10-12] Microfluidic systems can be readily interfaced with MALDI offline, either by depositing eluents from the device onto a MALDI target[13] or by directly using a substrate as the target.[14-16] With the development of MALDI MS imaging, spatial information can be added to the characterization process by allowing measurements of biomolecular distributions across samples.[17,18] As highlighted in Chapter 2, we demonstrated MALDI imaging from a poly(dimethylsiloxane) (PDMS) device comprised of a reservoir for accommodating cells and a derivatized surface for collecting secreted materials.[19] Direct

imaging of the surface revealed areas in the device containing both known and unknown analytes, without prior knowledge of their exact locations. Here, we adapt that earlier device to achieve improved accuracy and precision.

Although we are interested in obtaining qualitative information on the molecules present in a sample, it can also be important to know their quantity. However, MALDI is not considered quantitative because peak heights are not always directly related to the amount of analyte present.[20] The reasons for the disconnect between peak heights and analyte amounts include uneven distributions of analytes within matrix crystals, varied ionization efficiencies that depend on the molecular structure and environment, and ion suppression effects, especially from complex mixtures.[21,22] One solution is to use stable isotopic labeling, which overcomes several of the challenges of direct quantitation with MS.[23,24] For absolute quantitation, an internal standard that incorporates a heavy isotope (*e.g.*, ^{2}H, ^{13}C, ^{15}N, or ^{18}O) is added for each corresponding analyte and accurate measurements are done by comparing the intensity or area of paired peaks. For relative quantitation, peptides in two samples are differentially labeled with a distinguishable mass difference between two isotopic forms and are then combined for comparison. Stable isotopes can be incorporated into peptide molecules either through metabolic labeling[25] or by attachment with isotopic tags.[26] Owing to the development of a number of novel labeling schemes,[24,27,28] significant progress has been made in quantitative MS; it has been applied in the analysis of various biomolecules,[29-32] enabling measurement of contents from single cells.[33] However, using stable isotopic labeling within microfluidic devices presents several challenges: labeling adds multiple steps to the sample preparation process, organic labeling reagents may not be compatible with PDMS and are

toxic to live cells, and finally, the labeling reactions inevitably dilute the mass-limited samples. Therefore, a more amenable and simple quantitation strategy is needed for PDMS devices.

Here we modify an approach used in many diagnostic tests in which the length of color change along a strip is related to the amount of analyte. For example, in a home cholesterol test kit, a blood sample is drawn onto a test strip and cholesterol contained in the sample reacts with enzymes and chemicals deposited on the strip. The color of strip is changed during this reaction, and the zone of remaining cholesterol migrates further up the strip. The reaction continues until all the cholesterol is consumed. The final result is that the amount of cholesterol in the blood sample can be measured from the length of color band by using a standard conversion chart. The test is robust and offers a quantitative measurement that is independent of the viewer's color sensitivity, and is the approach adapted here. We combine this with off-line MALDI MS imaging to demonstrate that the adsorption length in a microfluidic channel is proportional to analyte amount. Because the ability of a surface to adsorb an analyte is fixed per unit length, the larger the quantity of sample, the longer the section of channel it will cover. This approach is label-free. We have adapted our prior device outlined in Chapter 2 for such measurements,[19] improving its design and implementing a more controlled solution flow. Calibration curves obtained with multiple standards show the expected linear relationship between length and amount; a model of the adsorption process supports the linear nature of length-to-amount for multiple analytes. We demonstrate the ability to measure peptide release from a small number of *Aplysia* bag cell neurons, a well-characterized

neurosecretory model,[34,35] and are able to extract absolute quantitative information for the released peptides.

3.3 Experimental

Appendix A contains a master list of all abbreviations used in this chapter.

3.3.1 Materials and Reagents

Unless stated otherwise, organic solvents were from Fisher Scientific (Fair Lawn, NJ) and all the other chemicals from Sigma-Aldrich (St. Louis, MO). The PDMS prepolymer kit, Sylgard 184, was purchased from Dow Corning (Midland, MI). Silicon wafers were obtained from WRS Materials (Spring City, PA); 2-[methoxy(polyethyleneoxy)propyl]trimethoxysilane (OEG, 90%) was from Gelest, Inc. (Morrisville, PA) and used as received. Negative photoresist SU-8 2050 and developer were obtained from MicroChem Corp. (Newtown, MA). Positive photoresist AZ 5214-E and developer were from AZ Electronic Materials Corp. (Somerville, NJ). Acidic peptide (AP) was synthesized at the Roy J. Carver Biotechnology Center (University of Illinois at Urbana-Champaign). α-bag cell peptide [1-9] (αBCP, 80%) was purchased from American Peptide Company, Inc. (Sunnyvale, CA). Angiotensin II (Ang II), (5-L-Isoleucine) [tyrosyl-3,5-^{3}H(N)] (specific activity = 50 Ci/mmol, concentration 1 mCi/mL) was from American Radiolabeled Chemicals, Inc. (Saint Louis, MO). Ultima Gold LLT liquid scintillation solution was purchased from Perkin Elmer. Filtered artificial sea water (ASW, pH 7.8) contained 460 mM NaCl, 10 mM KCl, 10 mM $CaCl_2$, 22 mM $MgCl_2$, 26 mM $MgSO_4$, 2.5 mM $NaHCO_3$, and 15 mM HEPES.

3.3.2 Substrate Derivatization

The derivatization process is illustrated in Fig. 3.1. A piece of silicon wafer was patterned with AZ 5214-E photoresist via standard photolithography so that about 2/3 of the bare silicon was exposed. The patterned substrate was dipped in a mixture of 15 mL chloroform and 35 mL hexane with octadecyltrichlorosilane (OTS, 0.8% v/v) for 10 min and then in hexane for 10 min, as modified from previous procedures.[19,36] The chip was rinsed with acetone to remove the photoresist and dried at 70 ℃ for 3 h. The partially derivatized surface was immersed in 50 mL toluene containing OEG (0.8% v/v) overnight, followed by immersion in toluene for 1 h, rinsing with methanol, and drying at 70 ℃ for 2 h.[37,38] Substrates were rinsed with methanol and water sequentially and dried with nitrogen directly before use.

3.3.3 Device Fabrication

Microfluidic devices consisted of PDMS with channel features sealed onto derivatized silicon substrates. The PDMS pieces were formed by molding Sylgard 184 onto a photolithographically patterned SU-8 master. Small pieces of silicone tubing (Helix Medical, LLC, Carpinteria, CA) were glued onto SU-8 features that served as device outlets.[39] The PDMS prepolymer was then poured onto the master and cured at 70 ℃ overnight. The inlet reservoir was made with an AcuPunch (Acuderm, Inc., Ft. Lauderdale, FL) biopsy punch of 1.5 mm diameter. To reduce sample loss to the PDMS material, the channels were sequentially treated with 5:1:1 H_2O:HCl:H_2O_2 for 5 min, H_2O for 5 min, OEG for 30 min, and finally flushed with 500 μL of deionized (DI) water (Milli-Q Biocel, Millipore Corporation, Billerica, MA) to yield OEGylated PDMS, as

described previously.[40] For plasma treatment, the PDMS was subjected to oxygen plasma for 30 s at 100 W with a March Plasmod (March Instruments, Concord, CA) oxygen plasma system and stored in DI water for future use. Extracted PDMS was prepared according to the previous procedure.[41] Prior to use, PDMS pieces were rinsed with methanol and water and dried with nitrogen.

3.3.4 Scintillation Measurements of Peptide Absorption

The radiolabeled Ang II was diluted to 1 pmol/μL with DI water, and 2 μL aliquots of the solution were incubated for 4 h in microchannels made of five different types of PDMS: native, plasma-treated, extracted, OEGylated, and OEGylated extracted. Incubated solutions were pushed out of each device through polytetrafluoroethylene tubing (Cole-Parmer Instrument Company, Vernon Hills, IL) and into microcentrifuge tubes. The devices were then rinsed with 2 μL of DI water and the rinsing solution was pushed into the same microcentrifuge tube. The combined Ang II and rinse solutions were pipetted into a 20 mL glass scintillation vial; 5 mL aliquots of liquid scintillation solution were added to each vial and counted with a liquid scintillation counter (Beckman LS 6500, Beckman Coulter, Inc., Brea, CA); 2 μL aliquots of the Ang II solution before incubation were also measured as a control.

3.3.5 Standard Peptide Calibration Experiments

AP and αBCP were used as received and dissolved in ASW to various concentrations (1–10 pmol/μL) for storage. The outlet tubing of the PDMS device was connected to a 25 μL syringe (Hamilton Company, Reno, NV) controlled by a Harvard

PHD 2000 syringe pump (Harvard Apparatus, Holliston, MA) set at the refill mode. For calibration with a single peptide, a desired amount of AP was loaded into the inlet reservoir and pulled through the channel to the outlet at the rate of 0.1 μL/min. For multiple peptide experiments, AP and αBCP were mixed in the inlet prior to assay. Three or more individual samples were tested for each amount, and the mean and standard error of adsorption length were calculated. The best-fit straight lines for adsorption length versus amount were obtained.

3.3.6 Cell Experiments

Aplysia californica (100–150 g, National Resource for *Aplysia*, Miami, FL) were anesthetized by injecting 390 mM of $MgCl_2$ solution equal to 1/2 of each animal's body weight. The abdominal ganglia with adjacent nerves were dissected and incubated in ASW containing 10 mg/mL protease from *Streptomyces griseus* at 34 ℃ for 90 min, modified from previous experiments.[42] This treatment facilitated removal of the connective sheath tissue around the ganglia and isolation of individual neurons. After washing with fresh ASW, individual bag cells were isolated and plated into the inlet chamber of a microfluidic device. Cells were allowed to attach to the substrate for at least 1 h and then stimulated by adding an elevated KCl solution (final concentration 55 mM). Following a 15 min incubation, released peptides were collected onto the OTS-functionalized surface by transporting the extracellular media with the syringe pump. The pump was stopped right before the inlet reservoir became completely empty and the remaining liquid was removed. The flow was then resumed until the solution in the channel was depleted.

3.3.7 MS Imaging

After peptide collection, the PDMS was peeled off of the silicon substrate. A MALDI matrix, 2,5-dihydroxybenzoic acid (DHB, 10 mg/mL in 50%/50% acetonitrile/water), was sprayed onto the surface with an airbrush (Paasche Airbrush Company, Chicago, IL) placed at a distance of ~15 cm. The substrate was then taped onto a modified target plate and MALDI characterization was performed with a Bruker UltrafleXtreme time-of-flight (TOF) mass spectrometer (Bruker Daltonics, Inc., Billerica, MA) in the reflectron mode. MS images were obtained at 100 or 200 μm resolution with each spot summed from 200 laser shots. Mass calibration was done with peptide calibration standard II (Bruker Daltonics). The images were analyzed with flexImaging software (Bruker Daltonics), with the threshold value for analyte detection set at 10% of the maximum intensity on the OTS surface. Individual mass spectra were analyzed with FlexAnalysis (Bruker Daltonics) and replotted with Origin, version 8.5 (OriginLab Corporation, Northhampton, MA).

3.4 Results and Discussion

3.4.1 Minimizing Peptide Losses to PDMS

Our goal was to design a device that allows the efficient collection of the media around cultured cells and its subsequent characterization via off-line MS. Because of the small scale of the fluidics, there is a large surface-to-volume ratio and so surface loss becomes a significant concern. Obviously, peptides that either partition into or adsorb onto surfaces in the culturing chamber or fluidic channels cannot be measured via MS

and are lost. Hence, we carefully minimized sample losses using surface derivatization protocols and then characterized those losses using sensitive radionuclide detection.

In order to minimize partitioning of the molecules into the PDMS material, its chemical properties have to be optimized. This includes adsorption due to the hydrophobicity of PDMS, and the even the diffusion of uncrosslinked oligomers and remaining platinum catalysts into bulk channel solutions.[41,43,44] Several surface treatment protocols have been employed in the past. Oxygen plasma treatment is a widely-used method that renders PDMS hydrophilic, making it more amenable to aqueous solutions.[45] PDMS extraction, which consists of a series of solvent washes to remove the uncured oligomers and remaining platinum catalysts used to cure the polymer, significantly improves cell viability in low-density cultures.[41] OEGylation, by derivatizing the PDMS surface with OEG, has been shown to reduce protein absorption and to provide more hydrophilic channels.[38,40] By measuring the amount of peptide lost by our devices with these treatments, we obtain a more accurate measurement of total peptide release from the neurons.

We measured these losses using radionuclide detection because of its low detection limits and absolute quantitation abilities. We incubated ^{3}H-labeled Ang II in a PDMS device containing 1 mm diameter reservoirs and a straight channel (200 μm wide, 100 μm high, 10 mm long), and then measured the loss of peptides from the surface-treated PDMS materials compared to the native. Recovered peptides from the native, plasma-treated, extracted, OEGylated and OEGylated extracted PDMS were quantified. Fig. 3.2 shows the signal from radiolabeled Ang II recovered from each type of PDMS compared to non-incubated solutions. Approximately 50% of the peptide was recovered

from native, plasma-treated, and extracted PDMS; whereas recovery of 70–75% was observed for OEGylated and OEGylated extracted PDMS, indicating a significant reduction in loss upon OEG treatment ($p < 0.05$, refer to Fig. 3.2). Furthermore, although the absorption of Ang II into the extracted PDMS (and also the plasma-treated one) was not appreciably different from the native PDMS ($p = 0.90$), absorption was significantly reduced ($p < 0.001$) when the extracted PDMS was OEGylated. While OEG treatment did not eliminate sample loss, it certainly reduced it. There was no significant difference ($p = 0.35$) between the OEGylated and OEGylated extracted PDMS. Therefore, OEGylated PDMS was utilized here; however, the combined OEGylated and extracted PDMS will be explored in future studies as it may aid cell viability. Peptide losses also depend on specific device dimensions, possibly making these treatments even more important for the smaller scale and longer serpentine channels explored below.

3.4.2 Minimizing Peptide Losses to Reservoir

In a microfluidic device, the area of a reservoir is significant compared to the area under the microchannel. For example, a circular reservoir with a diameter of 1.5 mm is equal to a 9 mm long channel with a width of 200 μm in terms of area. Therefore the loss of peptides into the reservoir is significant if the reservoir area is also able to adsorb peptides. The MS images in Fig. 2.4 and 2.5 show that strong signals were detected inside the reservoir, when the microfluidic device with a serpentine channel was used to sample different amounts of standard peptides, Ang II and substance P. The entire substrate of the device was coated with OTS. In order to reduce the nonspecific adsorption at the reservoir, the surface there needs to be nonadhesive to peptides.

Different methods were tested to pattern the substrate with the reservoir area resistant to peptide adsorption and the rest of area OTS-coated. In one method, an assembled device containing the PDMS with an open inlet and the OTS substrate was treated with oxygen plasma at 100 W for 30 s (Fig. 3.3A). With oxygen plasma treatment, the OTS layer was removed to expose the silicon surface. As only the reservoir was open to the air, that area would be deprived of OTS specifically. Fig. 3.3B shows a microscopic image of the surface after plasma treatment; the reservoir area appeared distinct from the other part. Because of the different hydrophobicity of silicon and OTS, water only wetted the reservoir (Fig. 3.3C). However, it was found that the silicon surface can also adsorb peptides. Moreover, the plasma penetrated into the channel and reacted with OTS there, causing nonconsistent results in terms of peptide adsorption. Another method was to partially coat the silicon substrate with OTS by dipping about 2/3 of the substrate into the OTS solution. The partial coating resulted in an evident boundary between silicon and OTS (Fig. 3.4A) and a difference in hydrophobicity of these two areas (Fig. 3.4B). The PDMS piece with the channel was then aligned with the boundary to ensure that the reservoir was on top of the silicon surface. However, because silicon could also capture peptide molecules, as mentioned above, this method was not able to reduce nonspecific adsorption.

The self-assembled monolayer (SAM) of alkanethiol on gold has different chemical properties based on its end functional group and is widely used for surface patterning. An OTS surface can be partially coated with gold by using a PDMS piece to block a portion of the surface. The gold part was then coated with a SAM of oligo(ethylene glycol) ((11-Mercaptoundecyl)tetra(ethylene glycol), abbreviated as OEG)

that prevents the adsorption of biomolecules. As a result, a surface patterned with OEG and OTS was formed. The effectiveness of OEG layer was first tested on a microfluidic device on a surface completely coated with OEG (Fig. 3.5A). In this device, 2 ng substance P was flowing through the channel. The MS image in Fig. 3.5B shows essentially no signals detected in the channel (substance P was visualized in the orange color). In a device with a partial gold coating (Fig. 3.5C), the PDMS was aligned with the boundary on the substrate so that the reservoir was on the gold side. 3 ng substance P was introduced into the system. No significant signals were detected in the channel on the OEG-coated gold, while strong signals were on the OTS side (Fig. 3.5D). The results demonstrate the capability of OEG to prevent peptide adsorption. Peptide signals in the reservoir were likely from the residual peptides left behind when the liquid in the reservoir was dried out.

The partial gold coating method is effective in reducing nonspecific adsorption, but gold deposition adds additional processing steps to chip fabrication and increases the cost. We modified this approach by utilizing a positive photoresist and OEG-silane instead, as depicted in Fig. 3.1. The photoresist was used to block a certain area of the silicon substrate and the OEG group was attached onto the substrate through silanization reaction. The detailed fabrication procedure was described in Section 3.3.2 above and the effectiveness of this treatment will be demonstrated in the next section.

3.4.3 Device Design and Fabrication

Our microfluidic device contains a serpentine channel (200 μm wide, 50 μm high, 110 mm long) with inlet and outlet ports (Fig. 3.6). The dimensions of the channel permit

a stable flow at the rate of 50 nL/min to 5 μL/min. Silicone tubing embedded into the PDMS structure ensures a good seal at the outlet and thus, stable liquid flow. The cell culture/sampling chamber is the inlet to the device; a diameter of 1.5 mm was optimal for ease of liquid handling and cell loading as well as minimizing sample losses that occur with too large an inlet reservoir. Fig. 3.7 compares the adsorption length of 3 pmol AP with different inlet sizes. The test was performed in a microfluidic device with a simple straight channel (200 μm width, 50 μm height, 30 mm length) on the OTS silicon substrate. Compared to the 2 mm diameter (Fig. 3.7A), the same amount of peptide covered a longer segment of channel with the 1.5 mm inlet (Fig. 3.7B), indicating a decrease in sample loss to the reservoir. By gluing a capillary (Polymicro Technologies, Inc.) onto the inlet feature of the SU-8 master before pouring the PDMS prepolymer, a void equal in size to the outer diameter of the capillary (370 μm) was formed after PDMS was cured and the capillary was removed. The longest adsorption length was achieved at this inlet size (Fig. 3.7C). However, it became very difficult to add liquid or load cells into the inlet when the reservoir diameter was 1 mm or less. In this case, the solution had to be added on top of the inlet, and be drawn into the inlet and channel by applying a negative pressure at the outlet. During this process, some liquid might not have been introduced into the channel, as the surface around the inlet was not completely flat, causing inconsistent sample loss and variation in adsorption length measurements between different experiments. Based on these considerations, the 1.5 mm inlet size was used for the following calibration and cell release experiments.

We divided the substrate into two regions, each with different surface chemistries. About 2/3 of the silicon substrate underneath the channel is functionalized with OTS for

peptide collection.[46,47] The other 1/3 is functionalized with our OEG treatments to reduce peptide losses from the sampling/inlet chamber. The PDMS device is carefully aligned with the OTS-OEG boundary, as shown in Fig. 3.6.

The effectiveness of OEG to reduce peptide adsorption is demonstrated in Fig. 3.8. In the two devices in Fig. 3.8A and B, the OTS-OEG boundary was aligned to intersect with channels in different directions. 5 pmol AP was added to the inlet reservoir and the solution was transported through the channel. Fig. 3.8A and B show the resulting MS images, with AP signals visualized in yellow. Essentially no AP signals were detected in the channel on top of OEG, indicating the excellent capability of OEG to repel adsorption of peptide molecules. In contrast, significant AP signals were detected on the OTS side. There were still AP signals in the inlet, most likely from residual peptides left behind as the liquid dried in the reservoir. The capability of OEG was further confirmed by comparing the adsorption length and intensity profile of 5 pmol AP in two devices with the surface coated with OTS completely and the OTS-OEG surface respectively. The MS images are shown in Fig. 3.8C and D, in which the signal intensity of AP at each spot is visualized in a rainbow color gradient. The white indicates the highest intensity, while the dark blue the lowest. In the OTS surface, strong signals were detected inside the reservoir, while the signals there were weaker on the patterned surface. The adsorption length on the OEG-OTS surface was much longer than the OTS surface, indicating that OEG is indeed efficient in preventing nonspecific adsorption.

3.4.4 Modeling the Molecular Adsorption and Separation in Microchannels

Before using the device to quantify peptides and to gain insight into the device design and operation, we developed a simplified kinetic model to describe the molecular adsorption in the microfluidic device. Consider a plug of analytes (A) with a width (W) of 200 μm, length (L) of 200 μm, and height (H) of 10 μm. The plug flows through a 10 cm-long microchannel at a linear velocity of v (Fig. 3.9A). The channel is divided into 200 μm-long segments of the same size as the plug (total 500 segments). In each segment the analytes are allowed to adsorb irreversibly onto adsorption sites (θ) at the bottom surface, occupying Aθ sites, with the adsorption rate constant k_A for the time period of τ = L/v.

$$A + \theta \xrightarrow{k_A} A\theta \tag{3.1}$$

The total number of binding sites is constant and determined by the surface area (W × L) and the size of the A molecule (assumed 1 nm for this study). From the site and material balance:

$$[\theta]_T = [\theta] + [A\theta] \tag{3.2}$$

$$[A]_O = [A] + [A\theta] \tag{3.3}$$

where $[\theta]_T$ and $[A]_o$ represent the total binding sites in a segment and the concentration of A when entering each segment, respectively. We assume a bimolecular elementary reaction, monolayer adsorption, no interaction between analytes, and no surface migration of analytes. Therefore, the adsorption rate is

$$\frac{d[A\theta]}{dt} = k_A[A][\theta] = k_A([A]_O - [A\theta])([\theta]_T - [A\theta]) \tag{3.4}$$

Upon completion of the reaction in a segment, the plug then discretely moves to the next segment where further adsorption takes place. The process repeats until the analyte plug migrates along the entire channel length.

The solutions are obtained for an initially clean substrate using ODE solvers in MATLAB, and Fig. 3.9B shows the surface coverage of the analyte ($[A\theta]/[\theta]_T$) versus channel distance for amounts ranging from 1 pmol to 30 pmol. k_A = 10000 $M^{-1}s^{-1}$ and v = 2.5 mm/s are used, and a coverage of 1 indicates saturation. The length covered by an analyte increases with amount. The linear result of length versus amount supports our concept of quantitation. When this sample is analyzed using MS imaging, the signal intensity is related to the surface coverage. We find that using the end point of the analyte band (i.e., adsorption length), rather than fitting the MS intensity profile directly to the model, is a robust measure for quantitation. Here we defined the threshold surface coverage above which the presence of analytes can be detected with MALDI to be 0.1. With this criterion the adsorption length versus amount is plotted at v = 2.5 mm/s for k_A values of 5000 $M^{-1}s^{-1}$, 10000 $M^{-1}s^{-1}$, and 50000 $M^{-1}s^{-1}$ (Fig. 3.9C). The adsorption length is linearly proportional to the amount, and turns out to be insensitive to k_A. The result suggests that our quantitation method, the amount-to-length conversion, can be applied to peptides with different adsorption characteristics.

For a given device design and a system to be analyzed, the only parameter under external control is flow rate. Understanding the effect of flow rate thus aids in obtaining reliable quantitation. In Fig. 3.9D, the surface coverage for 10 pmol is plotted at a linear velocity of 0.83 mm/s to 42 mm/s, which corresponds to 0.1 μL/min to 5 μL/min for continuous feed (k_A = 10000 $M^{-1}s^{-1}$). To fully utilize the adsorption capability of the

substrate, the flow rate should be low so that the convection timescale remains longer than the reaction timescale ($\tau > 1/k_A C_A$), where C_A denotes initial analyte concentration. When this condition is met, the adsorption length is insensitive to the flow rate and varies only with the amount of analytes, as shown in Fig. 3.9E.

For a mixture of analytes with different adsorption rate constants, a separation between them is expected due to their differential adsorption. We made several simplifying assumptions here. We assumed that each adsorbate molecule (A, B, and C) occupy the same area of 1 nm × 1 nm, and differ only by adsorption rate constants. The number of analyte binding sites per segment (200 μm × 200 μm) is therefore 4×10^{10} with 500 segments along the 10 cm-long channel. The size may be varied depending on the analytes of interest.

Consider adsorption of two analytes A and B. When two analytes adsorb onto the substrate, the adsorption is competitive between the two.

$$A + \theta \xrightarrow{k_A} A\theta \tag{3.5}$$

$$B + \theta \xrightarrow{k_B} B\theta \tag{3.6}$$

Using the site and material balance:

$$[\theta]_T = [\theta] + [A\theta] + [B\theta] \tag{3.7}$$

$$[A]_O = [A] + [A\theta],\ [B]_O = [B] + [B\theta] \tag{3.8}$$

the adsorption rate can be described:

$$\frac{d[A\theta]}{dt} = k_A[A][\theta] = k_A([A]_O - [A\theta])([\theta]_T - [A\theta] - [B\theta]) \tag{3.9}$$

$$\frac{d[B\theta]}{dt} = k_B[B][\theta] = k_B([B]_O - [B\theta])([\theta]_T - [A\theta] - [B\theta]) \tag{3.10}$$

The coupled differential equations can be solved for an initially clean surface ($[A\theta] = [B\theta] = 0$ at $t = 0$), and the solutions are plotted in Fig. 3.9F. We used the *ode15s* function in MATLAB (MathWorks, version 7.12, R2011a) to solve the coupled ordinary differential equations. $[A]_o$ and $[B]_o$ in each segment are determined based on the amount of A and B consumed by the previous segment. Consider 5 pmol each of A and B with adsorption rate constants $k_A = 10k_B = 100000\ M^{-1}s^{-1}$. The adsorption is now competitive between the two. When the analyte plug flows down the channel, preferential adsorption of A occurs, followed by adsorption of B as A in the solution is depleted. The result is two distinct analyte bands (Fig. 3.9F). The same principle applies to a mixture of three different analytes (5 pmol each of A, B, and C) as shown in Fig. 3.9G. The adsorption kinetics of the three analytes were obtained in a similar manner by solving three coupled differential equations. The parameters used in Fig. 3.9G are $k_A = 10k_B = 100k_C = 100000\ M^{-1}s^{-1}$ and $v = 0.83$ mm/s. In the actual experiments, analytes are continuously supplied to the channel as a long band rather than a plug, and a thin layer chromatography-like separation occurs as the mobile phase drives the adsorbates. This separation mechanism is not discussed further.

3.4.5 Validation of the Model with a Single Standard

Next, we experimentally validated our model using two neuropeptide standards, AP (*m/z* 2959.6) and αBCP (*m/z* 1122.6), two well-characterized peptides released from *Aplysia* bag cells and cleaved from the same egg laying prohormone.[48] We first performed the calibration experiments with only AP to determine optimized conditions. The flow rates of 0.1 and 0.05 μL/min and analyte concentrations of 1 and 0.5 pmol/μL

were tested with the same amounts of AP. As suggested by the model, the detected adsorption length was insensitive to the analyte concentration and the flow rate at 0.1 μL/min and below where $k_A C_A \tau > 1$ (Fig. 3.10). Therefore, the flow rate of 0.1 μL/min was used for subsequent experiments to minimize experimental times. The reproducibility of length measurements was tested in different devices with the same amount of 10 pmol AP. As shown in Fig. 3.11, the measured length remains essentially constant in all three devices. The mean of measured length is 28.3 mm. and the standard error of the mean (s.e.m.) is 0.7 mm. The variance of length measurement, defined as the ratio of s.e.m. to mean, is below 3%. The results demonstrate the robustness of our quantitation method.

Peptide standards (1, 3, 5, 10, or 15 pmol AP in ASW) were then added into the reservoir and pulled through the channel. The resulting MS images in Fig. 3.12A show the adsorbed AP, with AP signals visualized in yellow. A representative mass spectrum is shown in Fig. 3.12B. These images clearly demonstrate that the adsorption length increased proportionally with the amount of peptide introduced. Despite the large intensity fluctuation at individual pixels within the MS image, the signal remains obvious throughout until the front of the band. The observed profile well matches the model's predictions shown in Fig. 3.9B, suggesting the saturation of adsorption sites except for the band boundaries. A calibration curve (Fig. 3.12C) plotting the adsorption length of AP versus its amount shows a good linearity within the tested range (R^2 = 0.97). The variance of length measurement, defined as the ratio of standard error of the mean (s.e.m.) to mean, is from 3% to 12% from distinct microfluidic devices. The small negative intercept of the fit line is primarily due to sample lost to the sampling chamber. Indeed,

we detected AP signals in the inlet reservoir even with OEG functionalization. However, when the AP solution was pulled through the channel above the OEG-functionalized surface, no AP peaks were detected, demonstrating the ability of OEG to prevent peptide adsorption. Therefore, the signals in the inlet were unlikely from peptide adsorption, but most likely from residual peptides left behind as the liquid dried in the reservoir. It is possible that the presence of an inlet contributed to the variance of measured length, but the linear length-amount relationship indicates that this is not a large effect. The slope of the calibration equation suggests that the AP occupies 2.8 mm of channel length per pmol, equaling to a surface coverage of 1.8×10^2 pmol/cm^2. As indicated in Chapter 2, we previously measured the value of Ang II as 33 pmol/cm^2.[19] Peptide adsorption properties depend on chemical structure and polarity;[49] the slight differences in surface coverage for AP and Ang II are expected.

By plotting the signal intensity at each spot with the distance from the inlet, we can obtain an intensity profile of a peptide along the channel. The intensity profile of 10 pmol AP is shown in Fig. 3.13. The profile shows a large variation of signal intensity recorded with MALDI along the channel, demonstrating the nonquantitative nature of MALDI. However, a general trend is evident as indicated with a red guidance line in Fig. 3.13. This trend is consistent with the coverage profile predicted by the mathematical model shown in Fig. 3.9B, with saturated coverage of peptides along the whole band expect partial coverage at the end. In all, experiments on AP demonstrate that quantitation based on the adsorption length is feasible.

3.4.6 Validation of the Model with Multiple Standards

As mentioned previously, neurons often secrete multiple peptides during stimulation and MS can characterize each. Thus, we wanted to determine whether two peptides can be simultaneously measured and if the linear length-to-amount relationship is still maintained. We tested our device by mixing AP and αBCP in the reservoir; the amount of AP was fixed at 3 pmol and αBCP varied from 1 to 15 pmol. MS images for each amount of αBCP are shown in Fig. 3.14A, with yellow spots for AP and green for αBCP. For each sample tested, two distinct bands were clearly visible. A representative mass spectrum for each band is shown in Fig. 3.14B, confirming that these two peptides were separated. Based on our model and the fact that AP deposited first on the channel, it appears that AP has a higher adsorption than αBCP. From each image, the adsorption length of the αBCP band was measured, and the calibration curve for length versus amount (Fig. 3.14C) demonstrates a linear relationship ($R^2 = 0.98$) in the tested sample range. The variance of length measurement is in the range of 3 to 8%. From the slope of the linear fit, the surface coverage of αBCP was calculated as 1.6×10^2 pmol/cm^2, close to the value of AP. The small positive intercept of the straight line was likely caused by the variance in length measurement. The series of MS images also indicate that the length of 3 pmol of AP remained essentially constant, suggesting that the changing amounts of other analytes have limited influence on the band length. This was further confirmed by fixing the amount of αBCP at 3 pmol and varying AP from 1 to 5 pmol; the resulting αBCP bands were of constant length, and the length of AP was the same as the corresponding length when αBCP was not present (Fig. 3.15). Therefore, this quantitation method is applicable when more than one analyte is present. Moreover, because each of

the above experiments was done on a different device, the reproducibility of imaging profiles demonstrates the robustness of our measurement platform.

3.4.7 Measuring Neuronal Release

Aplysia bag cell neurons, located in the abdominal ganglion, are commonly used as a model to study activity-dependent neurosecretion. They were used in this study to document the capability of our approach for quantifying peptide release from neurons. When the surrounding KCl concentration is elevated, the membrane is depolarized, leading to the release of several peptides that originate from egg laying prohormone.[35,50] Previous studies used intact abdominal ganglia placed in perfusion systems and the secreted peptides in the perfusate were quantified by HPLC[51] or radioactivity.[50,52] The results showed high variability in the amounts of peptides released from different ganglia, but on average, the amount of each peptide from a single bag cell was in the upper femtomole range, assuming about 400 bag cells per ganglion. Compared to perfusion systems, microfluidic devices more efficiently collect the extracellular environment with minimal sample loss, and allow more precise timing of chemical stimulations. Here, 15 cells were loaded into the sampling chamber (Fig. 3.16A), and control experiments analyzed the media surrounding the cells without KCl stimulation. An MS image of a control is presented in Fig. 3.16B, in which yellow indicates AP and green, αBCP. The peptide signals in the reservoir were due to cell lysis occurring when the chamber was dried. No peptide signals associated with bag cell stimulation were detected there, indicating that the lysis products did not enter the channel. A representative mass spectrum from the channel area of the control device is shown in Fig. 3.16D. When the

cells were treated with 55 mM KCl for 15 min, the peaks for AP and αBCP were detectable in the channel (Fig. 3.16C and 3.16D). Both peptides were detected as separate, distinct bands, and their identities confirmed via MS. Based on the measured lengths and the calibration equations obtained with standards, the amount of AP released from 15 bag cells was estimated to be 2.3 ± 0.4 pmol, and αBCP, 1.9 ± 0.9 pmol (mean ± s.e.m., from 3 samples), meaning that the average isolated cell *in vitro* released 0.15 ± 0.03 pmol of AP and 0.13 ± 0.06 pmol of αBCP. These values are consistent with the femtomole release expected from a single cell.[51,52] The results presented here validate our approach for quantifying peptide release from a microfluidic device based on the adsorption length measured using MS imaging.

3.5 Conclusions

Microfluidics is receiving greater attention in analytical chemistry because of its ability to perform low-volume manipulations and work with samples such as cells. At the same time, MS has become the preferred technology for peptidomics and proteomics measurements. By combining MS with a microfluidic sampling system, we have successfully developed an off-line approach for quantifying the media located around cells for neuropeptides. The adsorption-length-based approach takes advantage of the imaging capability of MALDI while avoiding the challenges of conventional signal-intensity-based quantitation by offering a simple, robust and label-free solution for quantitative studies. Validated using peptide standards and releasate from *Aplysia* bag cell stimulation, this approach is flexible and can be adapted to many other molecular classes in addition to neuropeptides. Future work will use more complex devices with

multiple channels and collection areas so that our analyses will include monitoring multiple secretion events with time and/or spatial resolution and comparison of releasate under different physiological conditions.

3.6 Figures

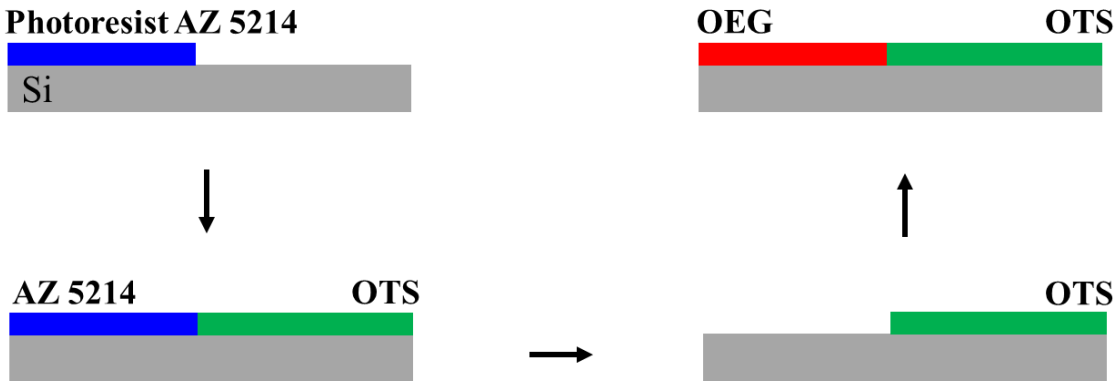

Figure 3.1 Fabrication process of a silicon surface patterned with OTS and OEG. A positive photoresist AZ 5214 is used to block certain area of the silicon surface from OTS treatment.

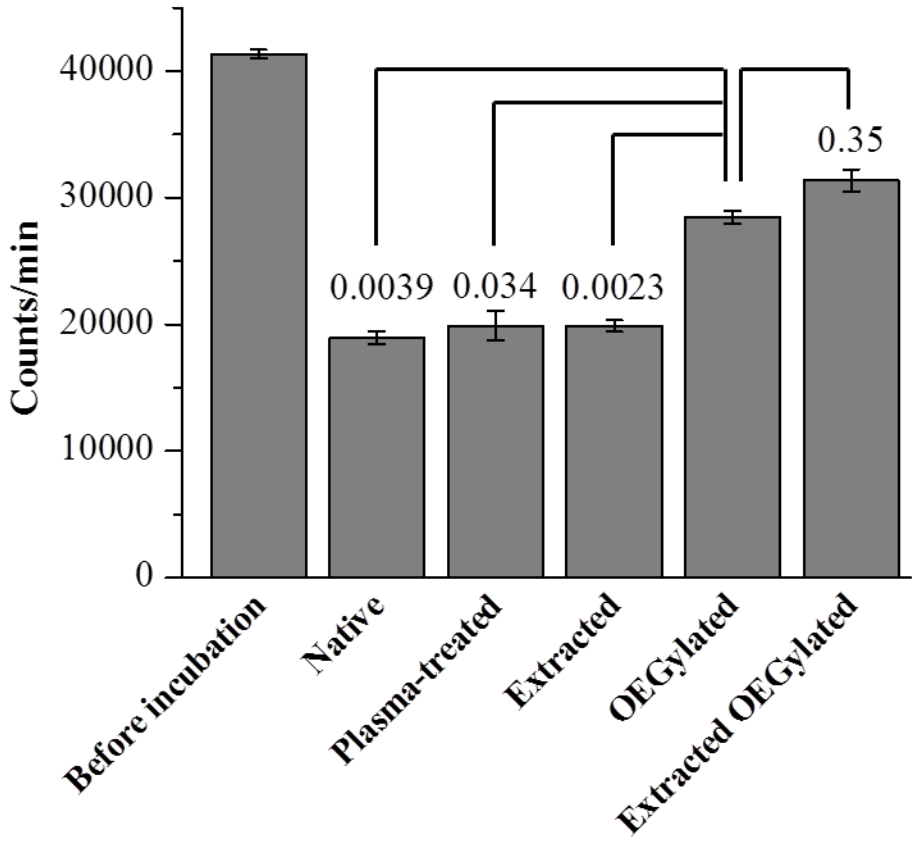

Figure 3.2 Radiolabeled Angiotensin II peptide recoveries following 4 h incubations from PDMS subjected to different treatments, as well as the control solution before incubation. The p-values comparing peptide recovery from OEGylated PDMS to other types of PDMS are listed above each corresponding bar; the significance ($p < 0.05$) demonstrates the ability of OEG to reduce peptide absorption. Error bars represent s.e.m.

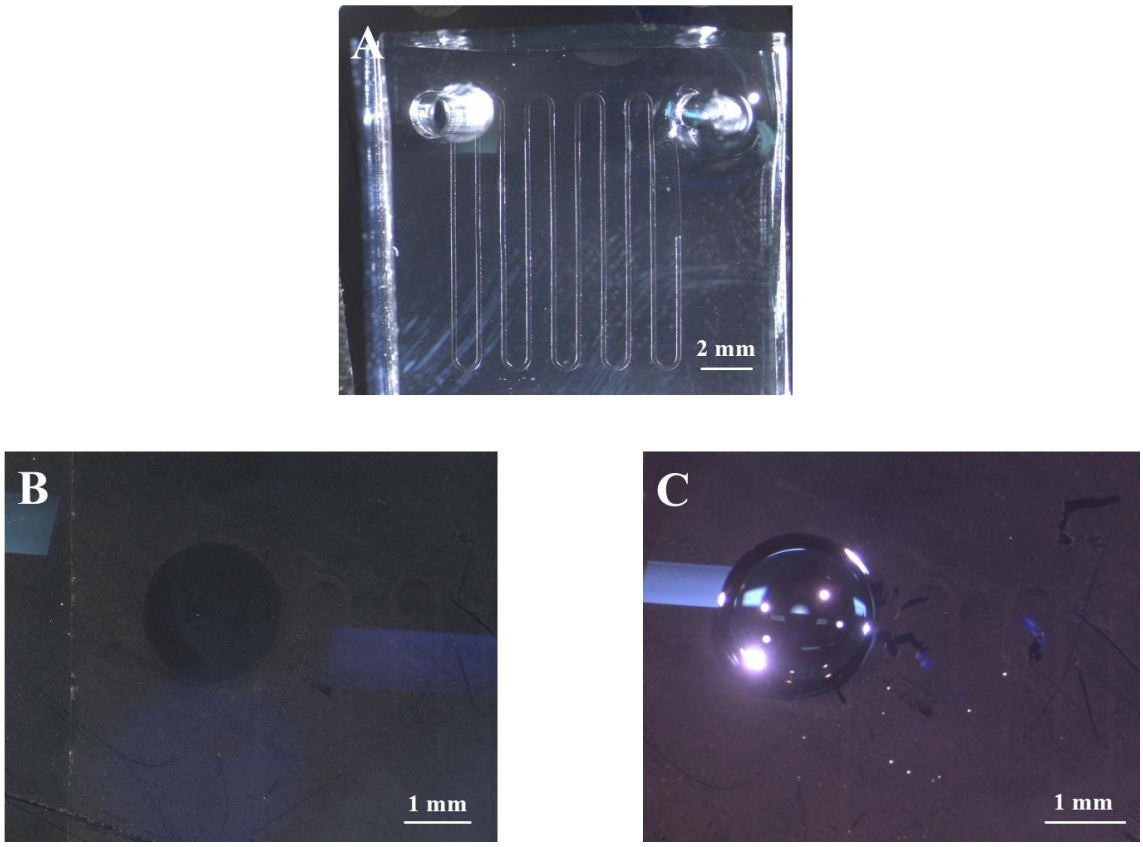

Figure 3.3 Removal of OTS in the reservoir with oxygen plasma treatment. (A) A PDMS chip with an open reservoir was placed on top of an OTS-coated silicon substrate. The whole device was subject to oxygen plasma treatment. (B) A microscopic image of the substrate after plasma treatment. The reservoir area was distinct from the rest area. (C) Water only wetted the reservoir area as it was more hydrophilic than the OTS surface.

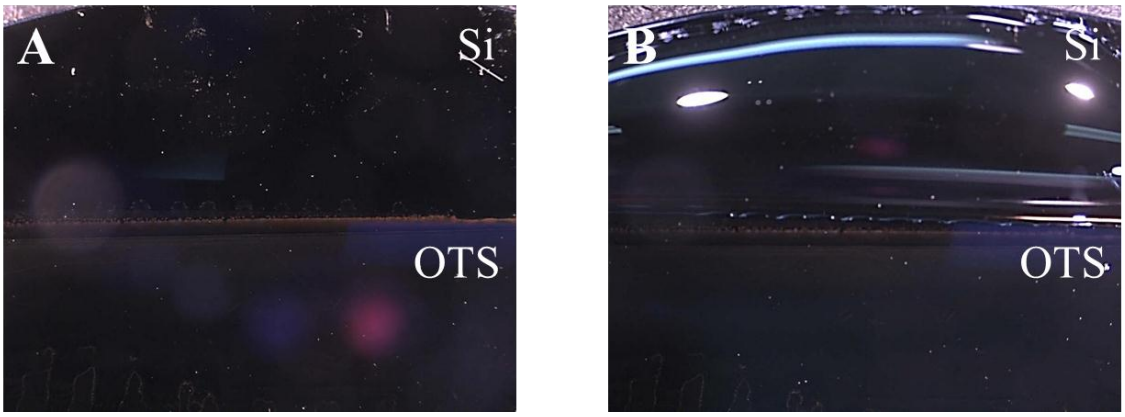

Figure 3.4 Partial coating of silicon with OTS. (A) A silicon substrate was partially dipped into the OTS solution. The boundary of bare silicon and OTS was clearly observed after treatment. (B) Water only wetted the silicon area.

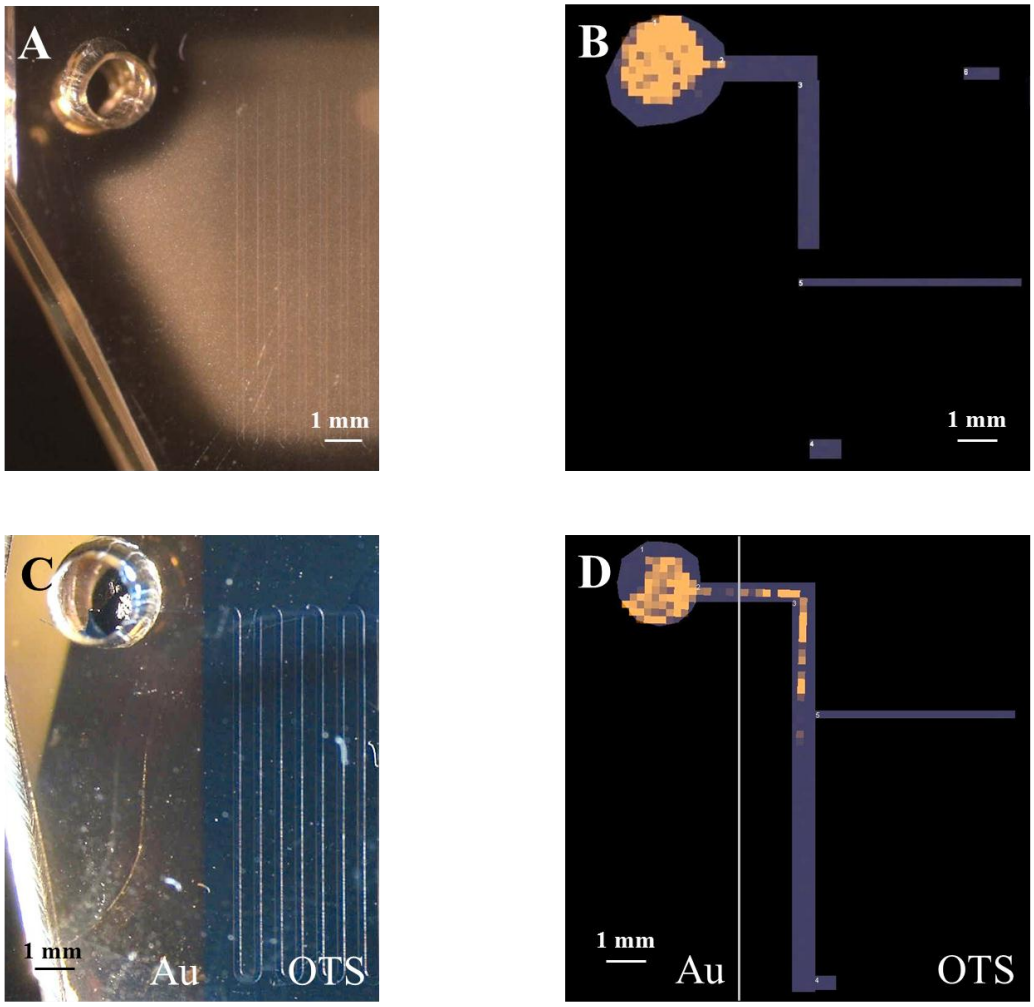

Figure 3.5 The method of gold patterning to reduce nonspecific adsorption in the reservoir area. (A) The OTS substrate was completely covered with gold, which was then coated with OEG. (B) A MS image of 2 ng substance P flowing in the device shown in (A). No substantial signals were detected in the channel area. The color of orange indicates the presence of substance P. (C) A microfluidic device on the silicon substrate patterned with OEG-gold and OTS. (D) A MS image of 3 ng substance P introduced into the device in (C). No significant signals of substance P were detected in the channel area on the gold side, while strong signals were on the OTS side.

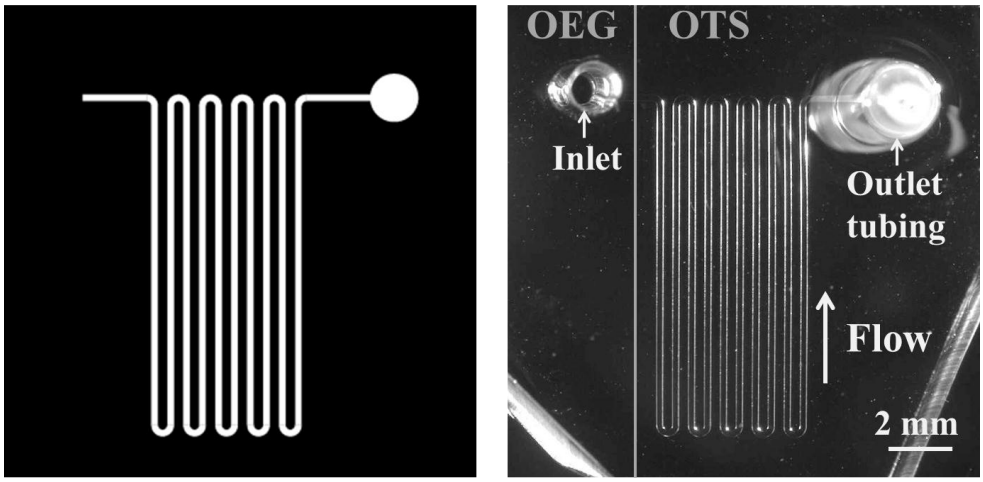

Figure 3.6 Device design. The microfluidic device contains a long serpentine channel (200 μm width × 50 μm height × 110 mm length). The inlet reservoir is made by punching PDMS with a biopsy punch, and the outlet has a short segment of tubing for connection to a syringe pump. (Left) The chip design on a transparency mask. (Right) A photomicrograph of the PDMS device. Note that the substrate is patterned with OEG and OTS, with their boundary visualized by the grey line. The inlet is on the OEG, and the channel and outlet on the OTS.

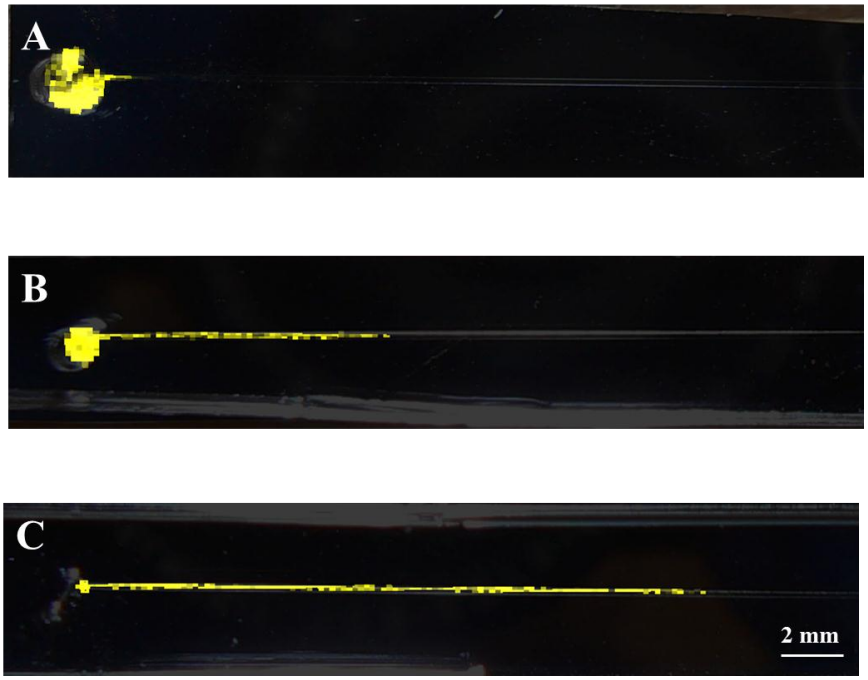

Figure 3.7 Influence of the reservoir size on adsorption length. A microfluidic device with a straight channel (200 μm width × 50 μm height × 30 mm length) was used. 3 pmol AP was introduced into each device and the signals are visualized in yellow. (A) The diameter of the inlet is 2 mm. (B) Diameter of 1.5 mm. (C) The reservoir was made by gluing a capillary with the outer diameter of 370 μm onto the master before PDMS curing.

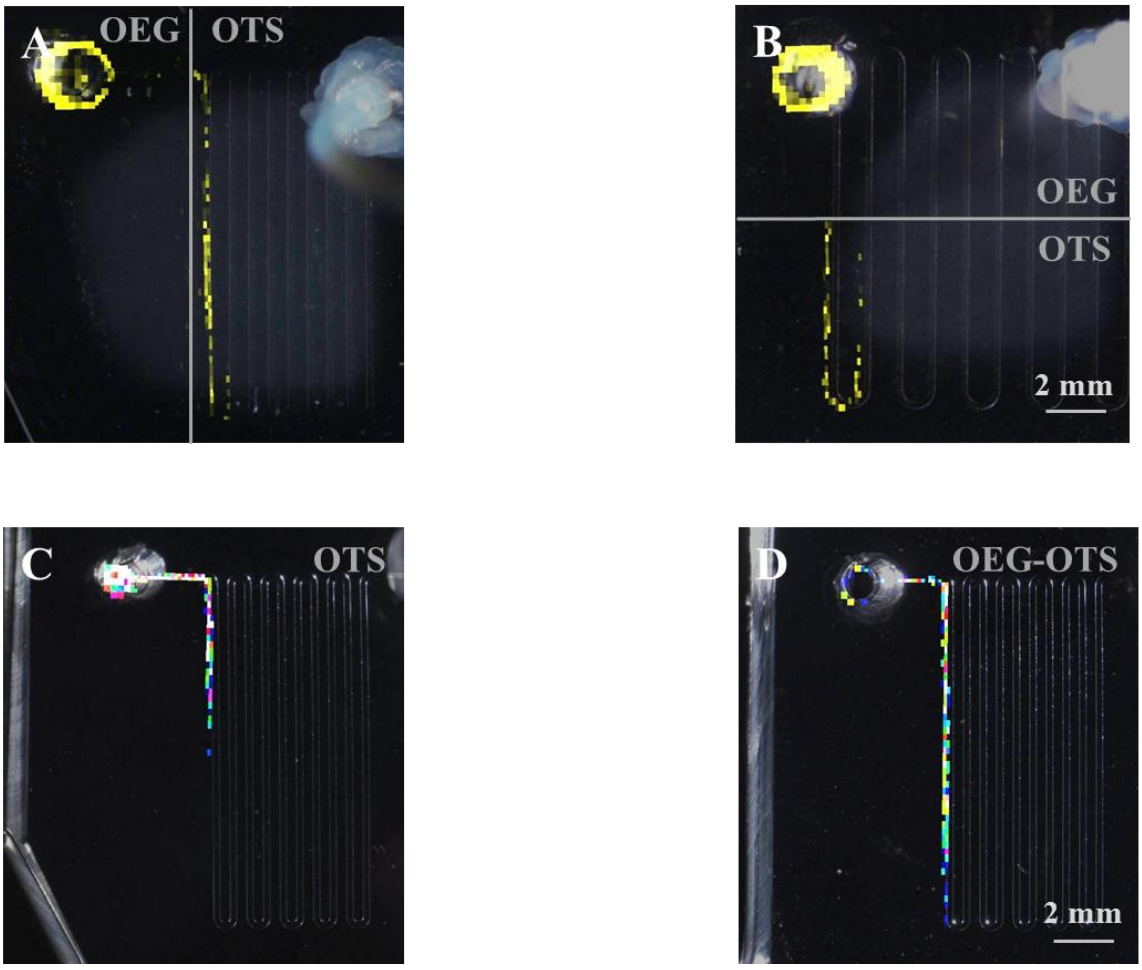

Figure 3.8 MS images of 5 pmol AP flowing through the channel on different surfaces. (A), (B) The OEG-OTS boundary was aligned with channels in different directions. AP signals are visualized in yellow. AP was detected in the channel on the OTS but not on the OEG. Signals in the inlet were due to residual peptides left behind when the liquid in the reservoir dried out. (C), (D) Comparison of the surface treated with OTS completely and the OEF-OTS pattern. AP signals are visualized in rainbow colors, with white indicating the highest intensity on the spot, and dark blue the lowest. The OTS chip had very strong signals in the reservoir and the OEG-OTS chip had weaker signals there. The adsorption length of AP was much longer with OEG-OTS patterning.

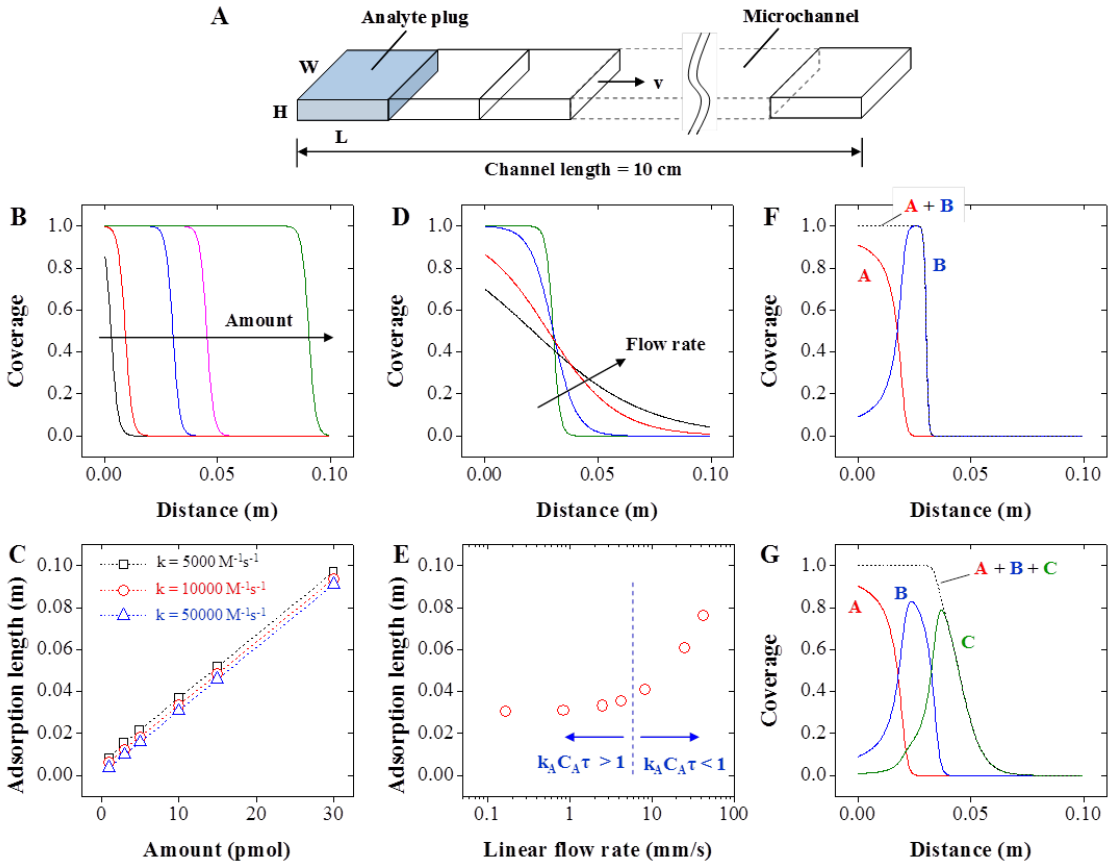

Figure 3.9 A simple kinetic model describes the molecular adsorption in the microfluidic device. (A) An analyte plug (W × L × H) flows through a microchannel with liner velocity of v. The channel is divided into multiple segments where the analytes in the solution are consumed by adsorption. (B) The adsorption length of analytes increases with the amount. (C) The adsorption length is insensitive to a wide range of k_A. (D) Collection efficiency decreases at high flow rates. (E) The relative timescale between the reaction and convection determines the sensitivity of adsorption length to flow rates. (F–G) Analytes with sufficiently different adsorption rate constants can be separated by the microchannel.

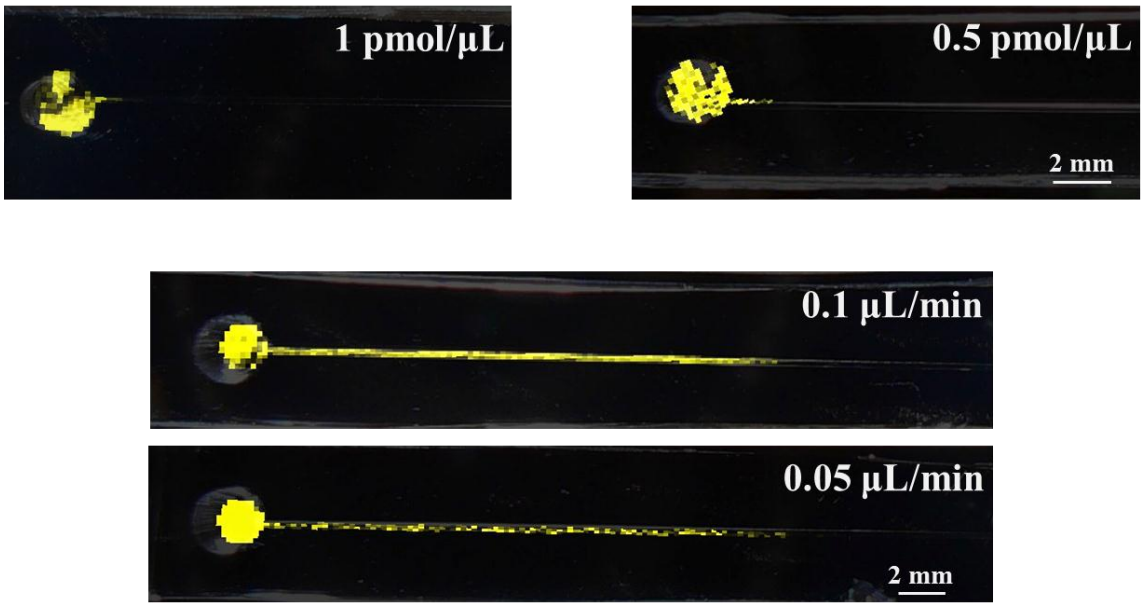

Figure 3.10 Influence of concentration and flow rate on length measurements. A microfluidic device with a straight channel (200 µm width × 50 µm height × 30 mm length) was used. The concentrations of 1 and 0.5 pmol/µL were compared with the sample amount of 3 pmol AP, and the flow rates of 0.1 and 0.05 µL/min were compared with 4 pmol AP. Yellow color indicates the presence of AP. In both cases, the measured lengths are insensitive to the changing parameter.

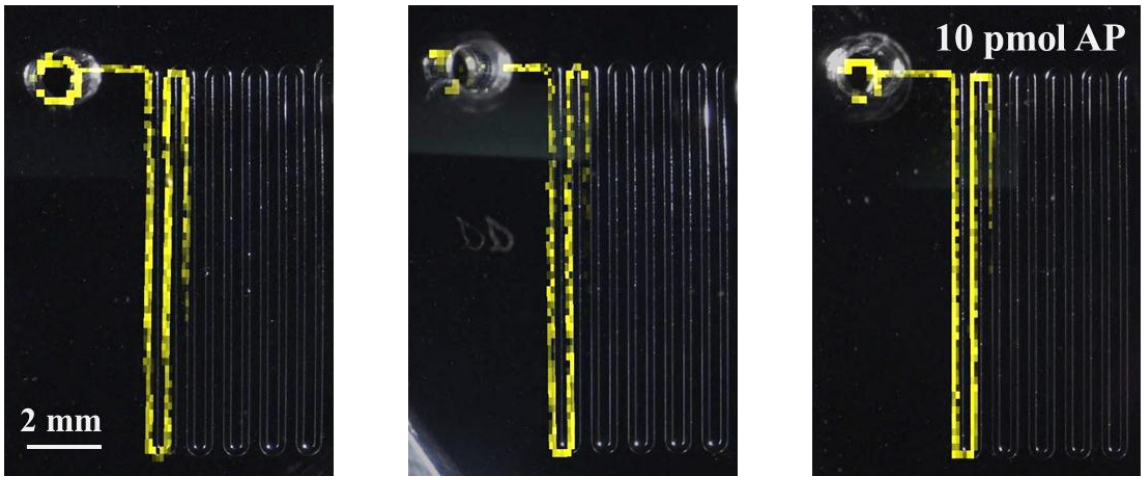

Figure 3.11 Reproducibility of quantitation approach in different devices. The experiment with 10 pmol AP was repeated in 3 devices. Yellow color indicates the presence of AP. The length of yellow band remains essentially constant between different devices.

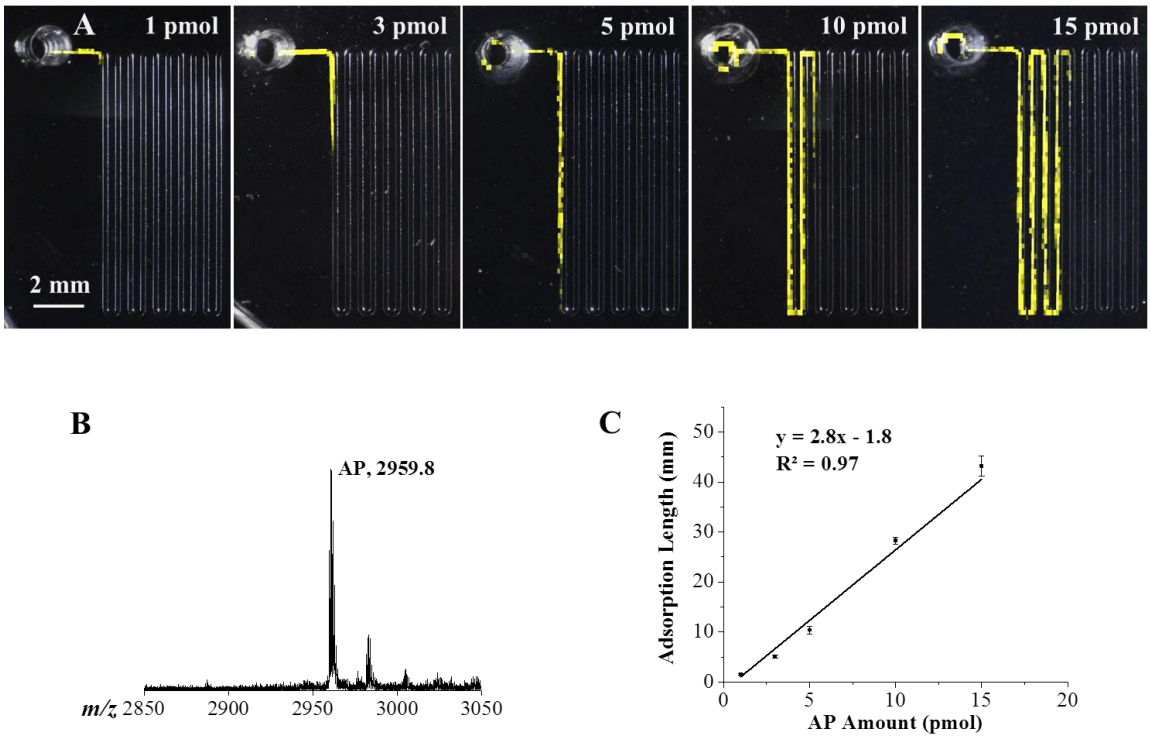

Figure 3.12 Characterization of AP peptide via MS imaging of the microfluidic device substrate. (A) A series of MS images of the adsorption of 1, 3, 5, 10, and 15 pmol of AP. Each spot where AP is detected is colored yellow. (B) Representative mass spectrum showing AP. (C) The calibration curve of adsorption length versus amount of AP obtained using the observed length from the MS image. Error bars represent s.e.m.

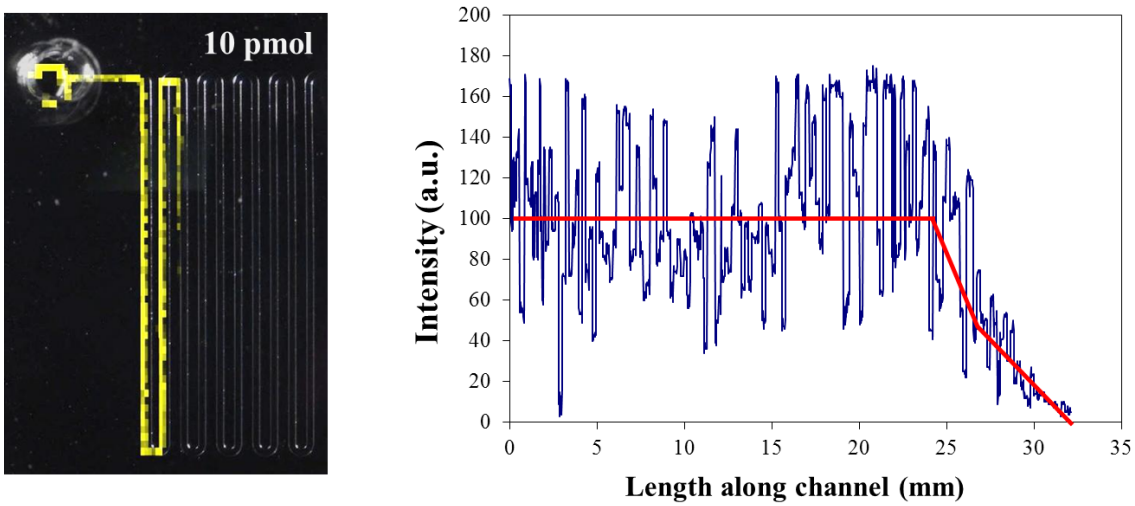

Figure 3.13 Intensity profile of 10 pmol AP along the channel. The red line was drawn for guidance purpose only. The coverage is saturated along the majority of the band expect the partial coverage at the end. This trend is consistent with the prediction from the mathematical model shown in Fig. 3.9.

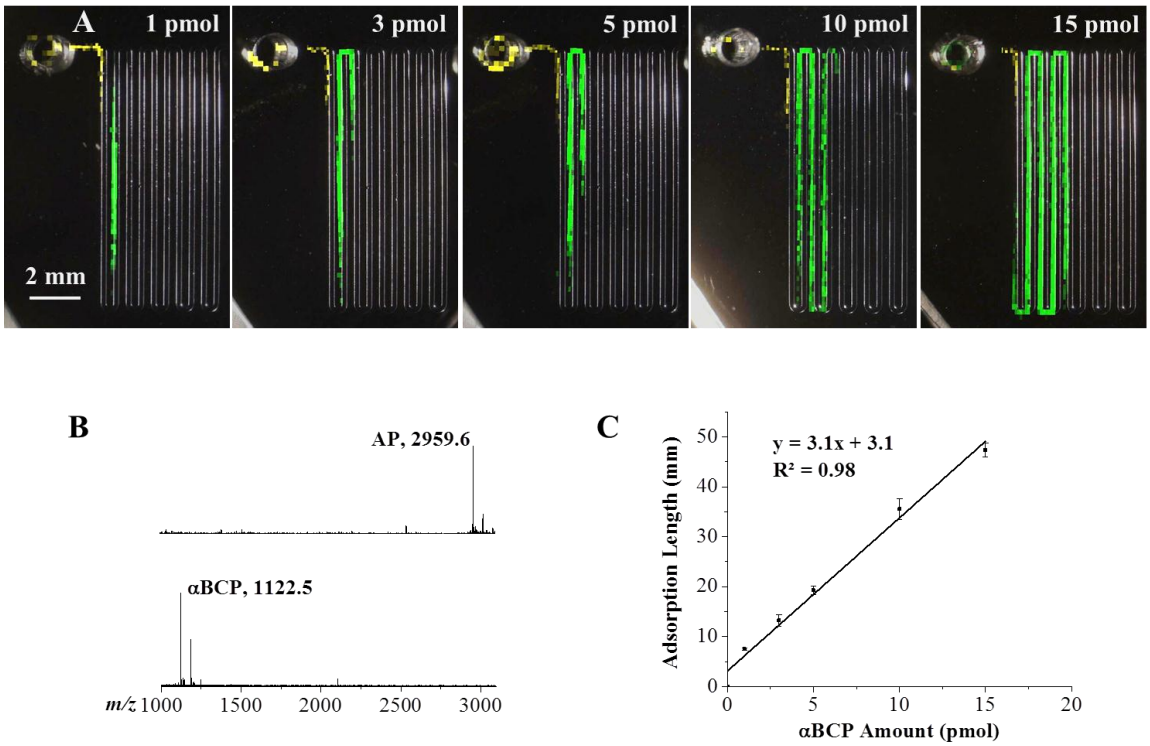

Figure 3.14 MS imaging of two peptides (AP and αBCP) from the microfluidic substrate. (A) A series of MS images of the adsorption of 1, 3, 5, 10, and 15 pmol of αBCP and 3 pmol AP. Yellow color indicates AP and green, αBCP. (B) Representative mass spectra for the AP and αBCP bands, respectively. (C) The calibration curve of adsorption length versus amount for αBCP. Error bars represent s.e.m.

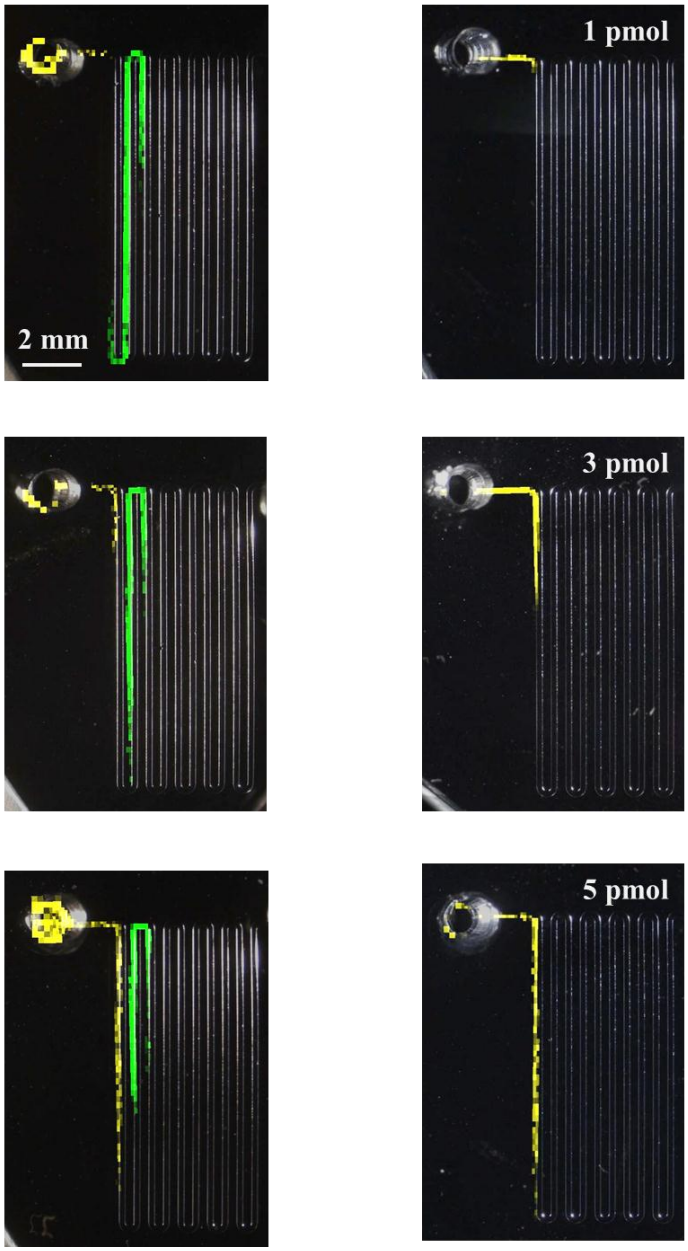

Figure 3.15 Comparison of MS images with AP alone and with the coexistence of AP and αBCP. In the two images in each row, the amount of AP was the same (1, 3, or 5 pmol) and the amount of αBCP added was fixed at 3 pmol. Yellow color indicates AP and green, αBCP.

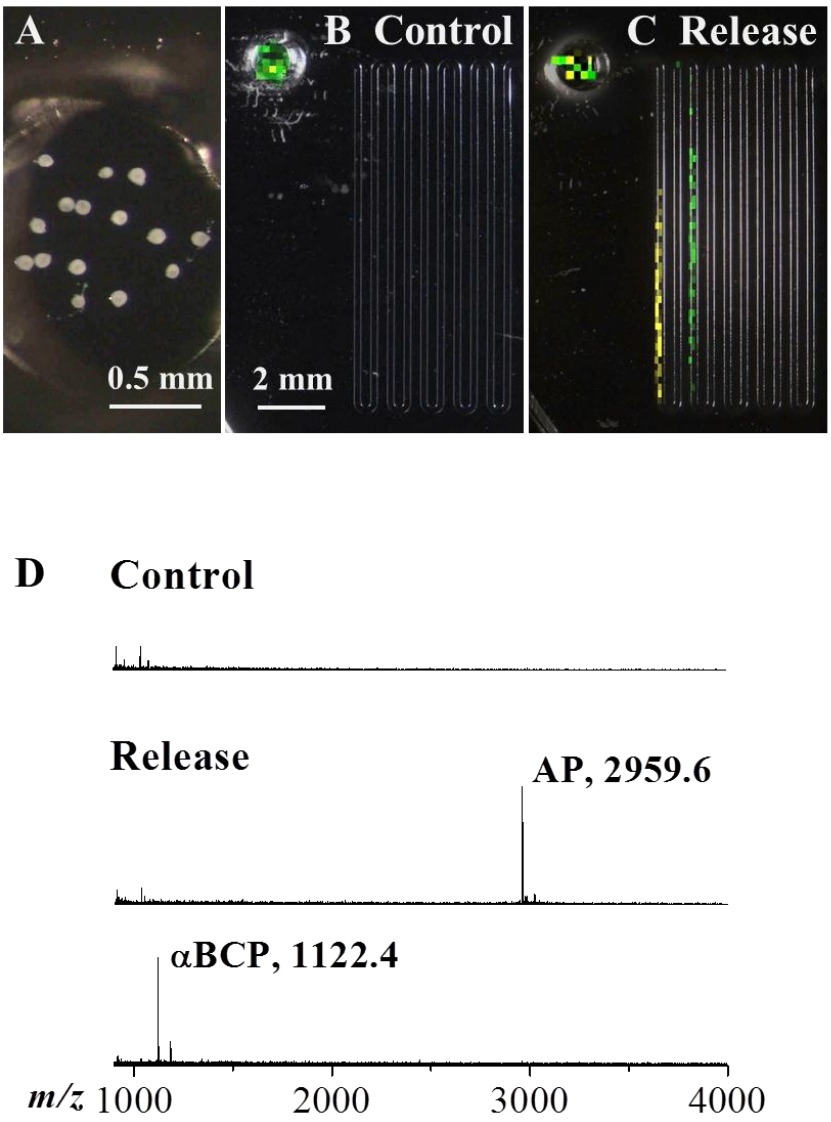

Figure 3.16 *Aplysia* bag cell release experiments with the microfluidic device. (A) Micrograph of the sample chamber showing the 15 neurons loaded into the inlet reservoir. (B) MS image for collection of peptide release when no stimulant was added. (C) MS image after neurons were treated with elevated KCl (final concentration = 55 mM). Yellow indicates AP and green, αBCP. (D) Representative mass spectra for the control, and for the AP and αBCP bands from the release experiments, respectively.

3.7 References

1. A. Manz, D. J. Harrison, E. M. J. Verpoorte, J. C. Fettinger, A. Paulus, H. Lüdi and H. M. Widmer, *J. Chromatogr., A*, 1992, **593**, 253-258.
2. K. Ohno, K. Tachikawa and A. Manz, *Electrophoresis*, 2008, **29**, 4443-4453.
3. B. Huang, H. Wu, D. Bhaya, A. Grossman, S. Granier, B. K. Kobilka and R. N. Zare, *Science*, 2007, **315**, 81-84.
4. N. A. Cellar and R. T. Kennedy, *Lab Chip*, 2006, **6**, 1205-1212.
5. Z. Zhuang, J. A. Starkey, Y. Mechref, M. V. Novotny and S. C. Jacobson, *Anal. Chem.*, 2007, **79**, 7170-7175.
6. A. M. Clark, K. M. Sousa, C. Jennings, O. A. MacDougald and R. T. Kennedy, *Anal. Chem.*, 2009, **81**, 2350-2356.
7. A. M. Taylor, M. Blurton-Jones, S. W. Rhee, D. H. Cribbs, C. W. Cotman and N. L. Jeon, *Nat. Methods*, 2005, **2**, 599-605.
8. M. L. Kovarik, P. J. B. Brown, D. T. Kysela, C. Berne, A. C. Kinsella, Y. V. Brun and S. C. Jacobson, *Anal. Chem.*, 2010, **82**, 9357-9364.
9. L. J. Millet, M. E. Stewart, R. G. Nuzzo and M. U. Gillette, *Lab Chip*, 2010, **10**, 1525-1535.
10. R. Predel, S. Neupert, S. F. Garczynski, J. W. Crim, M. R. Brown, W. K. Russell, J. Kahnt, D. H. Russell and R. J. Nachman, *J. Proteome Res.*, 2010, **9**, 2006-2015.
11. S. S. Rubakhin and J. V. Sweedler, *Nat. Protoc.*, 2007, **2**, 1987-1997.
12. N. G. Hatcher, T. A. Richmond, S. S. Rubakhin and J. V. Sweedler, *Anal. Chem.*, 2005, **77**, 1580-1587.
13. J. Lee, H. Musyimi, S. Soper and K. Murray, *J. Am. Soc. Mass Spectrom.*, 2008, **19**, 964-972.
14. J. Su, M. R. Bringer, R. F. Ismagilov and M. Mrksich, *J. Am. Chem. Soc.*, 2005, **127**, 7280-7281.
15. M. Fujita, W. Hattori, T. Sano, M. Baba, H. Someya, K. Miyazaki, K. i. Kamijo, K. Takahashi and H. Kawaura, *J. Chromatogr., A*, 2006, **1111**, 200-205.
16. K. P. Nichols and J. G. E. Gardeniers, *Anal. Chem.*, 2007, **79**, 8699-8704.
17. P. Chaurand, S. A. Schwartz and R. M. Caprioli, *Curr. Opin. Chem. Biol.*, 2002, **6**, 676-681.

18. S. S. Rubakhin, J. C. Jurchen, E. B. Monroe and J. V. Sweedler, *Drug Discovery Today*, 2005, **10**, 823-837.
19. K. Jo, M. L. Heien, L. B. Thompson, M. Zhong, R. G. Nuzzo and J. V. Sweedler, *Lab Chip*, 2007, **7**, 1454-1460.
20. E. Szájli, T. Fehér and K. F. Medzihradszky, *Mol. Cell. Proteomics*, 2008, **7**, 2410-2418.
21. R. W. Garden and J. V. Sweedler, *Anal. Chem.*, 1999, **72**, 30-36.
22. R. Knochenmuss, *Anal. Chem.*, 2003, **75**, 2199-2207.
23. L. Li and J. V. Sweedler, *Annu. Rev. Anal. Chem.*, 2008, **1**, 451-483.
24. L. D. Fricker, J. Lim, H. Pan and F.-Y. Che, *Mass Spectrom. Rev.*, 2006, **25**, 327-344.
25. S.-E. Ong, B. Blagoev, I. Kratchmarova, D. B. Kristensen, H. Steen, A. Pandey and M. Mann, *Mol. Cell. Proteomics*, 2002, **1**, 376-386.
26. S. Julka and F. Regnier, *J. Proteome Res.*, 2004, **3**, 350-363.
27. X. Yao, *Anal. Chem.*, 2011, **83**, 4427-4439.
28. F. Xiang, H. Ye, R. Chen, Q. Fu and L. Li, *Anal. Chem.*, 2010, **82**, 2817-2825.
29. S. S. DeKeyser and L. Li, *Analyst*, 2006, **131**, 281-290.
30. F.-Y. Che, I. Vathy and L. Fricker, *J. Mol. Neurosci.*, 2006, **28**, 265-275.
31. P. J. Boersema, R. Raijmakers, S. Lemeer, S. Mohammed and A. J. R. Heck, *Nat. Protoc.*, 2009, **4**, 484-494.
32. A. Brockmann, S. P. Annangudi, T. A. Richmond, S. A. Ament, F. Xie, B. R. Southey, S. R. Rodriguez-Zas, G. E. Robinson and J. V. Sweedler, *Proc. Natl. Acad. Sci.*, 2009, **106**, 2383-2388.
33. S. S. Rubakhin and J. V. Sweedler, *Anal. Chem.*, 2008, **80**, 7128-7136.
34. P. Conn and L. Kaczmarek, *Mol. Neurobiol.*, 1989, **3**, 237-273.
35. L. J. Jung and R. H. Scheller, *Science*, 1991, **251**, 1330-1335.
36. J. Sagiv, *J. Am. Chem. Soc.*, 1980, **102**, 92-98.
37. A. Papra, N. Gadegaard and N. B. Larsen, *Langmuir*, 2001, **17**, 1457-1460.
38. C. M. Dekeyser, C. C. Buron, K. Mc Evoy, C. C. Dupont-Gillain, J. Marchand-Brynaert, A. M. Jonas and P. G. Rouxhet, *J. Colloid Interface Sci.*, 2008, **324**, 118-126.

39. A. Tourovskaia, X. Figueroa-Masot and A. Folch, *Nat. Protoc.*, 2006, **1**, 1092-1104.
40. G. Sui, J. Wang, C.-C. Lee, W. Lu, S. P. Lee, J. V. Leyton, A. M. Wu and H.-R. Tseng, *Anal. Chem.*, 2006, **78**, 5543-5551.
41. L. J. Millet, M. E. Stewart, J. V. Sweedler, R. G. Nuzzo and M. U. Gillette, *Lab Chip*, 2007, **7**, 987-994.
42. S. S. Rubakhin, J. S. Page, B. R. Monroe and J. V. Sweedler, *Electrophoresis*, 2001, **22**, 3752-3758.
43. M. W. Toepke and D. J. Beebe, *Lab Chip*, 2006, **6**, 1484-1486.
44. K. J. Regehr, M. Domenech, J. T. Koepsel, K. C. Carver, S. J. Ellison-Zelski, W. L. Murphy, L. A. Schuler, E. T. Alarid and D. J. Beebe, *Lab Chip*, 2009, **9**, 2132-2139.
45. J. A. Vickers, M. M. Caulum and C. S. Henry, *Anal. Chem.*, 2006, **78**, 7446-7452.
46. S. Rocha, M. Carmo Pereira, M. A. N. Coelho, H. Möhwald and G. Brezesinski, *Langmuir*, 2007, **23**, 5022-5028.
47. G. Fragneto, R. K. Thomas, A. R. Rennie and J. Penfold, *Science*, 1995, **267**, 657-660.
48. N. G. Hatcher and J. V. Sweedler, *J. Neurophysiol.*, 2008, **99**, 333-343.
49. S. Margel, E. A. Vogler, L. Firment, T. Watt, S. Haynie and D. Y. Sogah, *J. Biomed. Mater. Res.*, 1993, **27**, 1463-1476.
50. N. L. Wayne and H. Wong, *Endocrinology*, 1994, **134**, 1046-1054.
51. R. W. Newcomb and R. H. Scheller, *Brain Res.*, 1990, **521**, 229-237.
52. N. L. Wayne, J. Kim and E. Lee, *J. Neuroendocrinol.*, 1998, **10**, 529-537.

CHAPTER 4

COMPARTMENTALIZED DEVICE FOR CONTROLLING AND SAMPLING SUBCELLULAR MICROENVIRONMENTS SURROUNDING NEURONS

4.1 Notes and Acknowledgements

This chapter describes a compartmentalized microfluidic device that can accommodate cultured neurons in the microchannel and isolate cell bodies (somata) and neurites. The overarching goal of this project is to develop microanalytical platforms that can define and sample the chemical microenvironments surrounding small areas down to subcellular regions of individual neurons in a neuronal network. Knowledge of the full complements of signaling molecules and trophic factors should help understand neuronal network formation and neuron damage recovery and even provide clues to potential treatments for neurodegenerative diseases. This project involves collaboration with Prof. Martha U. Gillett's group and Prof. Ralph G. Nuzzo's group at UIUC. This work was supported by the W. M. Keck Foundation, the National Science Foundation, Award No. DMI-0328162, the National Institute on Drug Abuse, Award No. P30DA018310, and the National Institute of Neurological Disease and Stroke, Award No. R01NS031609.

4.2 Introduction

In the nervous system, the processes of neurons extent over long distances and through different extracellular environments to form complex highly-branched networks.

The chemical environment surrounding a neuron, varying at the subcellular level (*e.g.* distinct areas of soma and processes of a neuron), affects the response of the neuron to chemical or electrical stimulation. Therefore, in order to gain reliable insights into signaling molecules in a neuronal network, it is important to mimic this *in vivo* situation and have culture platforms that separate control of the microenvironments of neurites and soma. In addition, it has been shown that distinct vesicles of neuropeptides are segregated into different terminal sites.[1-3] For example, in *Aplysia* bag cell neurons, the neuropeptides derived from the amino-terminal and carboxyl-terminal of the egg laying (ELH) prohormone are targeted to different processes[1] and are released from different locations[4]. Local release of different signals from the same cell may be important for creating complex physiology from simple networks. Therefore, it is necessary to have microanalytical platforms that are able to collect local peptide release from specific parts of neurons. However, the microfluidic devices described in Chapter 2 and 3 place entire neurons in a relatively large volume reservoir or introduce them into a single channel, thus not being able to selectively control the environments surrounding sub-regions of individual neurons or to allow analysis of local chemical signals.

Because of the small size, microfluidics is well suited for manipulating and monitoring extracellular microenvironments. This can be achieved by utilizing laminar flows in the microchannels.[5, 6] As the flow in a micron scale channel is laminar, different molecules mix by diffusion only. Therefore, a reagent can be specifically targeted to a certain area of individual cells, allowing control of subcellular environments. But as the neurites from cultured neurons can grow in various directions with regard to the channel, it is not always easy to direct the reagent to the area of interest. Also with laminar flows,

sampling environments of subcellular regions can be difficult to achieve with high spatial resolution.

Alternatively, physical barriers can be added to microfluidic devices to isolate one part of a neuron from others.[7-9] In fact, *in vitro* studies have employed Campenot chambers to isolate axons from other parts of neurons.[10] In this chamber, a Teflon divider is attached to a petri dish with a thin silicon grease layer to form two compartments. Processes of neurons placed in one side of the divider can be grown to penetrate the grease layer into the other side, and the grease serves as a hydrophobic barrier that prohibits substantial mixing of liquids in the two compartments. Campenot chambers have contributed significantly to axonal biology studies.[11-13] However, the imperfect silicon grease seal can lead to leaking, and even a slight mechanical force could damage the neurites. Microfluidics can overcome these challenges. In one culture platform, two parallel main channels with much larger dimensions were connected with a large number of small-diameter microgrooves. These microgrooves were used as the physical barrier and their high fluidic resistance provided a good isolation of these two main channels. A relatively large number of neurons (about 3000 cells) were loaded into one of the main channels, and after culture, the axons projected from the neurons were guided through the small connections into the other channel. The device was divided into a somal and an axonal side; either side could be separately manipulated.[7] In fact, this polydimethylsiloxane (PDMS) device has been commercialized (from Xona Microfluidics, LLC), but only a few formats are offered for sale.

In this study, we changed the channel width and depth of the compartmentalized device mentioned above according to the size of *Aplysia* neurons. We used smaller

reservoir and channel sizes to facilitate studies on small number of cells down to single neurons. The design of the device was also modified. Here it contains three parallel channels; cells are loaded into the middle main channel and the two secondary channels accommodate the outgrown neurites. Local releasate from different terminals can be sampled and compared to each other. The device was also adjusted to be better interfaced to the sample collection method described in the previous chapters. Because of the lower density of cells and more compact space, cell culture in microchannels presented challenges. We addressed these challenges with introduction of perfusion flow and solvent extraction of PDMS[14].

4.3 Experimental

Appendix A contains a master list of all abbreviations used in this chapter.

4.3.1 Materials and Reagents

Unless noted otherwise, all chemicals were purchased from Sigma-Aldrich (St. Louis, MO) and organic solvents were from Fisher Scientific (Fair Lawn, NJ). The PDMS prepolymer kit, Sylgard 184, was purchased from Dow Corning (Midland, MI). Silicon wafers were obtained from WRS Materials (Spring City, PA). Photoresist SU-8 and developer were from MicroChem Corp (Newtown, MA). Trideca-fluoro-1,1,2,2,-tetrahydrooctyl trichlorosilane was obtained from Gelest (Morrisville, PA). Glass coverslips (22 mm × 40 mm, No. 1 thickness) were from Corning (Product #: 2935-224, Corning, NY). The culture media for *Aplysia* bag cell neurons were made by supplementing artificial sea water (ASW) with antibiotics (final concentrations of 67.7 mg/L penicillin G, 100 mg/L streptomycin, and 50 mg/L gentamicin) and nutrients (final

concentrations of 1.1 g/L D-glucose, 0.3 g/L L-glutamine, and 0.1 g/L L-methionine). ASW (pH 7.8) contained 460 mM NaCl, 10 mM KCl, 10 mM $CaCl_2$, 22 mM $MgCl_2$, 26 mM $MgSO_4$, 2.5 mM $NaHCO_3$, and 15 mM HEPES.

4.3.2 Glass Surface Treatment

To facilitate observation of cells in the channels, glass coverslips were used as the substrates for the compartmentalized device. Glass coverslips were cleaned with methanol and water sequentially, and dried with nitrogen. Coverslips were then dipped into 1% (v/v) H_2SO_4 for at least 3 h to remove the metals doped in glass which might be toxic to neurons. Each coverslip was then covered with 1 mL 0.1% (v/v) poly-L-lysine (PLL) solution for 2 h and then rinsed with DI water 3 times to remove extra PLL. The PLL-coated coverslips were stored in the 4 ℃ refrigerator until use.

Alternatively, a pattern containing repeated straight lines of PLL and bovine serum albumin (BSA) was coated on the surface of glass. A PDMS piece with an array of parallel straight channels (Fig. 4.1, channel width: 50 or 100 μm, edge-to-edge spacing: 50 or 100 μm) was placed on top of a glass coverslip. Each channel was then filled with 0.1% (v/v) PLL solution according to the procedure of channel outgas technique reported previously[15]. A PDMS extension reservoir was added onto the top of the inlet reservoir to enable holding larger volume of filling solution. About 200 μL PLL solution was added to the extension reservoir and the whole device was put into a vacuum desiccator for 10 min so that PLL could fill all the channels without substantial air bubbles. The device was then removed from vacuum and placed in the ambient condition for 2 h. After that, the PLL solution in the reservoirs and channels was removed with vacuum as much as

possible and then DI water was flushed through the channels twice to wash away unattached PLL. The PDMS top was peeled off from the glass substrate afterwards. BSA was diluted to a 0.1 % v/v solution and was used to cover the glass substrate partially coated with PLL for another 2 h. After that, the substrate was rinsed with DI water and dried with nitrogen. The coated coverslips were stored in the 4 ℃ refrigerator until use.

4.3.3 Device Fabrication

Fabrication of the compartmentalized device consisted of two steps of photolithography and development, due to different heights of interconnects (3 μm high) and main/secondary channels (70 μm high). In order to ensure a good adhesion of small photoresist features to the silicon wafer, the wafer was first cleaned thoroughly with piranha solution (3:1 H_2SO_4:H_2O_2, **Caution!** Piranha is a strong oxidant. It reacts aggressively with organic materials and should be handled with great care). The silicon wafer was then rinsed with large amount of DI water and dried with nitrogen. After that, SU-8 2002 was spin-coated onto silicon to form a layer of 3 μm thick, and then exposed to UV light through the first mask containing high density of straight lines. Following development, a SU-8 pattern with interconnects was formed on the wafer. Subsequently, a second layer of SU-8 2075 (70 μm thick) was coated onto the silicon wafer. Before photolithography, the second mask containing the main/secondary channels was aligned against the interconnects on the wafer so that they intersected close to the middle of the main channel at almost 90°. After the second step of UV exposure and development, the master with the pattern of an entire compartmentalized device was made. This process is illustrated in Fig. 4.2. PDMS devices were made by molding Sylgard 184 onto the master.

To help release cured PDMS from the master, especially at the area of high-density small interconnects, the master was first treated with trideca-fluoro-1,1,2,2,-tetrahydrooctyl trichlorosilane by placing the master with 2-3 drops of the silanizing agent in an open dish together in a desiccator for 2 h. The PDMS prepolymer was then poured onto the master and cured at 70 ℃ overnight. The reservoirs were made with an AcuPunch (Acuderm, Inc., Ft. Lauderdale, FL) biopsy punch of 2 mm diameter.

4.3.4 Solvent Extraction of PDMS

The extraction procedure was modified from previous reports[14, 16]. Sequentially, PDMS pieces were immersed into pentane for 36 h, new pentane 7 h, xylenes 16 h, new xylenes 7 h, ethanol 16 h, another ethanol for 7 h, and finally DI water overnight, with continuous stirring. One PDMS piece required 100 mL of each solvent. After extraction, PDMS was dried at 70 ℃ overnight. Extracted PDMS was stored in the ambient condition until use.

4.3.5 Neuron Isolation and Loading

Aplysia californica were anesthetized by injection of magnesium chloride (50% of body weight) into the body cavity. Individual bag neurons were isolated after incubation in ASW with proteases (1% type IX and 1% type XIV) at 35 ℃ for 90 min as described in previous chapters. The cells were then introduced into the microchannel, which was prefilled with culture media for bag cell neurons. During the loading process, the microfluidic device was kept on the stage of an inverted microscope (Zeiss Axiovert 25) so that the movement of cells in the channel could be monitored. An ASW solution

containing about 20 cells was loaded into the inlet reservoir of the main channel, and an Eppendorf pipette immediately applied a negative pressure at the outlet. When the cells entered into the channel, as monitored by the microscope, the pipette was removed at once and another pipette was used to add to the outlet the amount of culture media equal to the volume of solution at the inlet to stop the flow. After loading, the cells in the channel were allowed at least 1 h to attach to the bottom glass surface.

4.3.6 Culturing Neurons inside Microchannels

The tip end of a 200 μL Pipette tip was cut off with a razor, and the flat end was glued with silicon grease on top of the reservoir hole to enlarge its holding volume. After that, equal amounts of culture media (about 200 μL) were used to fill the extended inlets and outlets of the main and secondary channels. 20 μL of media was added into the inlet reservoir to introduce a perfusion flow through the channel from inlet to outlet. Parafilm M (Bemis Flexible Packaging, Neenah, WI) was cut into small pieces and attached to the open ends of reservoir extensions to reduce evaporation of media during culturing. The whole device loaded with neurons was then placed in an incubator maintained at 14 ℃. To further reduce evaporation, small dishes of water were placed near the device. The device was replenished with fresh media every 24 h. The growth of neurons inside the microchannel was monitored with the Zeiss inverted microscope.

4.4 Results and Discussion

4.4.1 Device Design

The compartmentalized device contains one main channel (100 or 200 μm wide, 70 μm high, 20 mm long) and two parallel secondary channels (50 or 100 μm wide, 70 μm high, 15 mm in the middle segment). The edge-to-edge spacing between adjacent channels is 50 or 100 μm. The small channels connecting secondary channels to the main channel have the width of 3 μm, height of 3 μm, length of 2 mm, and center-to-center spacing of 10 μm. Because the main/secondary channels are much taller than the interconnects, fabrication of this device was performed in two steps of photolithography and development. The chip was designed in such a way that under appropriate conditions, the processes sprouted from neurons placed in the main channel could penetrate the small interconnects to enter into the adjacent secondary channels. The use of glass substrates here permits continuous monitoring of neurons in the microchannel. The design and picture of this microfluidic device is shown in Fig. 4.3.

4.4.2 Controlling Flows in Individual Microchannels

The compartmentalized device allows isolation of somata and neurites of neurons, and manipulation and sampling of each subcellular region. In order for this device to be feasible, the fluidic environment in each channel should be able to be controlled individually. The small dimensions of interconnects significantly reduced the liquid flow between large channels with high flow resistance. To counteract diffusion between adjacent channels, a hydrostatic pressure difference was established by adding slightly more liquid into the reservoirs of channels other than the one whose flow needed to be

separately controlled. For example, if the fluidic environment in one secondary channel needed to be isolated, 2 μL more solution was added into the middle main channel and the other secondary channel, as illustrated in Fig. 4.4A. The higher hydrostatic pressures at these two channels introduced a very slow flow inside the interconnects to the channel to be isolated, which canceled out the diffusion from that channel. This was visualized by a blue ink solution introduced in the left channel in Fig. 4.4A. With the hydrostatic pressure difference, the blue ink was confined into the left channel. No blue color was visible from the middle or right channel. The isolation of left channel was further confirmed with MALDI MS, which provided more sensitive detection. 5 pmol of a standard peptide, angiotensin II was added into the inlet of the left secondary channel. After 2 h, 1 μL of the solutions from the outlets of the left and middle channel were deposited to a MTP 384 polished steel target plate (Part No. 209520, Bruker Daltonics, Bremen, Germany). 1 μL 2,5-dihydroxybenzoic acid solution (DHB, 10 mg/mL in 50%/50% acetonitrile/water) was added to each spot to mix with the sample. The MALDI spectra are shown in Fig. 4.4B, which clearly demonstrates that the angiotensin II peaks were only detected from the left but not the middle channel. Given the high sensitivity of MALDI, no significant mixing of fluids in adjacent channels occurred during this time period. Based on the same principle, the middle main channel could also be specifically controlled by adding more liquids into the two secondary channels. As shown in Fig. 4.4C, the yellow color was restricted to the middle channel.

4.4.3 Introducing Neurons into Microchannel

Loading neurons into the microchannel presents challenges. After adding the cell solution into the inlet, a hydrostatic flow occurs due to the higher level of liquid in the inlet than the outlet. But by using gravity flow alone, the bag cell neurons attached in the reservoir instead. Cells could be moved by applying vacuum at the outlet with tubing connected to the vacuum line. However, the force was too fast as they were quickly drawn to the outlet, without leaving enough time to allow them to attach on the substrate. A narrower segment (25 μm wide) of channel was added near the outlet as an attempt to capture the cells (Fig. 4.5A). But with the force of applied vacuum, the cells could be still squeezed through the narrow restriction and some cells were lysed. Alternatively, a sharpened needle could be used to punch a hole near the middle of the main channel with the diameter of about 300 μm (Fig. 4.5B). Cells could then be placed into this open access hole without the need to introduce flow in the channel. But such a hole was too large and easily disrupted the adjacent secondary channels. Besides, it caused disturbance in the flow, leading to undesirable results during flow control.

The most reliable way to load neurons so far was achieved by using a pipette to draw the cell solution through the channel. The drawing force by the pipette was more controllable than vacuum, allowing cells to move slower and leaving enough time to stop them inside the channel. Glass beads with diameter of 40 μm, about the size of bag cell neurons, could be used here for practice purposes. After the beads or cells were entering the channel from the inlet, the pipette used to pull the solution was stopped immediately, and another pipette was used to add certain amount of culture media to the outlet to make the liquid levels in the outlet and inlet the same. After that, neurons gradually stopped

moving and started attaching onto the glass substrate. One example of an attached neuron is shown in Fig. 4.6A. Cells were kept undisturbed for at least 1 h to allow good attachment to the substrate, which was crucial to neuronal growth. With this approach, however, there were still many neurons adsorbed onto the inlet (Fig. 4.6B).

4.4.4 Increasing Neuron Viability inside Microchannels

Aplysia bag cell neurons are generally easy to culture on the open dish. Under appropriate conditions (14 ℃), they can be grown on different surfaces. Bag cells have been successfully grown on a culture dish (Falcon, Franklin Lakes, NJ), PLL-coated glass coverslip, bare silicon, silicon modified with octadecyltrichlorosilane (OTS), silicon modified with 2-[methoxy(polyethyleneoxy)propyl]trimethoxysilane (OEG), and PDMS (Fig. 4.7). The protocol for silicon derivatization was described in Chapter 2 and 3.

However, the environment in the microchannel is quite different from the open dish. In an open dish, both diffusion and convection help maintain a homogeneous chemical environment throughout the media, continually providing cultured neurons with a fresh supply of nutrients and diluting waste secretion from the cells quickly. In contrast, due to the small size of microchannel, only diffusion can occur in this confined space. After neurons consume the nutrients proximal to them, they have limited access to fresh media because of the slow diffusion of nutrient molecules. Also the waste secreted from neurons would accumulate surrounding them, which appears toxic for cell growth. Therefore, a local microenvironment is created that is not amenable to culturing neurons.[17] Another issue specifically with PDMS devices is PDMS itself. Although PDMS is generally biocompatible and gas-permeable, the untreated PDMS can absorb

nutrient molecules from the media, and oligomers and the platinum-containing catalyst used for curing PDMS, which are unhealthy for neuronal growth, can leach into the media.[14, 18] This issue becomes more significant as the surface-to-volume ratio increases with smaller channels. Because of these two reasons, bag cell neurons did not grow after several days of culture in the preliminary tests (Fig. 4.8A).

To overcome the challenges within local microenvironments, a gravity-induced perfusion flow was introduced into the system to continuously supply the neurons with fresh media. It was realized by adding more liquid into the inlet of a channel, causing a steady flow from the inlet to the outlet. Reservoir extension made from pipette tips was used to hold more media. Every 24 h, the liquid level difference was reestablished with fresh media. To solve the issue with PDMS, before assembling the device, PDMS was subject to serial solvent extraction. The extraction has been demonstrated to effectively remove the uncrosslinked oligomers and platinum catalyst.[14] After these additional treatments, about 1 out of 3 bag cell neurons grew well even after several days of culture. One example is shown in Fig. 4.8B.

4.4.5 Patterning Glass Surfaces with PLL/BSA for Guidance of Neuronal Growth

Fig. 4.8B also shows that the neurons preferred to grow along the channel instead of penetrating the interconnection channels. It was likely due to the highly restricted space of the small interconnects. In order to guide the neuronal growth through interconnects, the surface chemistry of glass needed to be modified to provide chemical cues for directing process outgrowth. We previously reported that neuronal growth aligned well with a pattern of repeated lines of PLL and BSA.[19] Here, we used a PDMS

device containing a large number of parallel straight channels (Fig. 4.2) to deposit PLL lines onto the glass surface; the remaining bare glass was then coated with BSA. It was difficult to fill all the parallel channels without introduction of significant air bubbles by applying vacuum at the outlet reservoir. Instead, a reservoir extension was added onto the inlet which could hold more PLL filling solution, and the whole device was placed under vacuum, according to the channel outgas technique procedure reported previously[15]. Fluorescein isothiocyanate (FITC)-labeled PLL was used here to visualize the liquid inside the microchannels with a Zeiss FluoArc fluorescence microscope, as shown in Fig. 4.9A. The image clearly indicates that all the channels were filled with FITC-PLL solution without substantial air bubbles. Fluorescence images of the glass substrate after coating also showed PLL lines (Fig. 4.9B), indicating that PLL adsorbed to the glass. Future work will be applying this surface patterning technique to the compartmentalized device to guide neuronal growth into the small interconnects.

4.5 Conclusions

Microfluidics allows control and sampling of chemical environments surrounding subcellular regions of individual cells. In a commercially available compartmentalized neuron culture platform, neurites from neurons can enter into a different channel from the somal channel so that the environments surrounding somata and neurites can be separately manipulated. Here we tailored the device to the cell sizes under investigation. We modified the chip design to include one main channel for somata and two secondary channels for processes, which are connected with small interconnects. In this way, the releasate from different terminals can be sampled separately and compared. With an

established hydrostatic pressure difference, each large channel could be fluidically separated from adjacent ones in this three-channel system. The challenges of culturing cells inside microchannels were addressed with introduction of a perfusion flow and PDMS extraction with serial solvents. A pattern of PLL/BSA was fabricated, which can guide the direction of process outgrowth. Future work includes combing this surface patterning technique with the compartmentalized microfluidic device to guide the neurites through the innterconects, and interface the sample collection method described previously to this device to sample local peptide release from each part of a single neuron.

4.6 Figures

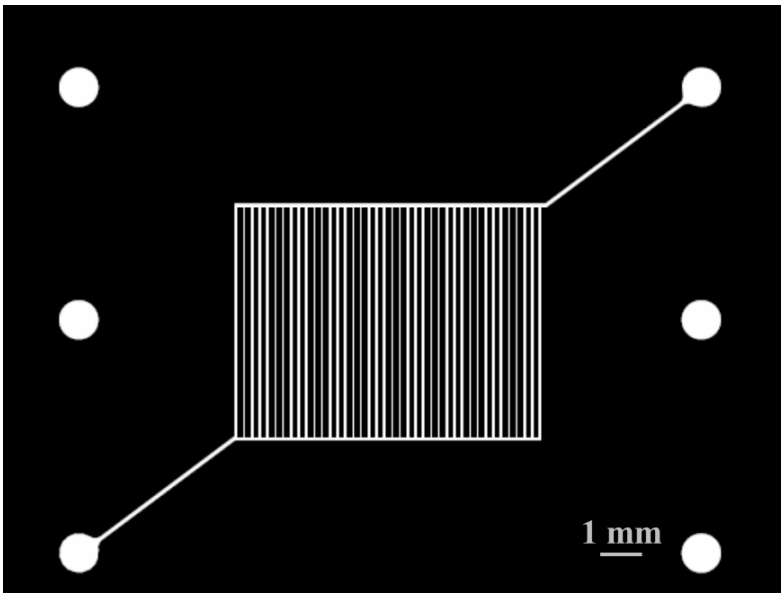

Figure 4.1 Mask design of the device used to pattern glass with repeated lines of PLL and BSA. Channels (transparent part on the mask) were filled with PLL. The width of channels was both 50 and 100 μm, and the edge-to-edge spacing was 50 and 100 μm.

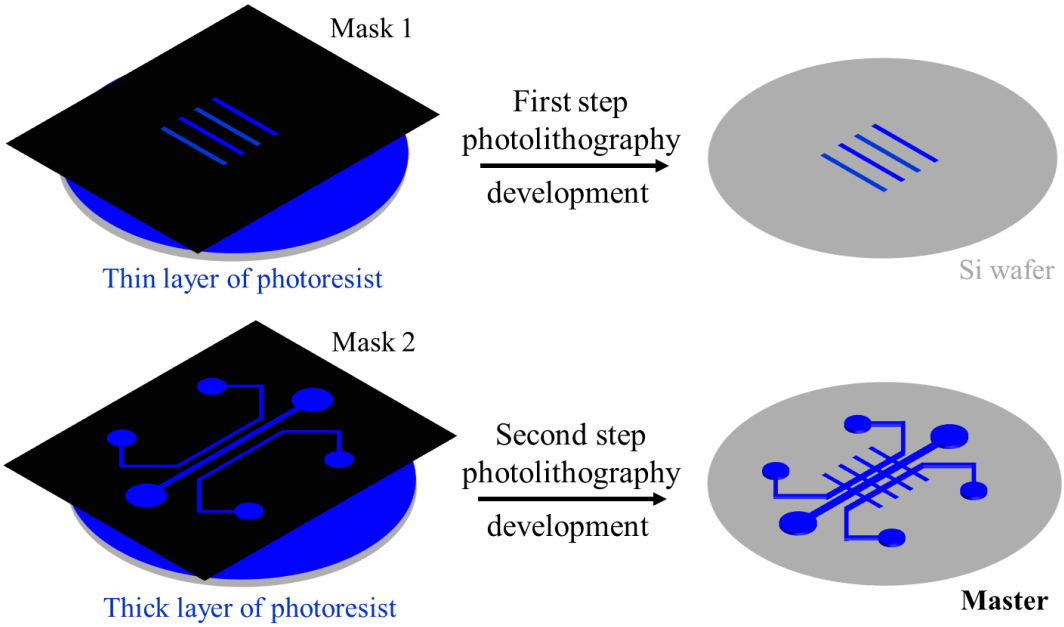

Figure 4.2 Fabrication process of compartmentalized microfluidic device. The blue color indicates photoresist. The process involves two steps of photolithography and development.

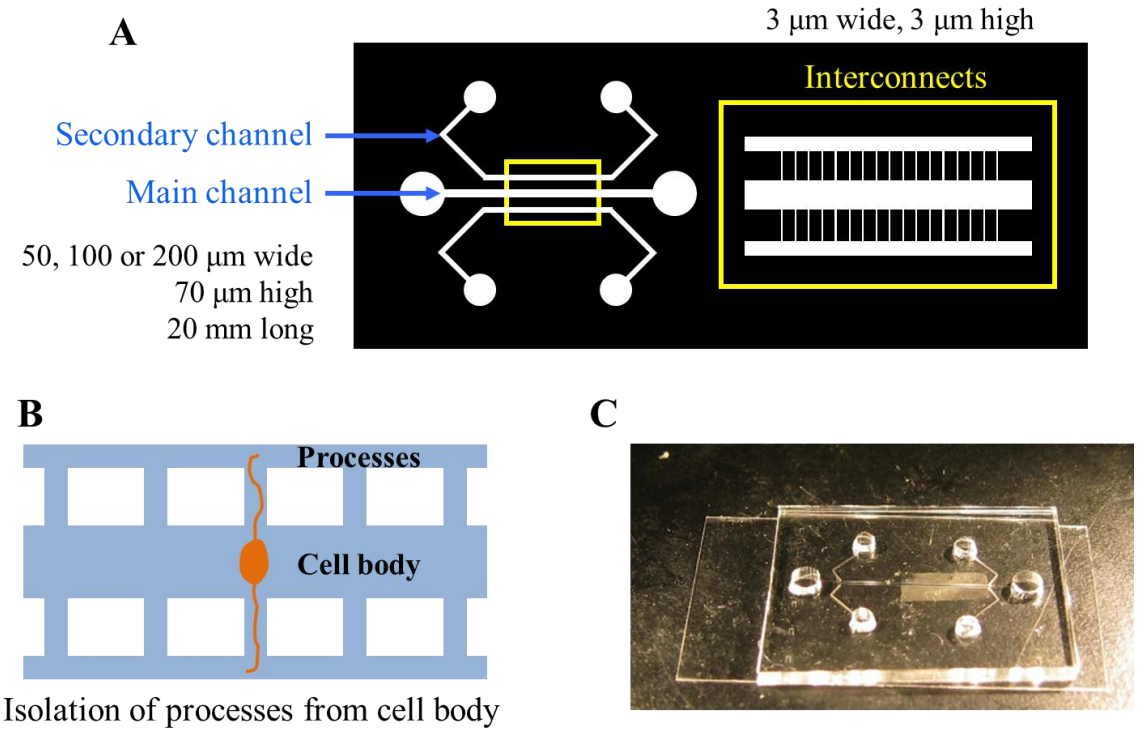

Figure 4.3 Design of compartmentalized microfluidic device. (A) Masks for the main/secondary channels and the interconnects. Individual feature sizes are listed. (B) A cartoon shows that the processes from a neuron penetrate the interconnects into the secondary channels. In this way, the processes and soma of a neuron can be separated. (C) A picture of the assembled compartmentalized PDMS device.

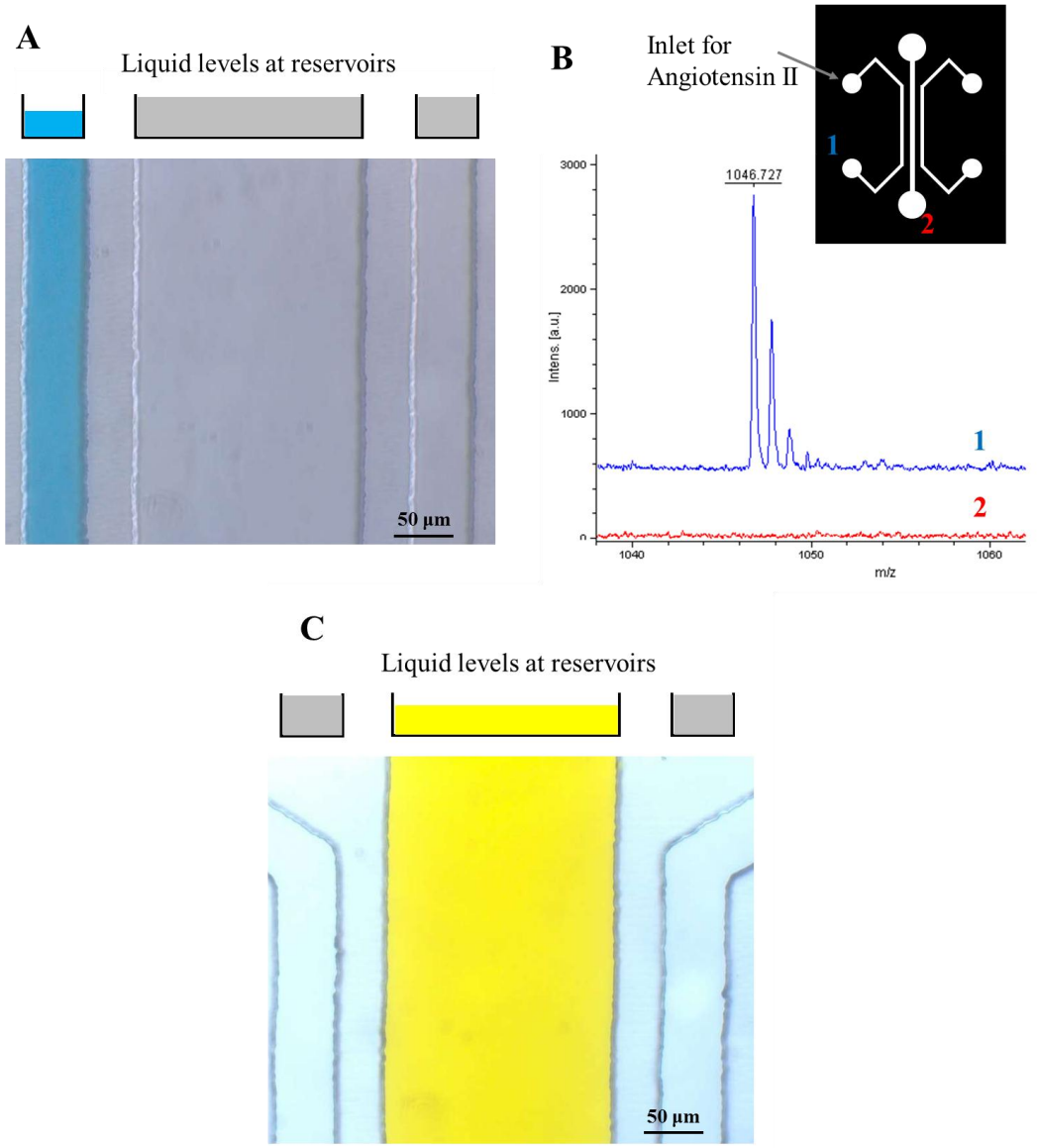

Figure 4.4 Controlling flows in individual channels. (A) Isolation of the left channel is visualized by blue ink. It was achieved by adding more liquids into the middle and right channels. (B) Confirmation of fluidic isolation in the left channel with MALDI MS. The liquid levels in each channel were the same as (A). After angiotensin II was added into the left channel, its signals could only detected from the left (1) but not the middle channel (2). (C) Isolation of the middle channel is visualized by yellow ink. It was achieved by adding more liquids into the left and right channels.

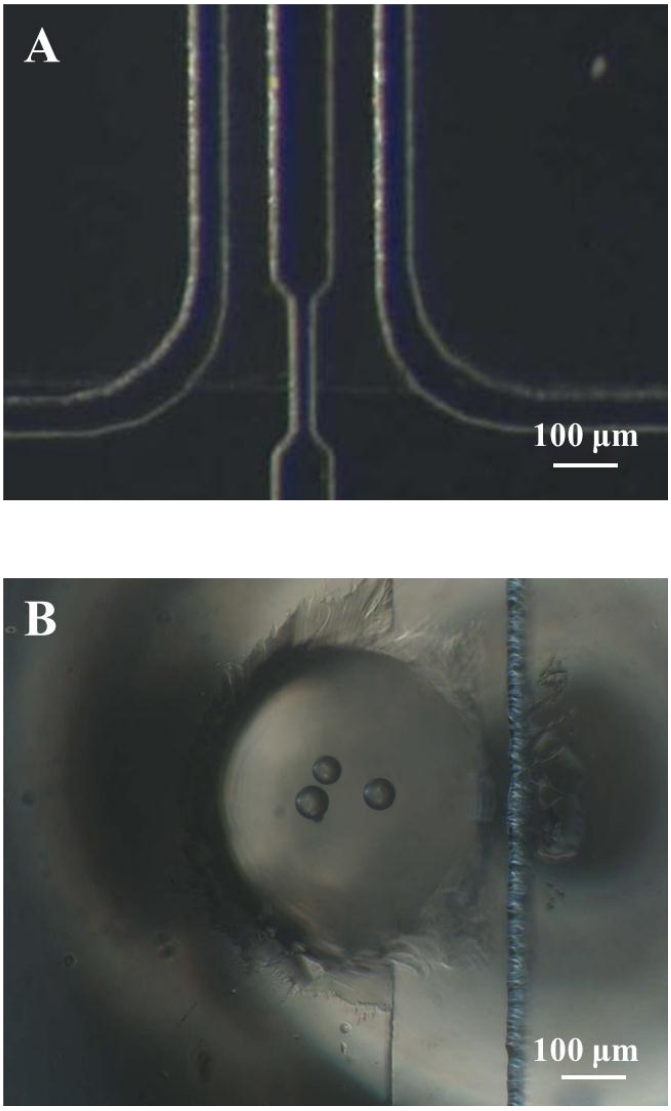

Figure 4.5 Loading neurons into microchannel. (A) A narrow segment of channel (25 µm wide) was added near the outlet to capture the moving neurons. (B) An open hole was punched near the middle of the main channel for loading cells. Note glass beads (diameter of 40 µm) were used here as a substitute for cells.

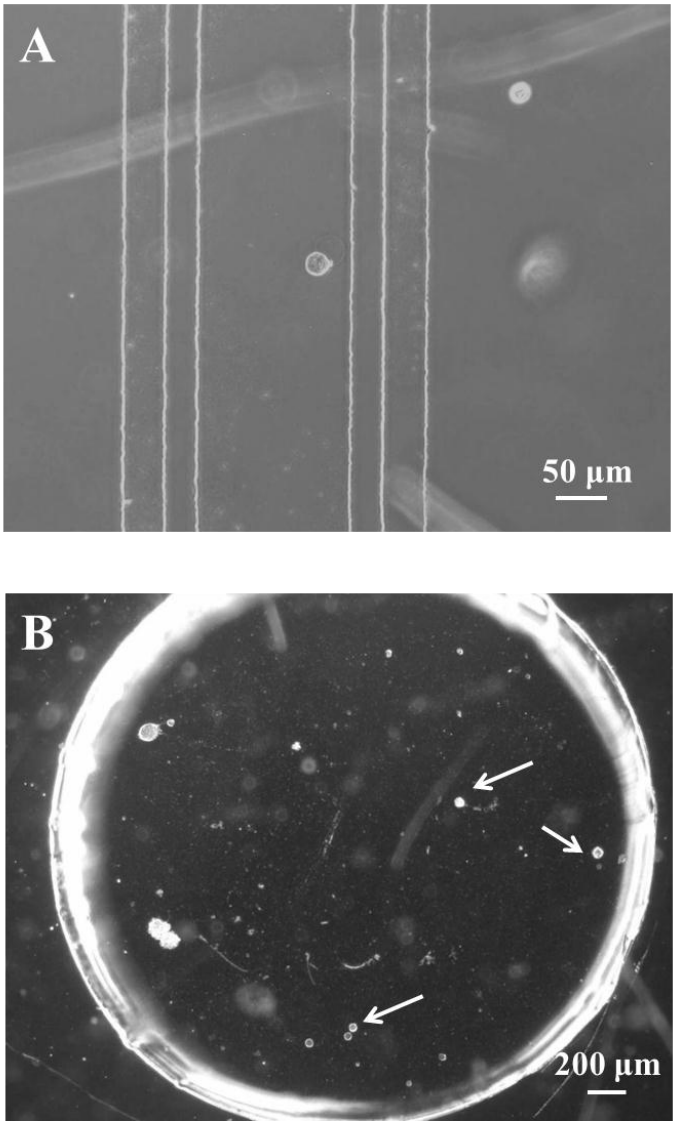

Figure 4.6 Loading neurons into microchannels with pipette. (A) A neuron was attached in the channel. (B) Many neurons attached in the reservoir instead of in the channel. The white arrows indicate the bag cells neurons.

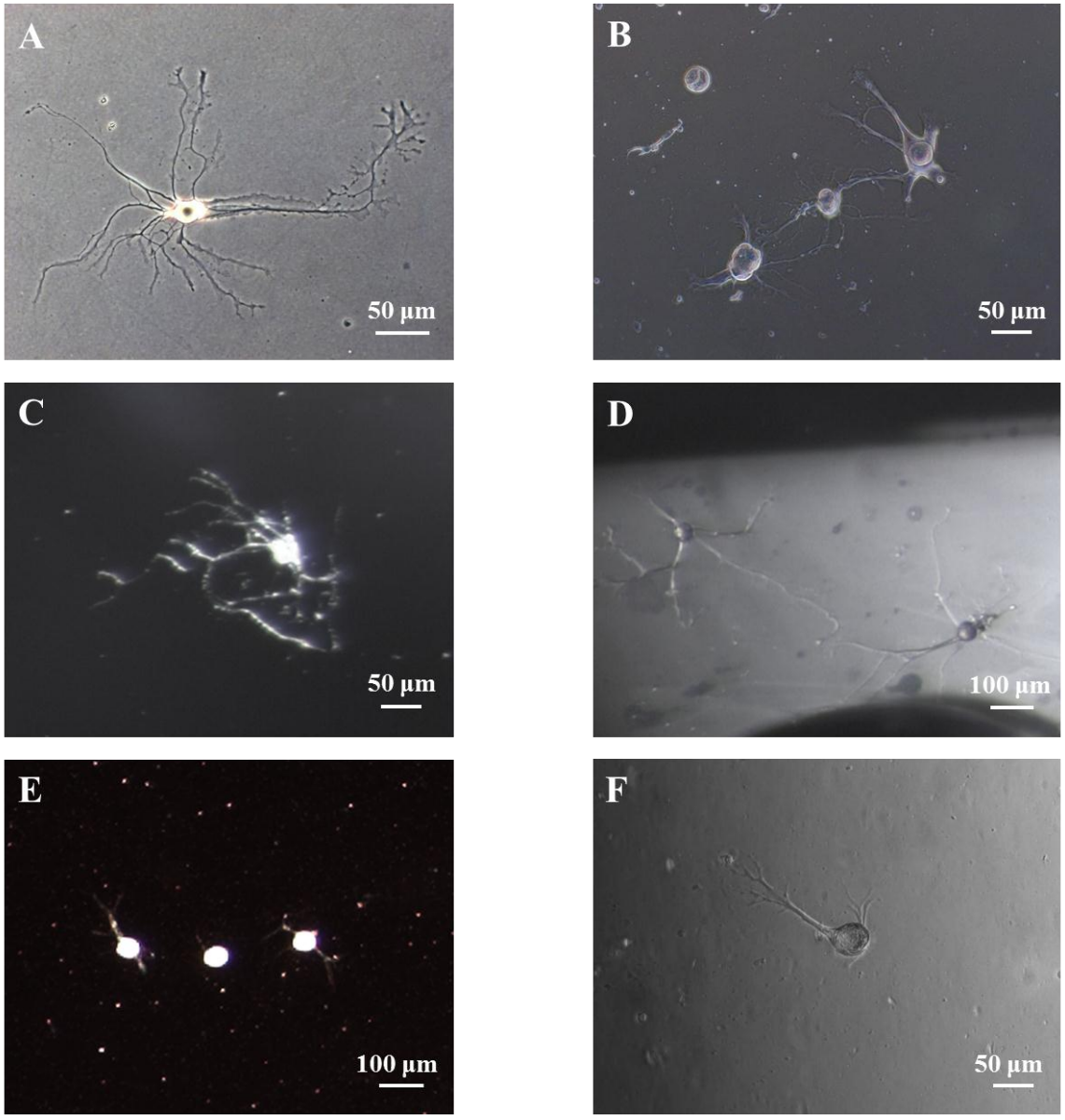

Figure 4.7 Growth of *Aplysia* bag cell neurons on different surfaces. (A) Culture dish, (B) PLL-coated glass coverslip, (C) bare silicon surface, (D) OTS-modified silicon surface, (E) OEG-modified silicon surface, and (F) PDMS layer.

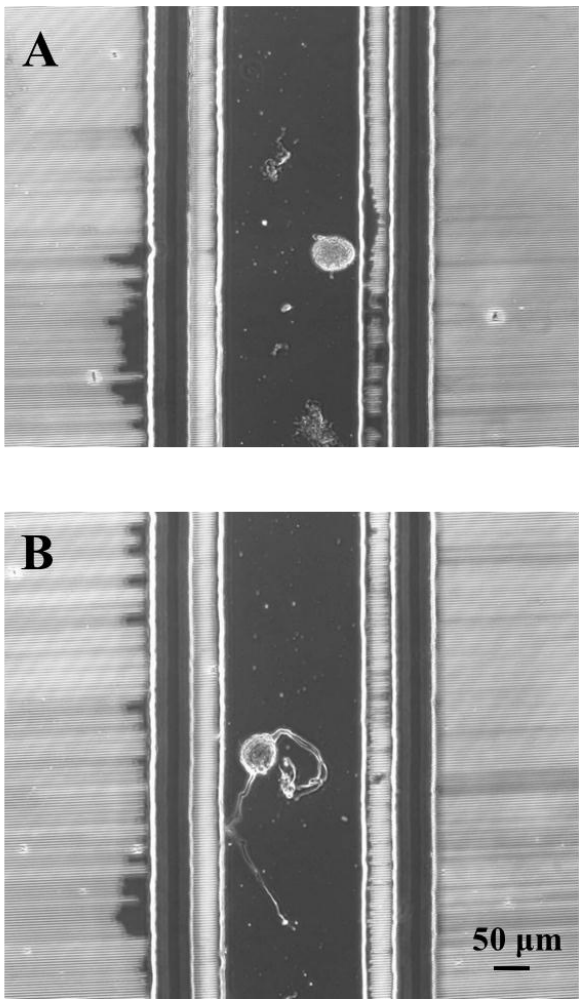

Figure 4.8 Culturing *Aplysia* bag cell neurons in microchannels. (A) Preliminary result after 3 days of culture, with native PDMS and no perfusion flow. (B) Neurons grew well after 3 days of culture, with extracted PDMS and perfusion flow.

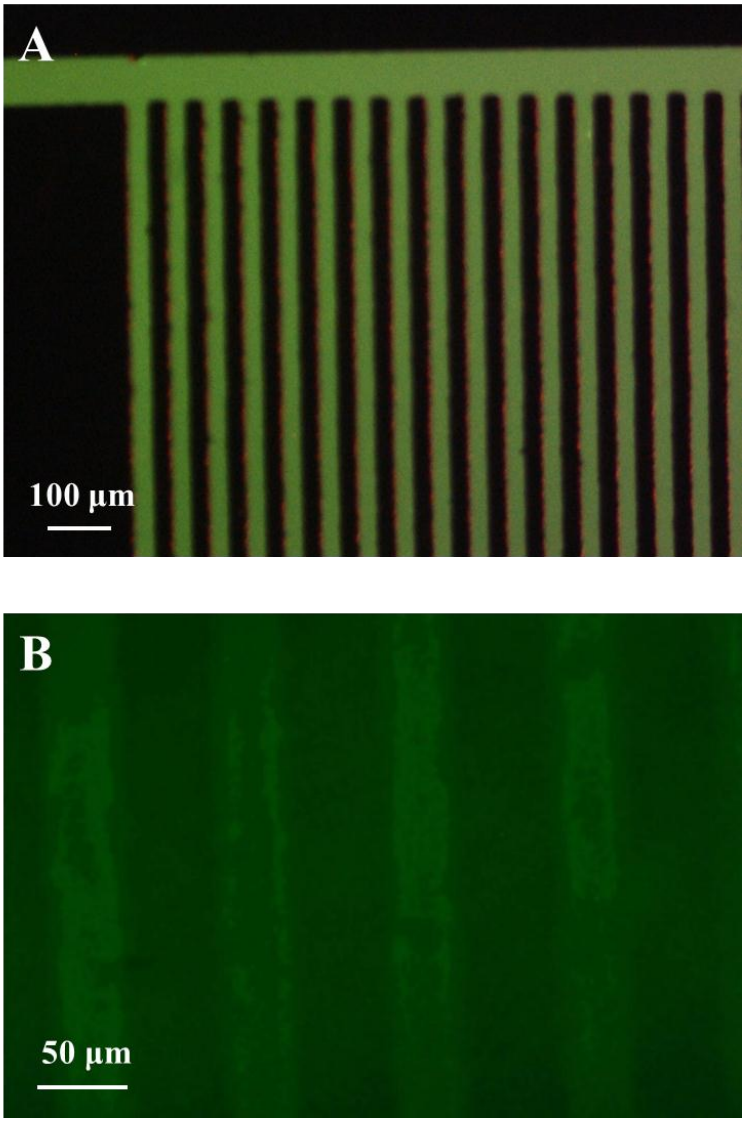

Figure 4.9 Patterning PLL/BSA lines on glass. (A) FITC-PLL solution filled the parallel channels without significant air bubbles. (B) Fluorescent image of PLL lines after PLL coating. The high background was due to ambient light.

4.7 References

1. W. S. Sossin, A. Sweet-Cordero and R. H. Scheller, *Proc. Natl. Acad. Sci. U. S. A.* , 1990, **87**, 4845-4848.
2. J. M. Fisher, W. Sossin, R. Newcomb and R. H. Scheller, *Cell*, 1988, **54**, 813-822.
3. T. Karhunen, F. S. Vilim, V. Alexeeva, K. R. Weiss and P. J. Church, *J. Neurosci.* , 2001, **21**, RC127.
4. N. G. Hatcher and J. V. Sweedler, *J. of Neurophysiol.*, 2008, **99**, 333-343.
5. S. Takayama, E. Ostuni, P. LeDuc, K. Naruse, D. E. Ingber and G. M. Whitesides, *Nature*, 2001, **411**, 1016-1016.
6. A. Tourovskaia, X. Figueroa-Masot and A. Folch, *Lab Chip*, 2005, **5**, 14-19.
7. A. M. Taylor, M. Blurton-Jones, S. W. Rhee, D. H. Cribbs, C. W. Cotman and N. L. Jeon, *Nat. Methods*, 2005, **2**, 599-605.
8. A. M. Taylor, S. W. Rhee, C. H. Tu, D. H. Cribbs, C. W. Cotman and N. L. Jeon, *Langmuir*, 2002, **19**, 1551-1556.
9. S. K. Ravula, M. S. Wang, S. A. Asress, J. D. Glass and A. Bruno Frazier, *J. Neurosci. Methods*, 2007, **159**, 78-85.
10. R. B. Campenot, *Proc. Natl. Acad. Sci. U. S. A.*, 1977, **74**, 4516-4519.
11. B. L. MacInnis and R. B. Campenot, *Science*, 2002, **295**, 1536-1539.
12. A. Salehi, J.-D. Delcroix and W. C. Mobley, *Trends neurosci.*, 2003, **26**, 73-80.
13. R. B. Campenot, J. Soin, M. Blacker, K. Lund, H. Eng and B. L. MacInnis, *Neuropharmacology*, 2003, **44**, 1107-1117.
14. L. J. Millet, M. E. Stewart, J. V. Sweedler, R. G. Nuzzo and M. U. Gillette, *Lab Chip*, 2007, **7**, 987-994.
15. J. Monahan, A. A. Gewirth and R. G. Nuzzo, *Anal. Chem.*, 2001, **73**, 3193-3197.
16. J. N. Lee, C. Park and G. M. Whitesides, *Anal. Chem.*, 2003, **75**, 6544-6554.
17. H. Yu, I. Meyvantsson, I. A. Shkel and D. J. Beebe, *Lab Chip*, 2005, **5**, 1089-1095.
18. K. J. Regehr, M. Domenech, J. T. Koepsel, K. C. Carver, S. J. Ellison-Zelski, W. L. Murphy, L. A. Schuler, E. T. Alarid and D. J. Beebe, *Lab Chip*, 2009, **9**, 2132-2139.

19. E. V. Romanova, K. A. Fosser, S. S. Rubakhin, R. G. Nuzzo and J. V. Sweedler, *FASEB J.*, 2004, **18**, 1267-1269.

CHAPTER 5

CONCLUSIONS AND FUTURE WORK

Deciphering the chemical signals in the nervous system is an important but challenging task. The main objective of this dissertation is the development of analytical platforms by coupling microfluidics to mass spectrometry to define and sample the chemical microenvironments surrounding small number of neurons. Microfluidic technology is well suited for studying mass-limited samples and controlling local environments. On the other hand, mass spectrometry (MS) offers high information content about analytes of interest without the need for prelabeling or preselection, serving as an excellent detection method for the samples collected within microfluidic devices. The specific group of chemical signals we investigated in this work is neuropeptides. However, the microfluidic systems and the detection scheme we developed here could be adapted to many other molecular classes.

Chapter 2[1] presented our interface of microfluidic devices and matrix-assisted laser desorption/ionization (MALDI)-MS imaging by using the substrate of the device directly as the MALDI target. The substrate was modified with octadecyltrichlorosilane (OTS) so that the surface resembled the C18 material used in liquid chromatography systems. The modified surface was able to collect the peptide molecules in the solution flowing down the channel by hydrophobic interaction; different molecules were separated on the surface due to different adsorption capability. This surface modification method

was demonstrated to be the optimal choice for collecting peptides by comparison to the surfaces derivatized with other chemicals in terms of sampling efficiency. The microfluidic device was dissembled after sample collection, and the substrate was directly introduced into the mass spectrometer for imaging after application of a matrix layer. This sampling and detection scheme is simple and adaptable to different applications; the sampling area can be fabricated at different locations of the chip with surface patterning techniques. The substrate used can be silicon or glass; in the case of glass, a layer of gold needs to be deposited on the surface to increase conductivity. The capability of the modified surface to adsorb peptides was independently confirmed by measurements of a captured radiolabeled peptide after the peptide solution flowed on top of the surface.

In Chapter 2, we also demonstrated different polydimethylsiloxane (PDMS) microfluidic devices used to investigate peptide release from neurons. We developed a device that contained an inlet reservoir connected to three branches of channels. A small number of *Aplysia* bag cell neurons were loaded into the inlet and were chemically stimulated to trigger peptide release. A negative pressure was sequentially applied to the outlet of each channel so that peptide release at different time points could be monitored. For example, we demonstrated that the media surrounding the neurons were sampled before, during, and after a simulation event; the fact that released peptides from bag cells, such as acidic peptide and egg laying hormone, were detected mainly in the "during" channel confirmed that the secretion of peptides was indeed due to the chemical simulation. In another device used for single cell analysis, one single neuron was loaded into a microchannel, and the released peptides in response to stimulation were collected

onto the sampling area of a C18-coated gold strip deposited down the channel. Before the sampling area, the cell loading channel was split into three branches, which were used to sample the microenvironment around the neuron before, during, and after simulation. Of course, more channel branches can be added to both chip designs, so that the device can be used to investigate the event of peptide release at greater temporal resolution. A microfluidic device containing an inlet reservoir and one long serpentine channel was designed to study the surface coverage of standard peptides. One intriguing result from these experiments was that a peptide, either angiotensin II or substance P, would be depleted before the surface was saturated; the length of the channel covered by a peptide increased with its amount. This result indicated that this device could be potentially used for quantifying the amount of released peptides, the basis of the follow-up work in Chapter 3. The applicability of the devices shown in this chapter clearly demonstrates that an efficient combination of microfluidics and mass spectrometry can be used for studying the small amount of peptides released, with the sensitivity allowing for single cell measurements.

A unique method to quantify peptides based on the adsorption length was described in details in Chapter 3.[2] We improved the microfluidic device with the serpentine channel mentioned in Chapter 2; here the outlet tubing was embedded into PDMS, ensuring a good seal at the outlet and a stable flow. The flow rate could now be precisely controlled by a syringe pump. The reservoir size was also optimized; the diameter of 1.5 mm was chosen to minimize sample loss to the reservoir while permitting easy liquid handling and cell loading. Most importantly, the issue of sample loss to the inlet reservoir and PDMS were addressed by oligo(ethylene glycol) (OEG) coating,

enabling more reliable and consistent quantitation results. Scintillation measurements of radiolabeled angiotensin II after incubated in PDMS channels showed that the OEG treatment of PDMS significantly increased the peptide recovery to more than 70% from about 50% with native, plasma-treated, or solvent-extracted PDMS. The nonspecific adsorption of peptides inside the reservoir was also reduced by derivatizing that area with an OEG-containing silane; the adsorption length of the same amount peptide was significantly longer than that on the surface completely coated with OTS. The OEG silanization reaction is a simple and effective way to make part of the substrate resistant to peptide adsorption, as compared to other surface patterning methods including deprivation of the OTS layer in the reservoir with oxygen plasma, partially coating the substrate with OTS, and the use of OEG-thiol on gold that was deposited on the reservoir area. In addition to the device enhancement, a mathematical model was proposed to describe the adsorption processes in the microchannel. The model was based on the kinetics of a simple adsorption reaction for a single peptide, and competitive adsorption of multiple peptides determined by adsorption rate constants. It predicted the linear correlation between the adsorption length and the amount of an analyte, and separation of multiple peptides by the channel. The model also examined the influence of experimental parameters and found that the adsorption length was insensitive to concentration and flow rate as long as the time scale of the flow was larger than that of the adsorption reaction. The conclusions from the model supported our quantitation method and were confirmed by the validation experiments. The test on 1 to 15 pmol acidic peptide showed a good linearity between length and amount (R^2 = 0.97). When both acidic peptide and α-bag cell peptide were present, these two peptides were separated in the channel and the linear

relationship still maintained for individual peptides (R^2 = 0.98 for 1 - 15 pmol α-bag cell peptide). The adsorption length of a peptide in a mixture remained the same to that of the same amount peptide when it was alone. The variance of length measurements, defined as the ratio of standard error of the mean to mean, was achieved as low as 3% between devices. By applying this quantitation approach on 15 chemically stimulated *Aplysia* bag cells, we detected two distinct bands of acidic peptide and α-bag cell peptide. The amounts of peptides released from one single neuron were determined to be 0.15 ± 0.03 pmol of acidic peptide and 0.13 ± 0.06 pmol of α-bag cell peptide, which matched measures from other methods. Our quantitation method based on adsorption length proved to be a simple, label-free, and robust way to quantify mass-limited analytes in microfluidic devices.

Chapter 4 demonstrated a compartmentalized PDMS microfluidic device that could separate one part of a neuron from the others, enabling spatial analysis of local chemical signals. The design was based on a commercially available device[3], which we modified according to the sizes of *Aplysia* neurons under investigation. The device contained one main cell loading channel and two adjacent secondary channels; they were connected by small interconnection channels. Under appropriate conditions, the neurites from the neurons could go through the interconnects to the secondary channels. Fabrication of this device involved two photolithography steps, sequentially making the features of the interconnects and the main/secondary channels on the wafer. We demonstrated that the liquid environment in each channel could be separately controlled by establishing a hydrostatic pressure difference between adjacent channels. The most efficient way for loading cells into the microchannel was by applying a pipette at the

outlet to draw the cell solution into the channel and then instantly stopping the pipette when some cells were inside. To increase the cell viability inside the microchannel, a perfusion flow was introduced into the system and the PDMS piece was extracted with serial solvents. We also found it necessary to pattern the substrate with repeated lines of poly-L-lysine and bovine serum albumin to guide the direction of process outgrowth from the neurons, so that the processes would penetrate the interconnects; otherwise the processes would follow the flow direction in the main channel. The pattern was made by introducing the poly-L-lysine solution through a device with a large number of parallel straight channels placed on top of the substrate, and then coating the substrate with poly-L-lysine lines with bovine serum albumin to fill the spaces between these lines. The success of pattern fabrication was confirmed by visualizing the surface with fluorescently labeled poly-L-lysine.

As for the future work, we will continue working on the compartmentalized device mentioned in Chapter 4 by applying the poly-L-lysine/bovine serum albumin pattern to cell culturing in the device. The culture conditions may need to be optimized to ensure that the outgrown neurites go through the interconnects and reach the adjacent channels, especially when there are only few to even single cells in the device. After the guided cell culture is achieved, we will use suitable collection methods to sample the subcellular environments of neurons. One promising method is to utilize the derivatized surface as in the previous devices. But as the substrate of the compartmentalized device is glass, for the sake of microscopic monitoring, the surface modification process used for the signal cell analysis chip in Chapter 2 will be adapted here. Briefly, a gold strip is deposited on the glass substrate, and then the self-assembled monolayer of

octadecanethiol is coated on the gold. In the assembled device, the gold strip is located downstream to where cells are to be attached; the releasate from the cells is captured by the thiolated surface.

While quantitation of released peptides during a single event is important, sometimes it is of more interest to be able to compare the components and quantities of releasate from the same neurons at different time points, in response to various chemical cues, or under different physiological conditions. Future work in this subject is based on the accomplishments described in Chapter 2 and 3. For this purpose, the serpentine channel design will be combined to the branching channels, one example shown in Fig. 5.1A. In this device, neurons are loaded into the inlet reservoir, and for instance, they can be treated with elevated potassium chloride, serotonin, and insulin sequentially. Each time after the chemical stimulation, the media surrounding the cells will be drawn into one of the channels with a syringe pump, and then the cells will be reconditioned with fresh media. The MALDI imaging profiles from the channels can be compared to each other. The device of this type offers flexibility in the chip design; more collection channels can be added if more conditions need to be compared or the release event needs to be monitored at greater temporal resolution. To eliminate the crosstalk between branching channels, a valve system can be applied to the device. In one valve system, a gas channel is placed on top of the fluidic channel and a thin PDMS membrane is sandwiched between these two channels.[4] The membrane can block or unblock the fluidic channel, which is controlled by the air pressure of the gas channel. The air pressure is adjusted by 3-way solenoid valves that can be easily interfaced to a computer for

controlling. The work on the valve system is currently underway by Callie Croushore and Dr. Chang Young Lee in our group.

To gain knowledge of the important chemical signals during neuronal network formation and neuron damage recovery, it is necessary to develop microfluidic devices that can monitor the neuronal wiring or regeneration within the device and sample the local chemical environments during the event. Fig. 5.1B shows one conceptual design of this kind device. The device contains five parallel channels connected by small interconnection channels, and two neurons (orange in the figure) are loaded into separate channels. Under appropriate conditions, the processes from the two neurons go through the interconnects into the adjacent channels and make a connection in the middle channel. The cell loading channel has a cell capturing chamber, and a small side channel attached to it to push a single cell into the capturing structure. Each of the channels can be fluidically separated from the others by using the principle of hydrostatic pressure discussed in Chapter 4, so that the local environment around the neuronal connection, the soma of either cell, and different process terminals can be individually defined and sampled. More channels can be added for finer spatial or temporal resolution for analysis. Since the amount of sample here is small, the sample collection method and the detection scheme need to be optimized for high-sensitivity analysis.

5.1 Figures

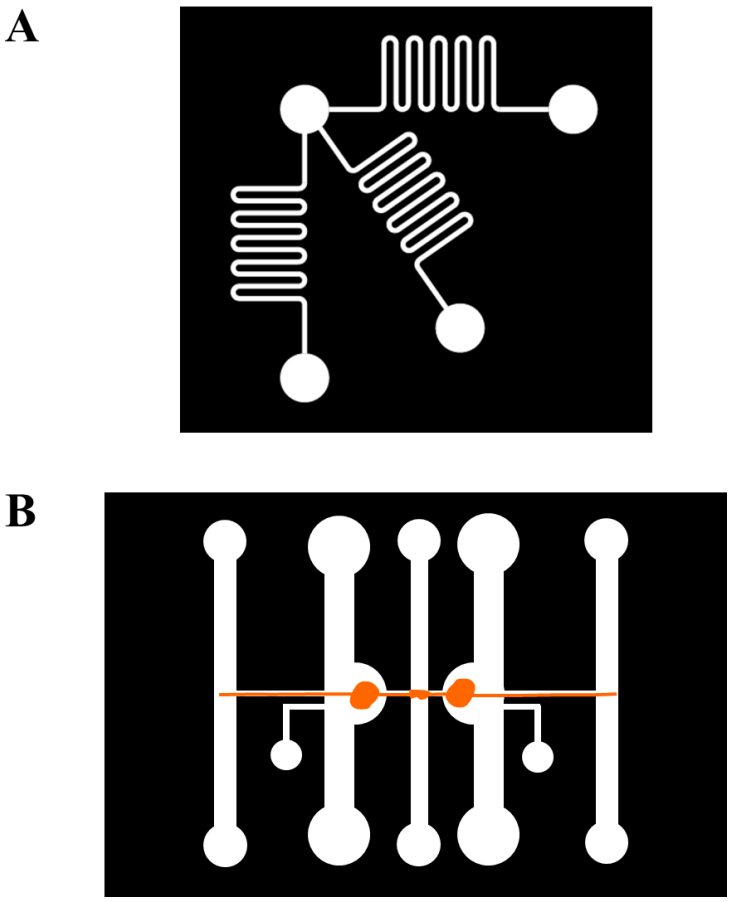

Figure 5.1 Design of microfluidic devices for future work. (A) A device contains three branches of serpentine channels. This device can be used for comparison of components and quantities of the releasate from neurons at different time points and conditions. (B) A device contains multiple channels connected by small interconnects. Two neurons (orange) can be loaded into separate channels and the event of neuronal connection or regeneration can be monitored. The local microenvironments surrounding the neuronal connection and different parts of the neurons can be sampled for studying the important chemical signals involved in neuronal network formation and neuron damage recovery.

5.2 References

1. K. Jo, M. L. Heien, L. B. Thompson, M. Zhong, R. G. Nuzzo and J. V. Sweedler, *Lab Chip*, 2007, **7**, 1454-1460.
2. M. Zhong, C. Y. Lee, C. Croushore and J. V. Sweedler, *Submitted to Lab Chip*, 2011.
3. A. M. Taylor, M. Blurton-Jones, S. W. Rhee, D. H. Cribbs, C. W. Cotman and N. L. Jeon, *Nat. Methods*, 2005, **2**, 599-605.
4. M. A. Unger, H.-P. Chou, T. Thorsen, A. Scherer and S. R. Quake, *Science*, 2000, **288**, 113-116.

APPENDIX A: LIST OF ABBREVIATIONS

αBCP	α-Bag cell peptide
Ang II	Angiotensin II
AP	Acidic peptide
APTS	(3-Aminopropyl)trimethoxysilane
ASW	Artificial seawater
BSA	Bovine serum albumin
C18	Octadecyl alkyl chains or octadecanethiol
CD	Compact disk
CIEF	Capillary isoelectric focusing
DHB	2,5-Dihydroxybenzoic acid
DI	Deionized
DMAPTS	(N,N-Dimethylaminopropyl)trimethoxysilane
DMOPAC	Dimethyloctadecyl[3-(trimethoxysilyl)propyl]ammonium chloride
ELH	Egg laying hormone
ESI	Electrospray ionization
FITC	Fluorescein isothiocyanate
HPLC	High performance liquid chromatography
m/z	Mass-to-charge ratio
MALDI	Matrix-assisted laser desorption/ionization
MS	Mass spectrometry

MSI	Mass spectrometry imaging
ODE	Ordinary differential equation
OEG	2-[Methoxy(polyethyleneoxy)propyl]trimethoxysilane or (11-mercaptoundecyl)tetra(ethylene glycol)
OTS	Octadecyltrichlorosilane
PC	Polycarbonate
PDMS	Poly(dimethylsiloxane)
PET	Polyethylenerephthalate
pI	Isoelectric point
PLL	Poly-L-lysine
PMMA	Poly(methyl methacrylate)
ROACHE	Rapid open-access channel electrophoresis
SAM	Self-assembled monolayer
s.e.m.	Standard error of the mean
SNR	Signal-to-noise ratio
TLC	Thin layer chromatography
TOF	Time of flight
UV	Ultraviolet

APPENDIX B: FABRICATION PROCESS OF MICROFLUIDIC DEVICES

The negative epoxy-based SU-8 2000 serial photoresists were purchased from MicroChem Corp. (Newtown, MA). The detailed fabrication procedure of SU-8 maters, used for molding poly(dimethylsiloxane) (PDMS) devices, is based on the datasheets found at http://www.microchem.com/Prod-SU82000.htm. First, a 3-inch silicon wafer (WRS Materials, Spring City, PA) is cleaned sequentially with acetone, methanol, and DI water and is blown dry with nitrogen. It is then placed on a hot plate maintained at 95 ℃ to dehydrate the surface. If fine structures of SU-8 (feature size < 5 μm) are to be fabricated, the wafer needs an immersion into piranha solution (H_2SO_4:H_2O_2 = 3:1, **Caution!** Piranha is a strong oxidant. It may explode on contact with organic residues) for 15 min and a rinse with a large amount of DI water. Piranha significantly removes organic contaminants on the silicon surface and ensures that small SU-8 features attach firmly to the wafer. The dehydrated wafer is then transferred to a CEE 100 programmable spinner that holds the wafer with vacuum. Approximately 5 mL SU-8 is dispensed onto the silicon wafer with a plastic dropper to cover the entire surface. Large air bubbles trapped in the photoresist should be removed with a new plastic dropper before spin-coating. The thickness of an SU-8 layer depends on the spin speed and the specific SU-8 product used, determining the height of structures in the final PDMS device. For instance, if a thickness of 10 μm is needed, SU-8 2010 can be used and spin-coated at 3500 rpm. Or if 50 μm is needed, SU-8 2050 is chosen and the spin speed is set at 3300 rpm. (Note: the relationship of spin speed versus thickness may change depending on the batch of products. Always check the protocol posted on the MicroChem website before starting.)

The program of spin-coating is usually set as follows: step 1: spinning at 500 rpm for 5 s, ramping at 100 rpm/s; step 2: spinning at the desired speed for 30 s, acceleration at 300 rpm/s. After that, a razor is used to remove the photoresist built up on the edge of the wafer. The coated silicon wafer is then put onto a hot plate for a soft bake. The purpose of soft bake is for the evolution of solvents and the formation of a uniform film. For a 50 μm film, the wafer is heated at 65 °C for 1 min and then 95 °C for 7 min. If wrinkles are still observable on the wafer after the prescribed time, the time of soft bake can be extended. After the soft bake, the wafer is left at room temperature for a sufficient time to allow cooling down completely.

A photolithography mask can be designed with Adobe Illustrator or AutoCAD. It can be printed on a transparency by ordering 5080 film production from the Printing Department at UIUC (http://www.printing.illinois.edu/L4SpecServ_5080.htm). The transparency mask is taped on a glass plate which is then mounted onto the mask holder of a Kasper mask aligner. (Note: make sure that the printed side of the mask faces the wafer.) The cooled wafer is also placed on the wafer area of the mask aligner and is fixed in position with vacuum. After the wafer and the mask have made a firm contact, their relative positions can be adjusted by the aligner. The exposure time is calculated by dividing the desirable exposure dosage (in mJ/cm^2) by the intensity of the UV lamp. To compensate the light loss due to absorption by the glass plate and the transparency, the practical exposure dosage usually doubles the recommended one in the SU-8 datasheets. For example, while the datasheet states that a 50 μm thick layer needs an exposure of 160 mJ/cm^2, 320 mJ/cm^2 is usually used in practice. Following exposure, the silicon is immediately removed from the aligner and placed on a hot plate for a post-exposure bake

for a prescribed time. Still take the 50 μm thickness as an example, a bake at 65 °C for 1 min and then at 95 ℃ for 6 min is utilized. The success of photolithography can be judged from the fact that the features of the mask appear in the photoresist layer after some time. After baking, the wafer is allowed for a sufficiently long time to cool down to room temperature. (Note: A sufficient cooling step is critical. Insufficiently cooled wafers will have the SU-8, especially the small and high aspect ratio structures, detached from the surface during the development step to be described below.)

The final step for fabricating masters is development; the wafer is dipped into the SU-8 developer to remove unexposed photoresist. Usually the development times recommended by the datasheets are used as a guideline only as the rate of development varies depending on the strength of agitation and the specifics of SU-8 structures. Being close to the end point of development is indicated by the observation that the majority of unexposed SU-8 is dissolved. The wafer is rinsed with fresh developer and then isopropyl alcohol. If a white films forms after rinsing, the development process is not completed. In this case, the wafer is again immersed into the developer solution for another 15 s. The cycle of rinse and reimmersion may need to be repeated until a clean surface is obtained after rinsing with isopropyl alcohol. (Note: too long a development can also lead to the detachment of exposed SU-8 from the surface. It is acceptable that some unexposed SU-8 remains on the wafer, as long as it does not interfere with the desired structures.) The exposed wafer is finally rinsed with DI water and blown dry with nitrogen. In this way, a master with the SU-8 features copied from the mask is formed. Before use, the master is usually inspected under a microscope to check for possible defects in the structures.

The top of a PDMS device is made by pouring the prepolymer, Sylgard 184 (Dow Corning, Midland, MI) onto the master and being cured at 70 ℃. It is found that different curing times above 6 h achieve similar results. The cured PDMS is cooled down to room temperature and peeled off from the master. For the feature sizes < 5 μm, it is difficult to remove the PDMS without breaking the fine structures on the master. In this case, the master is first treated with trideca-fluoro-1,1,2,2,-tetrahydrooctyl trichlorosilane (Gelest, Morrisville, PA) by placing the master and an open dish with 2-3 drops of the silanizing agent together in a desiccator for 2 h, before pouring the PDMS prepolymer. The layer on SU-8 formed by the silane facilitates the removal of cured PDMS. To assemble a device with sealed channels, the PDMS top is placed on a piece of silicon or glass, which is pre-cleaned by sequential rinse with methanol and DI water, through conformal bonding. If permanent bonding is needed, the PDMS piece is treated with oxygen plasma at 100 W for 30 s with a March Plasmod plasma system and then immediately bonded onto a substrate.

Although the positive photoresist, AZ 5214-E (AZ Electronic Materials Corp., Somerville, NJ), has only been used for surface derivatization purposes in this dissertation, the fabrication process involving it is also included here for completeness. Compared to the SU-8, the AZ 5214-E is less viscous and easier to handle. First, a 4-inch silicon wafer (WRS Materials, Spring City, PA) is cut with a diamond pen into small pieces of suitable size for a single device, and the pieces are cleaned sequentially with acetone, methanol, and DI water and blown dry with nitrogen. The silicon pieces are dehydrated at a hot plate set at 100 ℃ for at least 3 min. The dehydrated pieces are transferred to the CEE 100 programmable spinner one by one; the wafer holder may need

to be changed to accommodate the size of silicon pieces. The AZ 5214-E is dispensed onto the silicon with a plastic dropper to cover the entire surface. Since the AZ 5214-E is not very viscous, usually air bubble removal is not needed. The process of spin-coating is set as follows: step 1: spinning at 500 rpm for 5 s, ramping at 100 rpm/s; step 2: spinning at 3000 rpm for 30 s, ramping at 300 rpm/s. Because the photoresist is only used as a protection layer to block certain area of a silicon substrate from silanization reactions, the exact thickness of the photoresist layer is not important here. There is no issue of photoresist accumulation at the edge of the wafer either with the AZ photoresist. The silicon piece is then put on a hot plate at 100 ℃ for 1 min for a soft bake. After cooling down, the silicon is exposed to UV through a transparency mask for 10 s in the same mask aligner used for the SU-8 wafer. For positive photoresists, the exposed area becomes soluble in the developer solution. The mask for surface patterning has a simple design with one half black and the other blank. The black-blank boundary is carefully aligned with the silicon substrate in the mask aligner so that about 2/3 of the piece is exposed to UV light. For the AZ 5214-E, a post-exposure bake is not necessary. The purchased developer solution is diluted with DI water in 1:1, and the exposed silicon piece is dipped into the diluted solution until the exposed photoresist is dissolved and a clear pattern is visible. During development, an occasional agitation can be applied. The development time is about 45 s with the conditions used here. After that, the substrate is rinsed with DI water and blown dry with nitrogen. Now the substrate is ready for surface derivatization.